Università Politecnica delle Marche
Scuola di Dottorato di Ricerca in Scienze dell'Ingegneria
Curriculum in Energetica

---

# "Development and application of energy efficiency solutions in Water Supply Systems (WSSs)"

Ph.D. Dissertation of:
**Samuele Spedaletti**

……..

Supervisor:
**Prof. Gabriele Comodi, Ph.D.**

…….

Co-Supervisor
**Eng. Danilo Salvi**

……..

Curriculum supervisor:

**Prof. Giovanni Di Nicola, Ph.D.**

……..

XIX edition - new series

---

Università Politecnica delle Marche
*Dipartimento di Ingegneria Industriale e Scienze Matematiche*
Via Brecce Bianche — 60131 - Ancona, Italy

# Acknowledgements

I would like to express my gratitude to those around me to carry on my research work.

First of all, I would like to thank my Supervisor Prof. Gabriele Comodi, Ph.D., my Co-Supervisor Eng. Danilo Salvi, my colleague Eng. Matteo Lorenzetti, Ph.D., the Researcher Eng. Mosè Rossi, Ph.D., that sustained me on all the activities related to this thesis: their intuition, preparation and ideas had a great impact on the obtained results.

Moreover, I would like to give special thanks to all my family and girlfriend Sarah, whose patient love allowed me to achieve this important goal.

# Abstract

Energy efficiency interventions in Water Supply Systems (WSSs) can lead to significant energy, environmental and economic advantages. In this thesis, some strategies have been studied to predict water flow rates and improve WSSs efficiency. In particular, an Italian WSS located in Osimo town, located in Marche Region, has been analysed. The first part of this thesis presents a methodology for predicting flow rates in gravity adduction pipelines based on the electricity bills, so that the potential energy recovery through a small-scale hydropower plant is evaluated and subsequently validated through measured data. A Pelton turbine has been chosen as energy recovery unit with the aim of supplying electricity to a pumping station of a preloading tank where the water is treated to make it drinkable. In the year 2018, an energy saving of 475.26 MWh was achieved, which can be also expressed as 88.87 saved Tonnes of Oil Equivalent (TOE) and 204.36 $tCO_2$ not released into the atmosphere. The gross economic saving due to the installation of the Pelton turbine is equal to 94.29 k€/year and it can be further increased up to 116.51 k€/year if the energy efficiency certificates issued by the Italian Authorities are considered.

In the second part, a novel methodology to predict the yearly average flow rate in gravity adduction pipelines is presented and validated using measured data coming from a water meter installed on an adduction pipeline. Then, a methodology already developed was used to select Pump-as-Turbines (PaTs) and evaluate their Best Efficiency Point (BEP) to maximize the energy

recovery. On the selected WSS branch, two different installation layouts were investigated, namely one PaT and two PaTs in parallel. The first one showed the best economic profitability and led to a net economic saving of 1,325 €/year and a PayBack Period (PBP) of 11 years. Another branch with higher energy recovery potential was studied and a net economic saving of 4,915 €/year and a PBP of 6 years could be achieved.

Finally, the last part of the present study is focused on the efficiency of the WSS through the reduction of the electricity consumption of pumping systems acting on the volume of the supplied water. To achieve this goal, a method for monitoring and reducing network water losses has been developed. This method is based on the subdivision of the distribution water network into District Metering Areas (DMAs) and on the implementation of a remote reading system for hourly monitoring of the water balance of each water district. Subsequently, this methodology was applied to the water district of the historic center of the Osimo network, which was divided into 5 districts after having verified the resilience and hydraulic reliability of the water network divided into DMAs. An innovative 868 Mhz remote reading infrastructure was built and smart water meters were installed at the entrance of each district, as well as replaced the old residential ones.

In the analysed water district, 5,558.8 $m^3$of water savings, an energy saving $Ee_{saving}$= 7,332 kWh and an economic saving $EC_{saving}$= 1,857.45 € were achieved during the period between September and November 2020 with a PBP of the investement of 7 years and a 20-year NPV equal to 34,405.10 €.

# Contents

# List of Figures

# List of Tables

# Acronyms and Nomenclature

BEP = Best Efficiency Point

cc = Capital cost

dr = Discount rate

GSE = Gestore dei Servizi Energetici

HNU = Night Household Users consumption

MISE = Ministero dello Sviluppo Economico

MNF = Minimum Night Flow

NC = Night users Consumption

NHNU = Night Non-Household Users consumption

NPV = Net Present Value

NRW = Non Revenue Water

O&M = Operation & Management

OMS = Open Metering System

ONU = Operational Night Use

PaT = Pump-as-Turbine

PBP = PayBack Period

PID = Proportional-Integral-Derivative

PRV = Pressure Reducing Valve

rc = Market remuneration per each energy efficiency certificate

TOE = Tonnes of Oil Equivalent

WDN = Water Distribution Network

WSS = Water Supply System

$A_{ind}$ = Area occupied by industrial users [$m^2$]

$A_{res}$ = Area occupied by residential users [$m^2$]

C = Emitter coefficient

$C_p$ = Peak coefficient [-]

$C_w$ = Unit cost for purchase of water from an external source [€/$m^3$]

D = Impeller diameter [m]

$D_{Sp}$ = Specific diameter of a Pump-as-Turbine (PaT) in pump mode [-]

$D_{St}$ = Specific diameter of a Pump-as-Turbine (PaT) in turbine mode [-]

ec = Electricity cost [€/kWh]

$Ec_{cert}$ = Economic revenue due to the energy efficiency certificates [€/year]

$Ec_{saving\_gross}$ = Gross economic saving [€/year]

$Ec_{saving\_gross\_final}$ = Gross economic saving considering the energy efficiency certificates [€/year]

$Ec_{saving\_net}$ = Net economic saving [€/year]

$E_{e,i}$ = Specific electric energy consumption of j-th pump [kWh/$m^3$]

$\overline{En}_{after\_turbine}$ = Electric energy consumed by the pumping station after the installation of the hydraulic turbine [MWh]

$\overline{En}_{before\_turbine}$ = Electric energy consumed by the pumping station before the installation of the hydraulic turbine [MWh]

$\overline{En}_{electric\_bill}$ = Average electricity bill consumption of the pumping station [MWh]

$\overline{\mathrm{En}}_{\mathrm{electric\_pump}}$ = Average electricity consumption of the pumping station [MWh]

$\overline{\mathrm{En}}_{\mathrm{electric\_pump,i}}$ = Average electricity consumption of a hydraulic pump [MWh]

$\overline{\mathrm{En}}_{\mathrm{electric\_turbine\ avg\_monthly}}$ = Monthly average electric energy produced by the hydraulic turbine [MWh]

$\mathrm{En}_{\mathrm{saving}}$ = Energy saving [kWh]

$\overline{\mathrm{En}}_{\mathrm{saving\_after\_turbine}}$ = Electric energy saving after the installation of the hydraulic turbine [MWh]

$\mathrm{Fc}_{\mathrm{tCO2}}$ = Conversion factor from kWh to $tCO_2$ [$tCO_2$/kWh]

$\mathrm{Fc}_{\mathrm{TOE}}$ = Conversion factor from kWh to TOE [TOE/kWh]

$\mathrm{F}_{\mathrm{ec}}$ = Conversion factor from kWh to € [€/kWh]

$\mathrm{F}_{\mathrm{eec}}$ = Conversion factor from TOE to € [€/TOE]

g = Gravity acceleration [$m/s^2$]

H = Head [m]

$\mathrm{H}_{\mathrm{available}}$ = Available head [m]

$\mathrm{H}_{\mathrm{loss}}$ = Head losses [m]

$\mathrm{H}_{\mathrm{gross}}$ = Gross head [m]

$\mathrm{H}_{\mathrm{net}}$ = Net head [m]

$\mathrm{H}_{\mathrm{useful}}$ = Useful head [m]

$I_r$ = Resilience index of the original water network [-]

$I_r^*$ = Resilience index of the water network divided in DMAs [-]

$I_{r,d}$= Relative resilience index between original water network and divided in DMAs one [-]

$\overline{K}_{hi}$ = Average hourly coefficient of flow rates [-]

$\overline{K}_{gi}$ = Average daily coefficient of flow rates [-]

$\overline{K}_{mi}$ = Average monthly coefficient of flow rates [-]

$n_{ind}$ = Population density in industrial areas [person/$m^2$]

$n_{res}$ = Population density in residential areas [person/$m^2$]

$N_{Sp}$ = Specific speed of a Pump-as-Turbine (PaT) in pump mode [-]

$N_{St}$ = Specific speed of a Pump-as-Turbine (PaT) in turbine mode [-]

$P_D$ = Power dissipated along the water network [W]

$P_D^*$ = Power dissipated along the network divided into DMAs [W]

$P_{Dmax}$ = Maximum power dissipable along the water network to provide the minimum water service to users [W]

$P_h$ = Hydraulic power [kW]

$\overline{P}_{hydraulic\ avg\_yearly}$ = Average available hydraulic power [kW]

$P_{m\_BEP}$ = Mechanical power at the Best Efficiency Point [kW]

$P_r$ = Recovered power [kW]

$p_{t,m}$= Head pressure of m-th node at time t [m]

$\overline{P}_{turbine\ avg\_monthly}$ = Average power produced by the hydraulic turbine [kW]

Q = Flow rate [$m^3$/s]

$\overline{Q}_{a,t}$ = Yearly average flow rate from a water source to a tank [$m^3$/h]

$\overline{Q}_{a,tj}$ = Yearly average flow rate to the $j^{th}$ head compensation tank [$m^3$/h]

$\overline{Q}_{a,i}$ = Overall yearly average flow rate coming from each branch of a pipeline [$m^3/h$]

$\overline{Q}_{a,d,y}$ = Yearly average flow rate supplied by a head compensation tank to a water district [$m^3/h$]

$\overline{Q}_{app,y,m}$ = Average annual apparent losses of the m-th node of water network [l/s]

$\overline{Q}_{avg\_yearly}$ = Yearly average flow rate in a gravity adduction pipeline [$m^3/s$]

$\overline{Q}_{c,d,y}$ = Yearly average flow rate sold to the end users of water district [l/s]

$Q_{c,t,m}$ = Authorized billed flow rate consumed by users of m-th node of water network at time t [l/s]

$\overline{Q}_{c,y}$ = Yearly average flow rate used by all the end users [$m^3/h$]

$\overline{Q}_{c,y,gross}$ = Gross yearly average flow rate from a tank to the distribution network [$m^3/h$]

$\overline{Q}_{c,y,m}$ = Yearly average flow rate for the m-th node of water network [l/s]

$\overline{Q}_{d,y}$ = Total yearly average flow rate supplied to the water district [l/s]

$\overline{Q}_{hi,mis}$ = Average hourly flow rates [l/s]

$\overline{Q}_{gi,mis}$ = Average daily flow rates [l/s]

$\overline{Q}_{m,mis}$ = Average monthly flow rates [l/s]

$\overline{Q}_{loss}$ = Yearly average water losses [-]

$\overline{Q}_{loss,d}$ = Yearly average water losses in a water district network [-]

$\overline{Q}_{mis}$ = Yearly average flow rate measured through a flow meter [$m^3/h$]

$\overline{Q}_{mis,t}$ = Modal flow rate measured through a flow meter in one year [$m^3/h$]

$\overline{Q}_{pump\ avg\_monthly}$ = Monthly average flow rate elaborated by the pumping station [$m^3/s$]

$\overline{Q}_{pump,i\ avg\_monthly}$ = Monthly average flow rate elaborated by a hydraulic pump [$m^3/s$]

$\overline{Q}_{real,d}$ = Average annual real losses in water district [l/s]

$\overline{Q}_{real,m}$ = Average annual real losses of the m-th node of water network [l/s]

$Q_{real,t,m}$ = Real losses of the m-th node of water network at time t [l/s]

$\overline{Q}_{s,i,y}$ = Average yearly flow rate consumed by the users of each street of the district [l/s]

$Q_{t,m}$ = Flow rate of the m-th node at time t [l/s]

$\overline{Q}_{turbine\ avg\_monthly}$ = Measured monthly average flow rate elaborated by the hydraulic turbine [$m^3/s$]

$\overline{Q}_{turbine\ avg\_monthly\_meas}$ = Measured yearly average flow rate elaborated by the hydraulic turbine [$m^3/s$]

$\overline{Q}_{turbine\ avg\_monthly\_model}$ = Estimated monthly average flow rate potentially elaborated by the hydraulic turbine [$m^3/s$]

$\overline{Q}_{turbine\ avg\_yearly}$ = Measured average flow rate elaborated by the hydraulic turbine [$m^3/s$]

$\overline{Q}_{turbine\ avg\_yearly\_model}$ = Estimated yearly average flow rate potentially elaborated by the hydraulic turbine [$m^3/s$]

$\overline{Q}_{wells\ avg\_monthly}$ = Monthly average flow rate coming from the wells [$m^3/s$]

$\Delta\overline{Q}$ = Relative percentage error related to the flow rate estimation [%]

$\overline{V}$ = Overall water volume of a head compensation tank [$m^3$]

$V_{loss,avoided}$ = Avoided water losses [$m^3$]

$\overline{V}_c$ = Compensation water volume of a head compensation tank [$m^3$]

$V_{c,i}$ = Yearly average water volume used by each end user [$m^3$]

$V_{c,d}$ = Yearly authorized water volume invoiced in the district [$m^3$]

$V_{mis}$ = Yearly water volume measured through a flow meter [$m^3$/h]

$V_{monthly,end\ user,i}$ = Monthly water volume consumption of a generic end user [$m^3$]

$V_{monthly\_ind}$ = Monthly water volume consumption per each residential user [$m^3$]

$V_{monthly\_res}$ = Monthly water volume consumption per each industrial user [$m^3$]

$\overline{V}_g$ = Daily average water volume used by all the consumers in one year [$m^3$]

$\overline{V}_{g\_max}$ = Maximum daily water volume used by all the consumers in one year [$m^3$]

$\overline{V}_r$ = Reserve water volume of a head compensation tank [$m^3$]

t = Operational hours of the gravity adduction pipeline related to a Water Supply System [h]

$tCO_{2\_saving}$ = Tonnes of CO2 [tCO2] saving

$TOE_{saving}$ = Tonnes of Oil Equivalent [TOE] saving

$\alpha$ = Emitter exponent

$\eta_e$ = Electrical efficiency of a generator [-]

$\eta_{pump}$ = Total efficiency of a hydraulic pump [-]

$\eta_{turbine}$ = Total efficiency of the hydraulic turbine [-]

$\eta_p$ = Mechanical efficiency of a Pump-as-Turbine (PaT) in pump mode [-]

$\eta_t$ = Mechanical efficiency of a Pump-as-Turbine (PaT) in turbine mode [-]

$\rho_w$ = Water density [kg/m$^3$]

$\Phi$ = Flow coefficient [-]

$\psi$ = Head coefficient [-]

$\Psi(C_p)$ = Compensation function [-]

$\gamma$ = Water specific weight [N/m$^3$]

$\omega$ = Angular rotational speed [rad/s]

$\omega_s$ = Specific rotational speed [-]

# Chapter 1.

# Introduction

## 1.1. Background

Energy efficiency interventions are one the key points for lowering carbon dioxide emissions (CO2) into the atmosphere and, at the same time, enhancing the performance of both civil and industrial plants [89-91]. In particular, Water Supply Systems (WSSs) and Water Distribution Networks (WDNs) could lead to a high recovery potential due to their continuous operation throughout the day [92, 93].

Different solutions have been already studied so far; among them, the installation of particular or common hydraulic machines in determined pipelines is one of the most applied. In this regard, Oladosu et al. [94] proposed a vertical axis in-pipe turbine with NACA 0020 airfoils and performed numerical simulations to assess its performance and effects on the water flow. They found out that the minimum and the maximum percentage of pressure drop due to the presence of the turbine are equal to 1.94 and 9.70%, respectively, while the output power ranges between 242 and 1663 W. Du et al. [45] analysed the performance of a cross-flow turbine installed in the water pipelines, focusing on the runner geometry to achieve the optimal dimensions according to the operating conditions of the site. The optimal

sizing related to the analysed case led to an output power of 2285 W and an efficiency of almost 51%. Sinagra et al. [95] designed a 10 kW Banki micro-turbine renamed Power Recovery System (PRS) to be installed in the WDN of Palermo (Italy). Firstly, they carried out the laboratory tests on this hydraulic machine, showing that a maximum efficiency of 76% can be achieved. Yang et al. [96] designed, simulated and tested two types of vertical axis pipeline turbines lift- and drag-type based, respectively. Both turbines achieved the wanted requirements, even though the former showed higher performance.

Currently, the use of commercial pumps used as turbine, named Pumps-as-Turbines (PaTs) has taken the field in this sector, mainly due to i) their large availability in the market, ii) the high number of spare parts in case of failures and iii) their cheaper costs compared to traditional hydraulic turbines [97]. Several authors investigated the profitability of PaTs from both technical and economic points of view. Stefanizzi et al. [4] used PaTs to replace Pressure Reducing Valves (PRVs) to perform pressure regulations inside the pipelines and energy recovery as well. Knowing both available water flows and head of the WDN located in Apulia (Italy), they obtained the characteristic curve of a PaT suitable for this application through a 1-D prediction model to evaluate its Best Efficiency Point (BEP), so that a techno-economic evaluation of its installation can be assessed properly. Barbarelli et al. [69] carried out experimental activities on 12 PaTs in both direct and reverse modes to assess their statistical method for their performance prediction. After that, a case study has been analysed and used to evaluate the potential

energy recovery coming from the use of a PaT in the WDN of Cosenza (Italy). Kandi et al. [98] developed a PaTs selection process, whose effectiveness is based on capability, availability and adaptability, especially when these hydraulic machines are subjected to both variable flow rates and heads. Through a case study in Iran, they found out that this criterion can lead to an effectiveness up to 20%, since run-time values of flow rates and heads are used instead of the average ones.

However, another approach for improving the efficiency of both WSSs and WDNs is the reduction of water leakages throughout the pipelines, since they account for 20-30% of the water supply, achieving a peak of 50% in those countries where distribution systems are now old [99]. The optimization of their management, e.g. pressure regulation, could lead to satisfactory results in terms of both water and economic savings. In this regard, Cavazzini et al. [100] introduced a novel performance parameter named Leakage Performance Index (LPI) that allows the WDN management to minimize water leakages through flow rates and pressures measurements, focusing on the nodes of the water branches that have a greater impact on the water leakages due to high pressure values. A model of an Italian WDN was created by EPANET® and validated through the performed experimental campaign, assessing the effectiveness of the LPI performance parameter. Bonthuys et al. [101] created a hydraulic model using the management data and plans of the WDNs to identify zones having potential energy recovery and leakages reduction as well. In particular, they found out that the WDN of Polokwane (South Africa) has a potential energy recovery of 2.3 GWh/year if the

leakages losses are reduced between 3.3 and 4.2% of the overall supplied potable water. Latchoomun et al. [102] investigated the energy efficiency of the WDNs using an experimental network with low and high leakages. In particular, they developed a novel concept named Harmonic Oscillator Tank (HOT) that consists of modulating the pressure released by an hydropneumatic tank to provide constant flow rates, even though leakages are present. They obtained a specific consumption of 0.354 kWh/m3 per day using the HOT concept, which is sensibly lower than using only pumping stations and allows to reduce energy consumptions and leakages as well.

Currently, the installation of smart meters in both WSSs and WDNs leads to the monitoring of the water flows remotely, thus being able to make intervention quickly and creating the so-called District Metered Areas (DMAs). This method has a great impact on the energy efficiency improvement on the water system from both qualitatively and quantitatively points of view. In this regard, Naim et al. [103] proposed a fully Artificial Intelligence (AI)-based system capable of collecting data from smart meters to monitor both water supply and consumption of a sub-part, detecting eventual leakages and controlling potable water coverage. They used a neural network trained on a dataset that achieved an accuracy of 98.7% through tests and experiments. Bragalli et al. [104] proposed a Synchronous Water Balance (SWB) methodology to detect small leakages in water districts, considering the case study of the city of Fano (Italy), and assessed how the availability of near real-time synchronous water consumption measures can improve the WDN efficiency. Pesantez et al. [105] used the machine learning methods to

predict the water demand of 90 end-users through smart metered data. Among the machine learnings techniques, Random Forests (RFs) and Artificial Neural Networks (ANNs) performed better in all the analysed scenarios.

My research work starts with the aim to provide a contribution to the state of art in term of development and application of WSSs and WDNs energy efficiency methodologies and techniques.

The thesis is structured in 3 chapters and each chapter has a similar structure based on the following sections:

1) Introduction, which describes the WSSs energy efficiency solution in exam and the scientific state-of-art concerning the methodology analysed;

2) Design and explanation of a method that positively contribute to what the company has done so far;

3) Application and validation of this method on a real case study;

4) Description of benefits from energy and economic points of view, comparing the results with those available in the state-of-the-art.

In all the last three chapters, the case study is the WSS of the city of Osimo, a town located in the center of Italy in the Marche region.

The Osimo WSS consists of a water supply system and distribution network, pumping stations and water sources that are very complex. The planimetry and altimetry of the Osimo WSS cope with the geodetic height differences between the various districts of the city where the end users are located. Indeed, different compensation head tanks located at significantly different altitudes lead to water flow rates with high pressure energy content that can be exploited instead of being dissipated. The highest energy consumption

sites of the WSS of Osimo are water pumping stations in "Padiglione", hereinafter referred to as “water pumping station A”, and by the water pumping station of "Campocavallo", hereinafter referred to as “water pumping station B”. In addition to these pumps, other ones are present between compensation tanks, but they have a lower energy consumption. Concerning the planimetry of the Osimo WSS, see paragraph 2.2.1 with Figure 1 and Table 1 and paragraph 3.3 with Figure 9 and Table 8. In the year 2017, the water pumping station A consumed 1,647,195 kWh of electricity, while the water pumping station B 1,663,641kWh. The cost of this energy was equal to 529,800 €. These numbers show that the impact of the network management costs are high and their reduction is a primary goal. It is also important to highlight the part of these costs related to the water pumping, which are due to significant water losses that increase the volumes of water pumped to supply the end users. Indeed, in the year 2018 the water withdrawn from the water sources represented by Castreccioni dam and the two water fields was equal to 3,459,100 $m^3$, compared to 2,404,000 $m^3$ consumed by the users of Osimo, achieving a percentage of total water losses equal to 30.5 % with respect to the supplied water.

The first study is related to the development of a methodology capable of identifying the hydropower potential in WSSs through the estimation of the flow rates in gravity adduction pipelines that connect the water source to the preloading tanks downstream. Subsequently, the first study is applied to the WSS of Osimo to identify a site where a Pelton turbine with two nozzles can be installed, whose produced electricity is self-consumed by the pumping

station. On the other hand, in the second part of the thesis the developed methodology related to the estimation of the yearly average flow rate in gravity adduction pipelines is described. Then, in the same chapter the validation of the proposed methodology and an energy and economic assessment related to the installation of PaTs in gravity adduction pipelines in the analysed WSS of Osimo is presented. In the third part, a method to seek and reduce water losses and therefore the costs related to the energy consumed by the WSS pumping stations is described. This method is based on the hydraulic simulations of a water network subdivided in District Metering Areas (DMAs) and the creation of a remote reading system for monitoring the water balances of each district. This last study was also applied to a water district located in the historic center of Osimo.

# Chapter 2.

# 2. Hydropower recovery in energy consumption sites of WSS

## 2.1. Introduction

The water-energy nexus concept is becoming of great interest in the energy sector with the aim of ensuring a sustainable exploitation of the water source on both environmental and energy points of view [1, 2]. Within the water-energy nexus framework, one of the most important topics concerns the use of water for power production. Hydropower plants generate clean energy by exploiting the potential energy of a water reservoir and transforming it to electricity by a generator. Conversely, a considerable amount of energy is required by several processes to pump and treat water in civil and industrial contexts. The two perspectives can be combined in several applications, like in Water Supply Systems (WSSs), Water Distribution Networks (WDNs) [3, 4] and in wastewater treatment plants [5, 6] where a share of the energy required to run such plants can be potentially recovered. All the previous mentioned applications present facilities, such as pumping stations, that are highly energy consuming, but also with considerable hydraulic head potentials. For this reason, the recovered energy can lead to an increase of the

system efficiency, thus to a reduction of both consumed Tonnes of Oil Equivalent (TOE) and CO2 emissions released into the atmosphere [7, 8].

WSSs are typically constituted by a water source connected to loading/head compensation tanks downstream located at high geodetic altitudes, being in turn connected to other tanks [9] or directly to the end users via distribution network. The extension of WSSs depends on the number of inhabitants of a city/town, as well as on its dimensions. The water source can be a reservoir filled by water pumped from a low-level reservoir. About 2-3% of the electric energy consumption worldwide derives from pumping stations of WSSs [10, 11] and 80-90% of this consumption is addressed to pump motors [12, 13]. In this regard, some works in literature stated that the specific energy consumptions measured in WSSs are below 0.30 kWh/m3 in developing countries and reach values higher than 3 kWh/m3 in developed ones [14, 15]; in this last case, energy recovery interventions are strongly recommended to improve the WSSs efficiency.

The proper choice of the energy recovery intervention in WSSs depends on their design characteristics [16, 17] and several authors investigated on the potential energy recovery through hydropower solutions. Kucukali [18] estimated that this kind of potential recovery, which has been applied in 45 WSSs located in Turkey, led to 173 GWh saved per year. McNabola et al. [19] analysed ten cases related to water industries in Ireland, where the hydraulic power is recovered through small-scale hydropower plants ranging between 2 and 115 kW. The installation of hydraulic turbines in WSSs provides, beside the electricity production, the water pressure regulation

inside the network, which is usually performed by Pressure Reducing Valves (PRVs). Indeed, a reduction of the water pressure leads to a decrease of water losses throughout the pipelines [20, 21] that reached nowadays a remarkable average value of 26% worldwide [22]. PRVs are installed not only in WDNs, but also in other WSSs where high values of pressure are present. For instance, this situation occurs when an upstream water source is placed at a very high altitude and connected to a preloading or a loading/head compensation tank downstream that is at atmospheric pressure. The preloading tank has the aim to mix the water coming from the water source with the one coming from wells, whose chemical properties are not still acceptable. After the mixing process, the water becomes drinkable and it is pumped to loading/head compensation tanks; subsequently, it is distributed to end users via distribution network. However, pumping stations withdraw water from the preloading tank and provide it with the proper pressure in order to reach loading/head compensation tanks. Doing this, the potential energy content of the water due to the geodetic altitude difference between the water source and the preloading tank is lost, since it is dissipated through a PRV for being lowered down to the atmospheric pressure. It is worth noting that the mixing process can be also performed inside the pipelines, unless the water pressure is enough to provide the water to loading/head compensation tanks.
In order to improve the efficiency of WSSs, hydraulic turbines can be installed upstream the preloading tank, thus replacing the PRV in order to recover part of this water energy content and produce the electric energy required by the pumping station. The installation of small-scale hydropower

plants in WSSs presents low implementation costs [23, 24]. The produced electric energy can be consumed by facilities and auxiliary systems of WSSs, thus lowering the amount of electricity withdrawn by the national grid [18]. Energy recovery interventions through hydropower solutions in WSSs have also three main advantages [25]: i) reduction of greenhouse gas emissions due to the self-consumption of the produced electric energy, as well as its production by means of a renewable source, ii) limitation of civil works since they are adapted to the existing infrastructure, thus not requiring new spaces, and iii) to lower environmental impacts throughout the life cycle of WSSs.

Nevertheless, the correct average flow rate in gravity adduction pipelines has to be assessed in order to perform the energy recovery interventions properly, mostly when flow meters are not installed. In literature there are several works, based on the evaluation of the water demand of the end users, that analysed different deterministic, probabilistic and demand time-series approaches for predicting the peak one in WSSs, as well as the design flow rate in WDNs. In these regards, Wong et al. [26] carried out a literature review on the previous mentioned approaches and proposed the Bayesian one, which bridges the gap between model-based and field-measurement values, being more flexible and more reliable on the design point of view. Letting et al. [27] presented a simulation model for the water demand using a Particle Swarm Optimization (PSO) algorithm, which estimates the nodal water demand in each WDN branch, and compared the numerical results with real ones obtained by sensors installed in the network. Results showed that both nodal demands and pipe flows can be accurately determined. Balacco et al. [28]

analysed the water demand in several towns in Puglia (Italy), leading to the definition of a relationship between the peak factor and the number of inhabitants. They found out that the design of WSSs can be done without considering the use of monthly and weekly peak factors. Moreover, the magnitude of the peak factor obtained through measured data is considerably lower compared to literature values. However, detailed information related to WSSs and WDNs are usually required, which are not always affordable and make difficult, as well as time demanding, the calculation of the water demand, also considering the creation of optimization algorithms. Moreover, to the authors' knowledge, a methodology to estimate the yearly average flow rate in gravity adduction pipelines has not be discussed and presented so far.
In this work, a methodology based on the knowledge of the electricity bill consumption related to the pumping station of a preloading tank to predict the yearly average flow rate that can be potentially exploited for energy recovery purposes is presented. In particular, this methodology is thought to be applied in branches where flow meters are not installed. First of all, gravity adduction pipelines where the hydraulic turbine can be installed have to be identified, taking into account the connections between a water source and the preloading tank. The developed methodology was then validated through measured data obtained by a flow meter installed upstream the preloading tank, after the hydraulic turbine installation. Finally, energy, environmental and economic analyses have been performed to assess the advantages of this energy efficiency intervention.

This chapter is structured as follows: Section 2 describes the methodology developed for estimating the yearly average flow rate when flow meters are not installed; then, the head that can be exploited by the hydraulic turbine has been also calculated using a formula reported in literature. In addition, the procedure to select the proper machine is also presented. Section 3 deals with the case study of a WSS related to a mid-town located in the Center of Italy. After the analysis of the flow duration curve of the site of interest, the flow rates obtained through the methodology described in Section 2 have been confirmed and validated with measured data from a flow meter installed after the hydraulic turbine installation, whose selection process has led to the choice of a Pelton machine. Section 4 presents energy, environmental and economic analyses due to the energy efficiency intervention. Finally, Section 5 reports the conclusions of the work.

## 2.2. Methodology

This Section aims at describing a methodology capable of identifying the hydropower potential in WSSs through the estimation of the flow rates in gravity adduction pipelines that connect the water source to the preloading tanks downstream. The presented methodology is based on the knowledge of the electricity bill consumption of the pumping station installed in the preloading tank. After the estimation of the yearly average flow rate, the head is evaluated by knowing the geodetic heights of each element previously mentioned in the site of interest and the relative head losses. The methodology is divided in three phases:

i. analysis of the WSS structure of the site of interest, considering that the WSS layout composed by a water source, a preloading tank with a pumping station, loading/head compensation tanks and interconnections;
ii. estimation of the hydropower potential from sites identified in the previous phase, focusing the attention to the one having the connection between the water source and the preloading tank. Then, after the analysis of the flow duration curve, the yearly average flow rate, together with the useful head, are calculated. Finally, the calculation of the power produced by the hydropower system is also provided;
iii. assessment of energy, environmental and economic benefits due to the hydraulic turbine installation; specifically, the evaluation of the energy saving, also in terms of saved TOE and $tCO_2$ emissions not released into the atmosphere, and the economic saving due to the energy efficiency intervention are discussed.

### 2.2.1. Water Supply System (WSS) infrastructure and an overview of the site of interest

The water reservoir of the analysed WSS is located at 346 m a.s.l. with a height of 69.40 m (55 m of depth) and a capacity of 37.3 $Mm^3$. The water coming from this reservoir feeds one preloading tank and then 7 loading tanks placed in different zones, as reported in Figure 1 and Table 1.

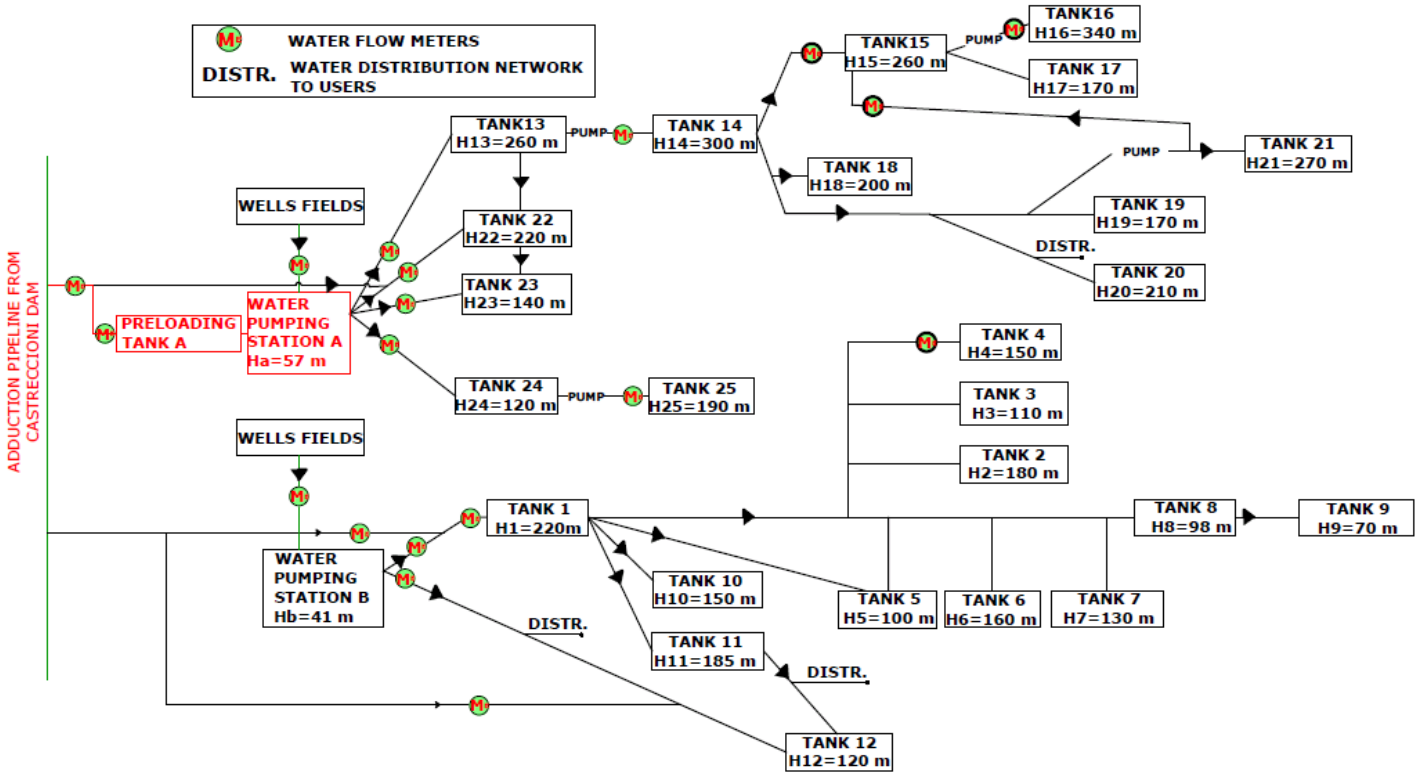


*Figure 1: Layout of the analysed WSS*

*Table 1: Water source, loading, preloading and head compensation tanks with respective geodetic heights*

| WATER SOURCE | LOADING AND PRELOADING TANK (GEODETIC HEIGTH) | HEAD COMPENSATION TANK (GEODETIC HEIGTH) | GEODETIC HEIGTH DIFFERENCE |
|---|---|---|---|
| CASTRECCIONI DAM (346 m) | TANK A (57 m) | - | 346-57=289 m |
| | - | TANK 1 (220 m) | 346-220=126 m |
| | - | TANK 22 (220 m) | 346-220=126 m |
| | - | TANK 12 (120 m) | 346-120=226 m |

| | | |
|---|---|---|
| TANK 13 (260 m) | TANK 22 (220 m) | 260-220=40 m |
| TANK 22 (220 m) | TANK 23 (140 m) | 220-140=80 m |
| TANK 14 (300 m) | TANK 18 (200 m) | 300-200=100 m |
| | TANK 19 (170 m) | 300-170=130 m |
| | TANK 20 (210 m) | 300-210=90 m |
| | TANK 15 (260 m) | 300-260=40 m |
| TANK 15 (260 m) | TANK 17 (170 m) | 260-170=90 m |
| TANK 1 (220 m) | TANK 2 (180 m) | 220-180=40 m |
| | TANK 3 (110 m) | 220-110=110 m |
| | TANK 4 (150 m) | 220-150=70 m |
| | TANK 5 (100 m) | 220-100=120 m |
| | TANK 6 (160 m) | 220-160=60 m |
| | TANK 7 (130 m) | 220-130=90 m |
| | TANK 8 (98 m) | 220-98=122 m |
| | TANK 10 (150 m) | 220-150=70 m |
| | TANK 11 (185 m) | 220-185=35 m |
| TANK 11 (185 m) | TANK 12 (120 m) | 185-120=65 m |
| TANK 8 (98 m) | TANK 9 (70 m) | 98-70=28 m |

In particular, Tank A is the preloading tank that collects the water coming from both water source and wells with the aim of making it drinkable after a mixing phase process. The preloading tank presents a pumping station that supplies water to Tanks 13, 22, 23 and 24 located at higher altitudes with

respect to the preloading tank itself. Figure 2 shows a simplified scheme of the site of interest, namely the preloading tank where a hydraulic turbine has been subsequently installed.

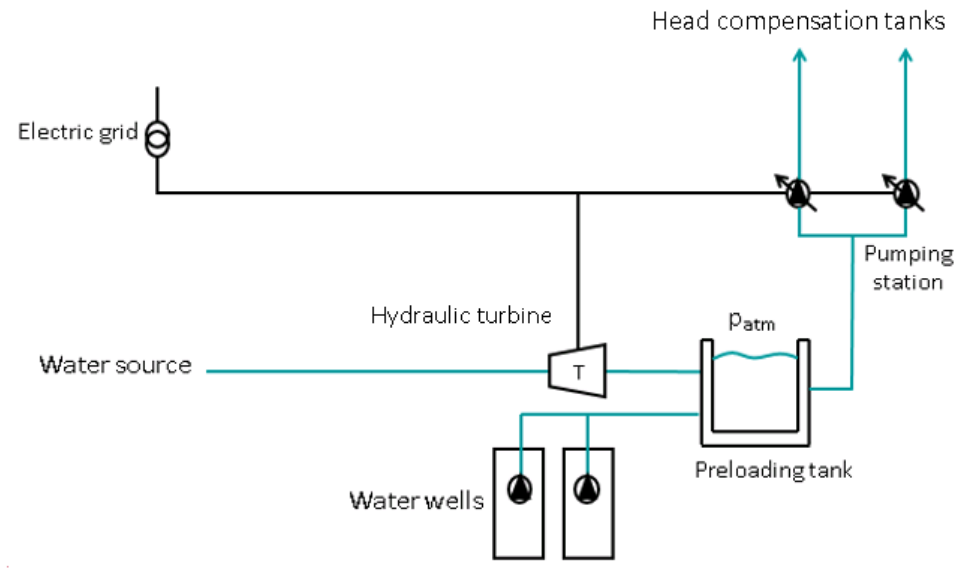


*Figure 2: Simplified scheme of the site of interest (preloading tank plus the new hydraulic turbine)*

### 2.2.2. Estimation of both yearly average flow rate and useful head of the hydraulic turbine

The flow rate elaborated by the hydraulic turbine can correspond either to the overall one that flows in gravity adduction pipelines or to a part of it, according to the number of deviations and design characteristics of the WSS.

The evaluation of the flow rate can be done instrumentally through flow meters installed in pipelines that recreate the flow duration curve.

Generally, flow meters are installed in adduction pipelines that connect the pumping stations to a loading/head compensation tank located at high altitude, while it is rare to find them in gravity adduction pipelines since they are costly. If a gravity adduction pipeline connects the water source to a loading/head compensation tank directly, the yearly average flow rate $\overline{\mathrm{Q}}_{\mathrm{avg\_yearly}}\ [\mathrm{m}^3/\mathrm{s}]$ is evaluated through Eq. (1), which takes into account the population density $\mathrm{n}_{\mathrm{res}}$ and $\mathrm{n}_{\mathrm{ind}}$, the occupied areas and the monthly water volume consumptions $\mathrm{V}_{\mathrm{monthly\_res}}\ [\mathrm{m}^3]$ and $\mathrm{V}_{\mathrm{monthly\_ind}}\ [\mathrm{m}^3]$ of both residential and industrial end users, respectively:

$$\overline{Q}_{avg\_yearly} = \frac{(n_{res} \cdot A_{res} \cdot V_{monthly\_res} + n_{ind} \cdot A_{ind} \cdot V_{monthly\_ind}) \cdot \#\ of\ months\ in\ a\ year}{86{,}400s \cdot \#\ of\ days\ in\ a\ year}\ [m^3/s] \quad (1)$$

It is worth noting that Eq. (1) is valid when the flow rate coming from the water source is the same of the one that flows inside a loading/head compensation tank; indeed, the balance of the water consumption related to the end users served by a loading/head compensation tank returns the volume of water entered the loading/head compensation tank itself. That said, Eq. (1) can be considered be a good starting point for estimating the flow rate of an ex-novo WSS.

However, when preloading tanks are located at lower geodetic heights than loading/head compensations ones, another approach for the evaluation of the

flow rate is used. In this case, the monthly average flow rate pumped by the pumping station $\overline{Q}_{\text{pump avg\_monthly}}\ [m^3/s]$ is estimated by knowing its electricity consumed per month $\overline{En}_{\text{electric,pump}}\ [MWh]$. The steps used in the presented methodology are explained hereinafter through bullet points:

1. the number of end users served by each pump of the pumping station, as well as the monthly water volume consumption of each end user $V_{\text{monthly,end user,i}}\ [m^3]$, are known; thus, the multiplication of the previous mentioned terms returns the water volume consumption of all the end users. Then, this value is divided by the period of operation of the WSS equal to 86,400 s times the number of days in a month, leading to the monthly average flow rate $\overline{Q}_{\text{pump,i avg\_monthly}}\ [m^3/s]$ elaborated by each pump;
2. both dimensions and physical characteristics of the adduction pipelines that connect each pump to the respective loading/head compensation tank are known as well. The monthly average flow rate elaborated by each pump $\overline{Q}_{\text{pump,i avg\_monthly}}\ [m^3/s]$ previously evaluated is used to calculate the head losses along each adduction pipeline, being a quadratic function of the flow rate;
3. the useful head $H_{\text{useful}}\ [m]$ provided by each pump is equal to the sum of the geodetic height difference between the head compensation tank and the preloading one $H_{\text{available}}\ [m]$ plus the head losses along the adduction pipelines $H_{\text{loss}}\ [m]$ using the one-term quadratic formula valid for fully turbulent flow regimes [29];

4. since the pumps are installed in parallel, the same hydraulic efficiency within all the operating range is assumed, since they operate close to their Best Efficiency Point (BEP) most of the time. Therefore, Eq. (2) provides the monthly average electric energy $\overline{\mathrm{En}}_{\mathrm{electric\_pump,i}}$ [MWh] consumed by each pump:

$$\overline{En}_{electric_{pump},i} = \frac{\rho \cdot g \cdot \bar{Q}_{pump,i\ avg_{monthly}} \cdot H_{useful}}{\eta_{pump} \cdot 10^{6}} \cdot (24\ h \cdot \#of\ days\ in\ a\ month)$$

$[MWh]$ (2)

5. the sum of the electric energies consumed by each pump has to be equal to the one in the electric bill; if not, the monthly water volume consumption $\overline{\mathrm{V}}_{\mathrm{monthly,end\ user,i}}$ $[\mathrm{m}^3]$ of each end user is modified iteratively until the solution converges;
6. finally, when the convergence of the solution is reached, the sum of the monthly average flow rates elaborated by each pump $\overline{\mathrm{Q}}_{\mathrm{pump,i\ avg\_monthly}}$ $[\mathrm{m}^3/\mathrm{s}]$ leads to the monthly average flow rate elaborated by the pumping station $\overline{\mathrm{Q}}_{\mathrm{pump\ avg\_monthly}}$ $[\mathrm{m}^3/\mathrm{s}]$.

In order to have a better overview of the entire process, Figure 3 shows the flow diagram related to the procedure previously explained, where the free parameter and the known values are highlighted in dark blue and in red, respectively.

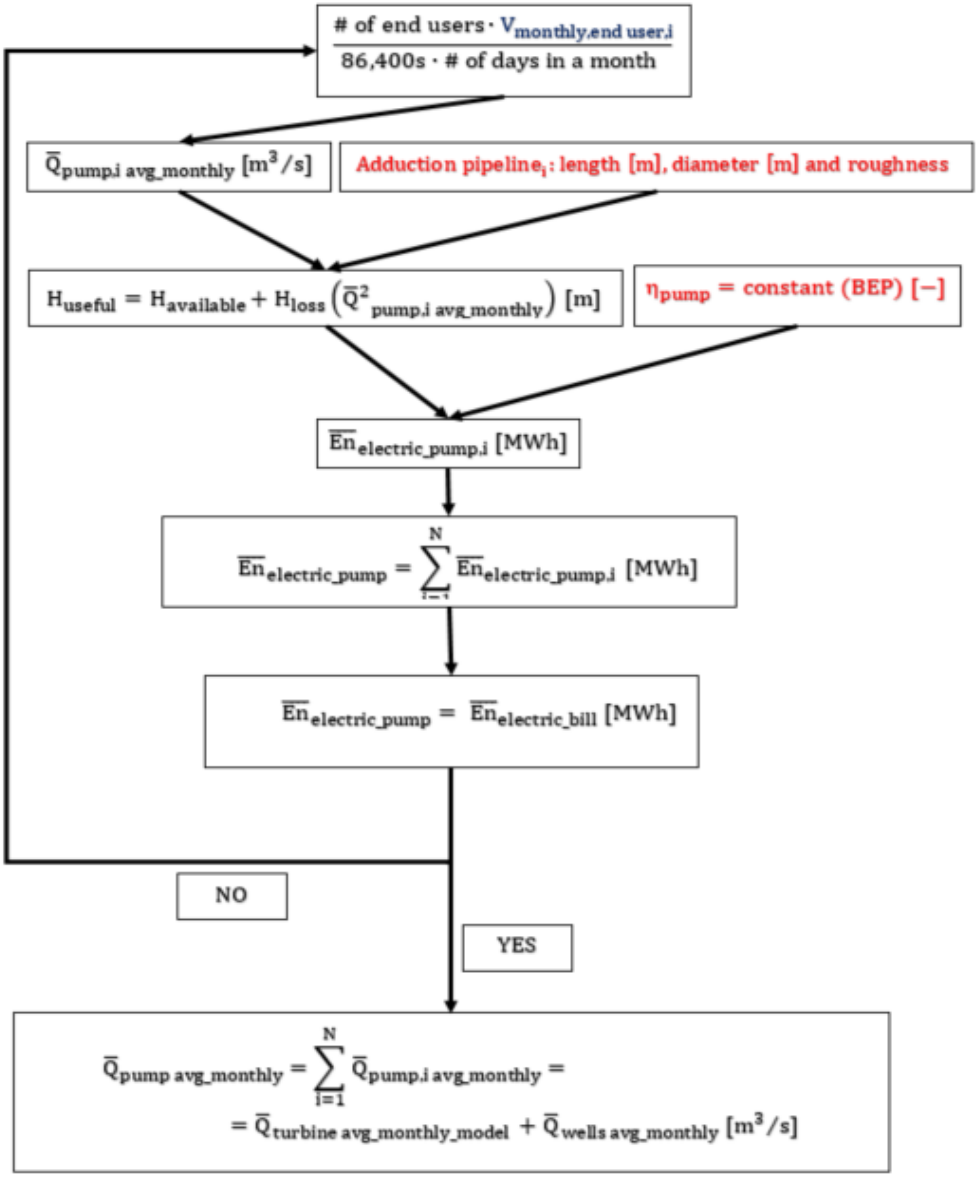


*Figure 3: Flow diagram related to the estimation of the flow rate elaborated by the pumping station*

As reported in Figure 3, the monthly average flow rate elaborated by the pumping station $\overline{\mathrm{Q}}_{\mathrm{pump\ avg\_monthly}}$ $[\mathrm{m}^3/\mathrm{s}]$ is equal to the one elaborated by the hydraulic turbine $\overline{\mathrm{Q}}_{\mathrm{turbine\ avg\_monthly\_model}}$ $[\mathrm{m}^3/\mathrm{s}]$ sum with the monthly average water flow rate coming from the well $\overline{\mathrm{Q}}_{\mathrm{wells\ avg\_monthly}}$ $[\mathrm{m}^3/\mathrm{s}]$, which are measured by flow meters installed in correspondence of the wells themselves. Using this procedure, the water mass balance in the preloading tank is assessed; however, it is worth noting that this methodology is valid only if the variability of the flow rate in gravity adduction pipelines is restricted close to its average value.

Knowing the monthly average flow rate elaborated by the hydraulic turbine $\overline{\mathrm{Q}}_{\mathrm{turbine\ avg\_monthly\_model}}$ $[\mathrm{m}^3/\mathrm{s}]$, the yearly average flow rate $\overline{\mathrm{Q}}_{\mathrm{turbine\ avg\_yearly\_model}}$ $[\mathrm{m}^3/\mathrm{s}]$ is obtained through Eq. (3), where 12 stands for the number of months in a year:

$$\overline{Q}_{turbine\ avg\_yearly\_model} = \frac{\sum_1^{12} \overline{Q}_{turbine\ avg\_monthly\_model}}{12} \quad (3)$$

Then, knowing both dimensions and physical characteristics of the gravity adduction pipeline as well, the head losses in gravity adduction pipelines are obtained according to [29]. The useful head $\mathrm{H}_{\mathrm{useful}}$ $[\mathrm{m}]$ that the hydraulic turbine has to exploit is equal to the difference between the available head $\mathrm{H}_{\mathrm{available}}$ $[\mathrm{m}]$ and the pressure losses $\mathrm{H}_{\mathrm{loss}}$ $[\mathrm{m}]$ that the water encounters along the gravity adduction pipeline using the one-term quadratic formula valid for fully turbulent flow regimes [29], as described by Eq. (4):

$$H_{useful} = H_{gross} - H_{loss}\left(\overline{Q}^2{}_{turbine\ avg\_yearly\_model}\right)\ [m] \quad (4)$$

### 2.2.3. Selection of the hydraulic turbine together with power and energy calculations

The values of both flow rate Q $[m^3/s]$ and head H [m] of the hydraulic turbine, along with its angular rotational speed $\omega\,[rad/s]$ that is dependent on both grid frequency and characteristics of the electric generator, allows to select the proper machine to be installed close to the preloading tank. In particular, the most important dimensionless parameter that characterizes which machine better suits the available operative conditions is the specific speed $\omega_s$ $[-]$, as expressed by Eq. (5).

$$\omega_s = \omega \cdot \frac{Q^{0.5}}{(gH)^{0.75}}\ [-] \tag{5}$$

However, a machine capable to operate in a quite wide range of flow rates has to be selected, preferably with a quite flat efficiency trend. Among traditional turbines, the Pelton one could be the best choice according to what previosluy said: indeed, the efficiency trend is quite flat close to the BEP, thus being suitable for this case study. Nevertheless, attention must be paid at strong part-load conditions, since a consistent efficiency drop occurs. This situation mainly happens in the summer season, when the water availability could be low [30]. The monthly average power that can be produced by the hydraulic turbine $\overline{P}_{\text{turbine avg\_monthly}}$ [MW] is evaluated through Eq. (6), while the potential monthly average energy

recovery $\overline{\mathrm{En}}_{\mathrm{electric\_turbine\ avg\_monthly}}$ [MWh] is evaluated using Eq. (7), where a WSS operation of 24 h times the number days in a month has been considered. The results can be widened to a yearly basis with equations similar to Eq. (3).

$$\bar{P}_{turbine\ avg\_monthly} = \frac{\eta_{turbine} \cdot \rho \cdot g \cdot \bar{Q}_{turbine\ avg\_monthly} \cdot H_{useful}}{10^6} = \frac{\eta_{turbine} \cdot \bar{P}_{hydraulic\ avg\_monthly}}{10^6}\ [MW] \quad (6)$$

$$\overline{En}_{electric\_turbine\ avg\_monthly} = \bar{P}_{turbine\ avg\_monthly} \cdot (24h \cdot days\ in\ a\ month)\ [MWh] \quad (7)$$

## 2.3. Case study

### 2.3.1. Evaluation and assessment of the yearly average flow rate in gravity adduction pipelines

As already stated in Section 2, the monthly average electric energy $\overline{\mathrm{En}}_{\mathrm{electric\_turbine\ avg\_monthly}}$ [MWh] consumed by the pumping station, together with the useful head $\mathrm{H}_{\mathrm{useful}}$ [m] and their efficiencies $\eta_{\mathrm{pump}}$ [−] (see Table 2), allows to estimate the monthly average flow rate elaborated by the pumping station $\overline{\mathrm{Q}}_{\mathrm{pump\ avg\_monthly}}$ [$\mathrm{m}^3/\mathrm{s}$] through Eq. (2). Furthermore, the obtained monthly average flow rate elaborated by the pumping station $\overline{\mathrm{Q}}_{\mathrm{pump\ avg\_monthly}}$ [$\mathrm{m}^3/\mathrm{s}$] has to be shortened by the the water flow rates

coming from the wells $\overline{Q}_{\text{wells avg\_yearly}}$ $[m^3/s]$. Finally, the monthly average flow rate elaborated by the hydraulic turbine $\overline{Q}_{\text{turbine avg\_monthly\_model}}$ $[m^3/s]$ is obtained, which can be also expressed as yearly average flow rate $\overline{Q}_{\text{turbine avg\_yearly\_model}}$ $[m^3/s]$ according to Eq. (3). Table 3 sums up the numerical values of the magnitudes previously mentioned related to the year 2018.

It is worth noting that the overall efficiency of each pump $\eta_{\text{pump}}$ has been set equal to 0.65, according to point 4 of Subsection 2.2 and the available datasheets. Furthermore, the monthly water consumption of each end user $V_{\text{monthly,end user,i}}$ $[m^3]$ provided by each pump is considered the same and equal to 12 $m^3$, taking into account an average water volume consumption of about 0.4 $m^3$/day per each end user [29]. This was possible since the distribution of end users per each pump is homogeneous in terms of both residential and industrial consumers.

*Table 2: Input and known values used in the proposed methodology*

| **# of the PUMP** | **# of end users** | **$V_{\text{monthly,end user,i}}$ [$m^3$]** | **Adduction pipeline length [km]** | **Adduction pipeline diameter [m]** | **$H_{\text{available}}$ [m]** | **$\eta_{\text{pump}}$** |
|---|---|---|---|---|---|---|
| 1 (TANK A to TANK 13) | 7203 | 12 | 2.94 | 0.25 | 203 | 0.65 |
| 2 (TANK A to TANK 22) | 668 | 12 | 2.65 | 0.15 | 163 | 0.65 |

| | | | | | | |
|---|---|---|---|---|---|---|
| 3 (TANK A TO TANK 23) | 379 | 12 | 2.02 | 0.15 | 83 | 0.65 |
| 4 (TANK A TO TANK 24) | 710 | 12 | 2.84 | 0.15 | 63 | 0.65 |

*Table 3: Estimated monthly average flow rates in the analysed gravity adduction pipelines (year 2018)*

| **MONTH (YEAR 2018)** | **PUMP** | **$En_{electric\_pump,i}$ [MWh]** | **$Q_{pump,i\ avg\_monthly\_model}$ [$m^3/s$]** | **$Q_{pump\ avg\_monthly\_model}$ [$m^3/s$]** | **$Q_{well\ avg\_monthly}$ [$m^3/s$]** | **$Q_{turbine\ avg\_monthly\_model}$ [$m^3/s$]** |
|---|---|---|---|---|---|---|
| JANUARY | 1 | 83.55 | 0.03543 | 0.04406 | 0.00793 | 0.03613 |
| | 2 | 6.00 | 0.00328 | | | |
| | 3 | 1.73 | 0.00186 | | | |
| | 4 | 2.51 | 0.00349 | | | |
| FEBRUARY | 1 | 73.86 | 0.03468 | 0.04313 | 0.007763 | 0.03537 |
| | 2 | 5.31 | 0.00321 | | | |
| | 3 | 1.53 | 0.00182 | | | |
| | 4 | 2.22 | 0.00342 | | | |
| MARCH | 1 | 94.37 | 0.04002 | 0.04977 | 0.02241 | 0.02736 |
| | 2 | 6.79 | 0.00371 | | | |
| | 3 | 1.96 | 0.00210 | | | |
| | 4 | 2.83 | 0.00394 | | | |
| APRIL | 1 | 84.27 | 0.03693 | 0.04593 | 0.01791 | 0.02802 |
| | 2 | 6.06 | 0.00342 | | | |
| | 3 | 1.75 | 0.00194 | | | |
| | 4 | 2.53 | 0.00364 | | | |

| | | | | | | |
|---|---|---|---|---|---|---|
| MAY | 1 | 91.42 | 0.03877 | 0.04822 | 0.01917 | 0.02905 |
| | 2 | 6.57 | 0.00359 | | | |
| | 3 | 1.90 | 0.00204 | | | |
| | 4 | 2.75 | 0.00382 | | | |
| JUNE | 1 | 91.32 | 0.04002 | 0.04977 | 0.0214 | 0.02837 |
| | 2 | 6.57 | 0.00371 | | | |
| | 3 | 1.89 | 0.00210 | | | |
| | 4 | 2.74 | 0.00394 | | | |
| JULY | 1 | 99.67 | 0.04227 | 0.05258 | 0.02156 | 0.03102 |
| | 2 | 7.18 | 0.00392 | | | |
| | 3 | 2.07 | 0.00222 | | | |
| | 4 | 3.00 | 0.00417 | | | |
| AUGUST | 1 | 101.63 | 0.04310 | 0.0536 | 0.02091 | 0.03269 |
| | 2 | 7.30 | 0.00399 | | | |
| | 3 | 2.11 | 0.00226 | | | |
| | 4 | 3.05 | 0.00425 | | | |
| SEPTEMBER | 1 | 91.89 | 0.04027 | 0.05009 | 0.02254 | 0.02755 |
| | 2 | 6.61 | 0.00373 | | | |
| | 3 | 1.91 | 0.00212 | | | |
| | 4 | 2.76 | 0.00397 | | | |
| OCTOBER | 1 | 97.32 | 0.04127 | 0.05133 | 0.02258 | 0.02875 |
| | 2 | 6.99 | 0.00382 | | | |
| | 3 | 2.02 | 0.00217 | | | |
| | 4 | 2.93 | 0.00407 | | | |
| NOVEMBER | 1 | 91.32 | 0.04002 | 0.04977 | 0.0229 | 0.02687 |
| | 2 | 6.57 | 0.00371 | | | |

| | | | | | | |
|---|---|---|---|---|---|---|
| | 3 | 1.89 | 0.00210 | | | |
| | 4 | 2.74 | 0.00394 | | | |
| DECEMBER | 1 | 97.50 | 0.04135 | 0.05143 | 0.02211 | 0.02932 |
| | 2 | 7.01 | 0.00383 | | | |
| | 3 | 2.02 | 0.00217 | | | |
| | 4 | 2.93 | 0.00408 | | | |

After the estimation of the monthly average flow rate that can be elaborated by the hydraulic turbine $\overline{\mathrm{Q}}_{\text{turbine avg\_monthly\_model}}\,[\mathrm{m}^3/\mathrm{s}]$, the WSS management decided to install a flow meter in the gravity adduction pipeline that connects the water source to the preloading tank. The flow meter allows to evaluate the exact flow rate values that can be elaborated by the hydraulic turbine and, at the same time, to validate the estimated results obtained with the proposed methodology. Figure 4 shows the hydraulic turbine installation site highlighted in red and connected to the gravity adduction pipeline highlighted in purple. The location of the PRV to be dismissed is also present. Table 4 lists the estimated monthly average flow rate $\overline{\mathrm{Q}}_{\text{turbine avg\_monthly\_model}}\,[\mathrm{m}^3/\mathrm{s}]$ and the measured ones $\overline{\mathrm{Q}}_{\text{turbine avg\_monthly\_meas}}\,[\mathrm{m}^3/\mathrm{s}]$, along with the relative percentage errors expressed by Eq. (8).

$$\Delta\bar{Q}\ (\%) = \frac{\bar{Q}_{turbine\ avg\_monthly\_model} - \bar{Q}_{turbine\ avg\_monthly\_meas}}{\bar{Q}_{turbine\ avg\_monthly\_meas}}\ [-] \qquad (8)$$

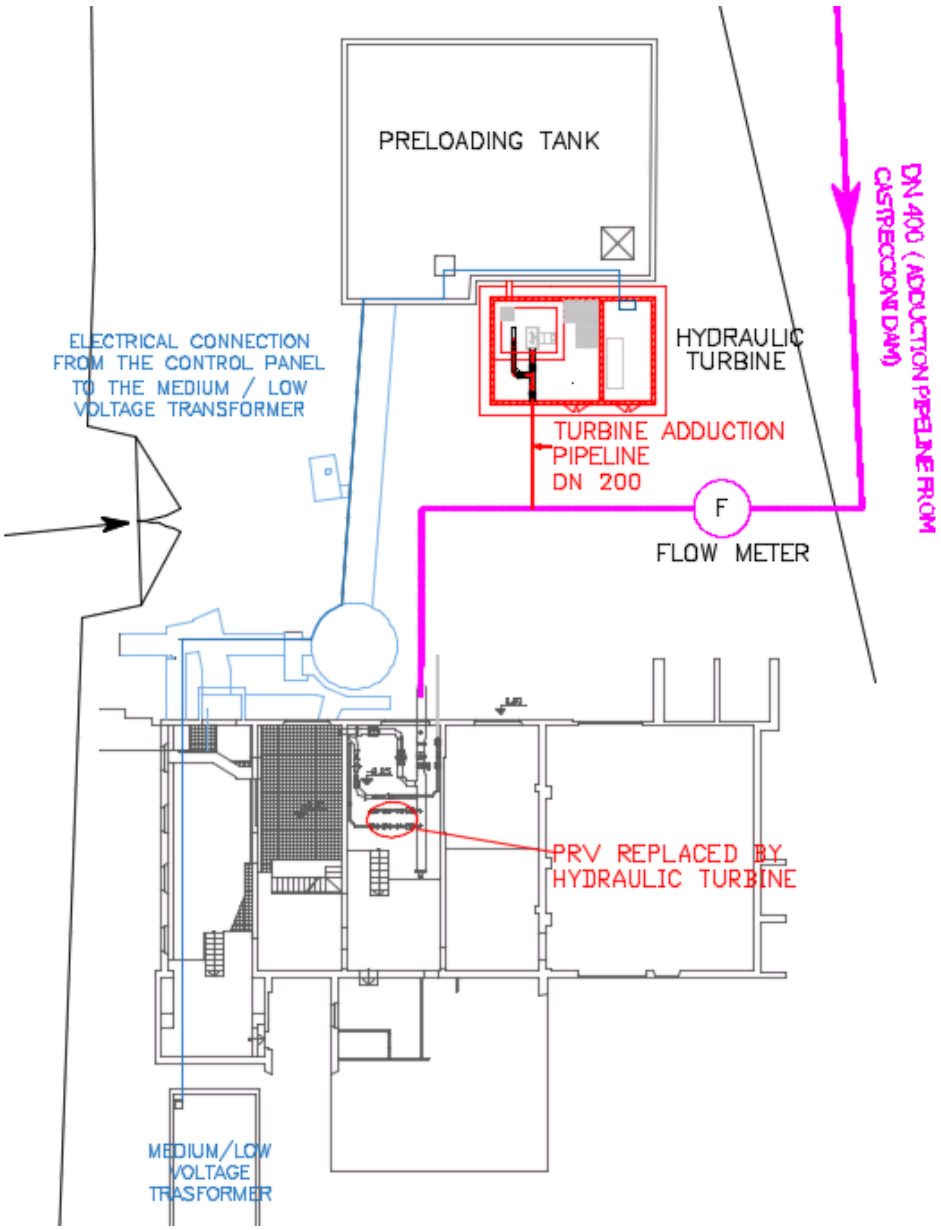


*Figure 4: Detailed view of the hydraulic turbine installation site*

*Table 4: Monthly average flow rates elaborated by the hydraulic turbine (model. vs meas.)*

| **MONTH (YEAR 2018)** | **$Q_{turbine\ avg\_monthly\_meas}$ [$m^3/s$]** | **$Q_{turbine\ avg\_monthly\_model}$ [$m^3/s$]** | **Δ (%)** |
|---|---|---|---|
| JANUARY | 0.03600 | 0.03613 | 0.36 |
| FEBRUARY | 0.02940 | 0.02674 | -9.05 |
| MARCH | 0.02881 | 0.02736 | -5.03 |
| APRIL | 0.02994 | 0.02802 | -6.41 |
| MAY | 0.03074 | 0.02905 | -5.50 |
| JUNE | 0.02983 | 0.02837 | -4.89 |
| JULY | 0.03183 | 0.03102 | -2.54 |
| AUGUST | 0.03497 | 0.03269 | -6.52 |
| SEPTEMBER | 0.02628 | 0.02755 | 4.83 |
| OCTOBER | 0.02955 | 0.02875 | -2.71 |
| NOVEMBER | 0.02935 | 0.02687 | -8.45 |
| DECEMBER | 0.02939 | 0.02932 | -0.24 |
| **2018** | **0.03050** | **0.03000** | **-1.64** |

Table 4 shows that the relative percentage errors related to the monthly average flow rates in the year 2018 are lower than 5% in six out of twelve months, while they are slightly higher (5-7%) in four out of twelve months in the same year. The remaining months present relative percentage errors between 7-10%, which are still acceptable. Nevertheless, it is pointed out that the relative percentage error referred to the yearly average flow rate potentially exploited by the hydraulic turbine

$\overline{Q}_{\text{turbine avg\_yearly\_model}}$ $[m^3/s]$ is sensibly lower than 5%, namely 1.64% in absolute value. It can be stated that the methodology presented in this paper is anyway a good approach for estimating the yearly average flow rate in gravity adduction pipelines when flow meters are not installed.

Knowing the measured yearly average flow rate $\overline{Q}_{\text{turbine avg\_yearly\_meas}}$ $[m^3/s]$, which will be renamed $\overline{Q}_{\text{turbine avg\_yearly}}$ $[m^3/s]$ hereinafter, the pressure losses $H_{loss}$ [m] between the water source and the preloading tank is calculated, being equal to 68.13 m. Therefore, the useful head that can be exploited by the hydraulic turbine $H_{useful}$ [m], considering the respective geodetic heights of the water source (346 m) and the preloading tank (57 m), is equal to 220.87 m. Finally, the operative yearly average measured flow rate $\overline{Q}_{\text{turbine avg\_yearly}}$ $[m^3/s]$ of 0.0305 $m^3/s$ and the useful head exploited by the hydraulic turbine $H_{useful}$ [m] of 220.87 m allow to evaluate the available yearly average hydraulic power $\overline{P}_{\text{hydraulic avg\_yearly}}$ [kW], which is approximately equal to 66 kW.

### 2.3.2. Flow duration curve

In Section 2, the main operating magnitudes to evaluate the performance of the hydraulic turbine to be installed in the gravity adduction pipeline of interest have been assessed. Nevertheless, the yearly average flow rate that can be exploited by the hydraulic turbine $\overline{Q}_{\text{turbine avg\_yearly}}$ $[m^3/s]$ must be

checked through the flow duration curve, which is fundamental to obtain the flow rate value that leads to the highest energy recovery. Immediately downstream the water reservoir, a flow meter is installed. Using data measured by this flow meter between the years 2012 and 2016 (see Table 5), both yearly average water volumes and flow rates coming from the water source are determined.

*Table 5: Yearly average water volumes and flow rates coming from the water reservoir (2012-2016)*

| YEAR | WATER VOLUMES [$km^3$] | YEARLY AVERAGE FLOW RATE [$m^3/s$] |
|---|---|---|
| 2016 | 946.08 | 0.03000 |
| 2015 | 1151.56 | 0.03652 |
| 2014 | 923.39 | 0.02928 |
| 2013 | 898.77 | 0.02850 |
| 2012 | 911.16 | 0.02889 |
| AVERAGE VALUE | 966.19 | 0.03064 |

The maximum and minimum monthly average flow rates in the five years of measurements reported in Table 5 are approximately 0.047 $m^3/s$ and 0.019 $m^3/s$, respectively. However, all the flow rates recorded in the five years of measurements provided the flow duration curve reported in Figure 5.

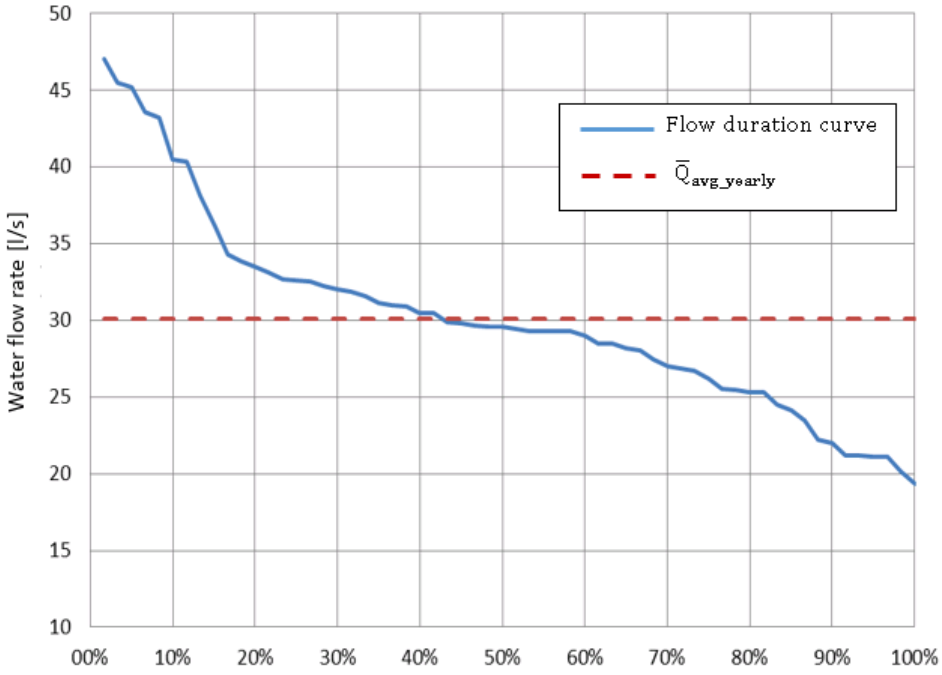


*Figure 5: Flow duration curve of the gravity adduction pipeline of interest*

Figure 5 clearly shows that the monthly average flow rate of about 0.03064 $m^3/s$ occurred more than 40% of the measured time period. That said, if a flow rate range of ±0.005 $m^3/s$ is considered during the operation of the hydraulic turbine, flow rates that occur up to 60% of the measured time period can be elaborated, thus further maximizing the potential energy recovery since the hydraulic turbine will be designed to have the miximum efficiency at almost 0.03064 $m^3/s$.

### 2.3.3. Selection of the hydraulic turbine

After the flow duration curve analysis, which confirmed the correct evaluation of the yearly average flow rate $\overline{Q}_{\text{turbine avg\_yearly}}\ [\text{m}^3/\text{s}]$ of 0.0305 $m^3/s$, this value and the useful head $H_{\text{useful}}\ [\text{m}]$ of 220.87 m, together with the rotational speed of the hydraulic turbine equal to 1000 rpm that is imposed by the electric generator, are used to evaluate the specific speed value, which is equal to 0.057, in order to select the proper hydraulic machine by means of Eq. (5). It is worth noting that this value is within the range of Pelton turbines (0.05-0.35); for this reason, this kind of hydraulic machine with two jets has been chosen for being installed in the WSS site of interest. Pelton turbines have a wide range of operation in terms of flow rates; indeed, the efficiency curve is quite flat and constant down to 30% of the maximum load and between ±40% with respect to the design flow rate [30]. For this reason, quite sensible flow rate variations from the design one do not affect too much the efficiency of this machine. The efficiency of the turbine is always constant during its operation since a Proportional-Integral-Derivative (PID) controller switch its functioning from one nozzle to two according to the operative flow rate by checking the water level of the preloading tank. Table 6 resumes the main characteristics of the Pelton turbine at its BEP, while Figure 6 shows the hydraulic machine installed in the site of interest.

*Table 6: Pelton turbine characteristics at its BEP*

| MAGNITUDE | VALUE |
|---|---|
| Flow rate [$m^3/s$] | 0.0305 |
| Useful Head [m] | 220.87 |
| Rotational speed [rpm] | 1000 |
| Total efficiency [-] | 0.82 |
| Power [kW] | 54.19 |

b)

*Figure 6: Pelton turbine installed close to the preloading of the analysed WSS*

## 2.4. Energy, environmental and economic analyses

The values listed in Table 6 related to the Pelton turbine have been used to carry on the energy analysis deriving by the installation of a small-scale

hydropower plant in WSSs. It is worth noting that the measured flow rate value at BEP has been used in these analyses.

The energy saving $\overline{\mathrm{En}}_{\mathrm{saving\_after\_turbine}}$ [MWh] is evaluated by the difference between the electricity consumption before, $\overline{\mathrm{En}}_{\mathrm{before\_turbine}}$ [MWh], and after, $\overline{\mathrm{En}}_{\mathrm{after\_turbine}}$ [MWh], the installation of the small-scale hydropower plant, as reported by Eq. (8).

$$\overline{En}_{saving\_after\_turbine} = \left(\overline{En}_{before\_turbine} - \overline{En}_{after\_turbine}\right)[MWh] \quad (8)$$

Precisely, 475.25 MWh per year are saved. To better highlight this aspect, Figure 7 shows the energy consumed by the pumping station before and after the energy recovery intervention, where the produced electric power is used for supplying electric energy to the pumping station.

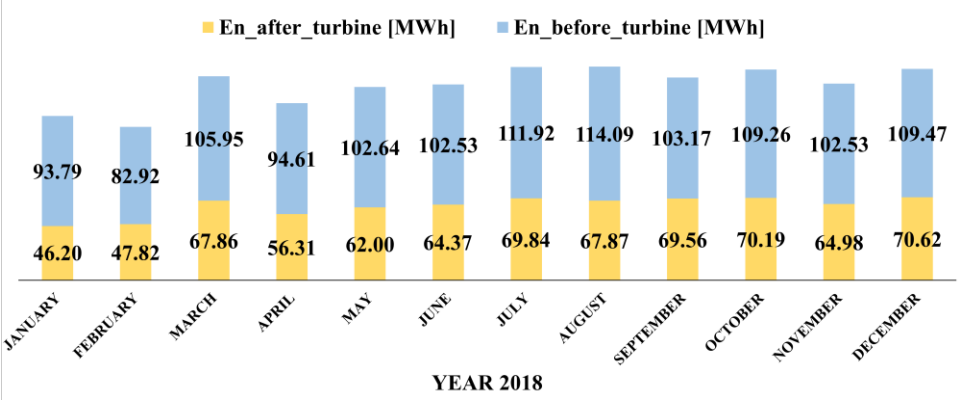


*Figure 7: Electric energy consumed by the pumping station before and after the hydraulic turbine installation*

It is worth noticing that the electricity consumption after the energy recovery intervention includes: i) the electricity withdrawn from the grid to feed the pumping station that is lowered due to the installation of the hydraulic turbine and ii) the electricity consumed by auxiliary devices of both pumps and turbine. Knowing the energy saving $\overline{\mathrm{En}}_{\mathrm{saving\_after\_turbine}}$ [MWh], 88.87 TOE are saved according to Eq. (9):

$$\boldsymbol{TOE_{saving} = \overline{En}_{saving\_after\_turbine} \cdot Fc_{TOE}} \; [TOE] \qquad (9)$$

$\mathrm{Fc}_{\mathrm{TOE}}$ [TOE/kWh] is the conversion factor equal to 0.000187 TOE/kWh [31] for the Italian scenario. This saving can be also expressed by means of $tCO_2$ not released in the atmosphere, as expressed by Eq. (10), that leads to a value of 204.36 $tCO_2$:

$$tCO_{2\_saving} = \overline{En}_{saving\_after\_turbine} \cdot Fc_{tCO2} \; [tCO_2] \qquad (10)$$

$\mathrm{Fc}_{\mathrm{tCO2}}$ [$\mathrm{tCO_2}$/kWh] is the conversion factor equal to 0.43 $\mathrm{tCO_2}$/MWh [32]. Finally, the gross economic saving is then obtained using Eq. (11), being equal to 94.29 k€/year:

$$\boldsymbol{Ec_{saving\_gross} = \overline{En}_{saving\_after\_turbine} \cdot F_{ec}} \; [€/year] \qquad (11)$$

$\mathrm{F_{ec}}$ [€/year] is the gross electricity cost in 2018 for non-residential consumers with an overall consumption of 20-500 MWh [33]. The gross economic saving $\mathrm{Ec}_{\mathrm{saving\_gross}}$ [€/year] has to be reduced by the Operation & Management (O&M) costs that have not been taken into account in this

work. Nevertheless, Italian Authorities introduced incentives for energy efficiency interventions: in this regard, energy efficiency certificates are issued according to the amount of saved TOE. In this case, the possible economic income is calculated through Eq. (12) and it is equal to 22.22 k€/year:

$$\boldsymbol{Ec_{eec} = TOE_{saving} \cdot F_{eec}} \ [€/year] \quad (12)$$

$F_{eec}$ [€/TOE] corresponds to the economic income obtained per each saved TOE, considering a maximum value of 250 €/TOE [34]. Then, $Ec_{eec}$ [€/year] is summed to the net economic saving $Ec_{saving\_gross}$ [€/year], obtaining 116.51 k€/year that is the new economic saving $Ec_{saving\_gross\_final}$ [€/year]. This value is sensibly high and it is expected to keep such interesting results also in the upcoming years since the flow rate elaborated by the Pelton turbine is almost constant throughout the year. Table 7 resumes main energy and economic items reported in this Chapter.

*Table 7: Resume of energy, environmental and economic analyses of the energy efficiency intervention*

| $\overline{En}_{saving_{after_{turbine}}}$ [MWh] | $TOE_{saving}$ | $tCO_{2\_saving}$ | $Ec_{saving_{gross}}$ [k€/year] | $Ec_{cert}$ [k€/year] | $Ec_{saving\_gross\_final}$ [k€/year] |
|---|---|---|---|---|---|
| 475.26 | 88.87 | 204.36 | 94.29 | 22.22 | 116.51 |

## 2.5. Conclusions

In this first work, a methodology to estimate the average flow rate in a gravity adduction pipeline upstream the preloading tank of a WSS located in amid-town in the Center of Italy has been developed. This methodology is based on the electric energy consumption of the pumping station, since the sum of flow rates supplied by each pump is equal to the one flowing in the gravity adduction pipeline reduced by the flow rate coming from wells. It is worth noting that this methodology is valid only if the variability of the flow rate in gravity adduction pipelines is restricted close to its average value. A Pelton turbine has been selected for recovering the water energy content, supplying electricity to the pumping station. The useful head exploited by the hydraulic turbine is evaluated by knowing the flow rates and the dimensions, as well as the physical characteristics, of the gravity adduction pipeline in which it can be installed.

This methodology has been then validated using flow rates values recorded by a flow meter installed in the gravity adduction pipeline after the installation of the Pelton turbine. Considering the yearly average flow rate value, an absolute relative percentage error of 1.64% with respect to measured value has been obtained, which is considered satisfying. Always using the measured data, an energy saving equal to 475.26 MWh (88.87 TOE and 204.36 $tCO_2$) is obtained, which results to a gross economic saving of 94.29 k€/year. The gross economic saving increases up to 116.51 k€/year if energy efficiency

certificates issued by Italian Authorities are considered. In year 2019 it is obtained an energy saving equal to 507.77 MWh.

This study confirmed that energy recovery interventions improve the efficiency of a WSS when a proper methodology for the evaluation of the flow rates in gravity adduction pipelines is performed, which is fundamental for assessing its profitability when flow meters are not present. Furthermore, since the flow rate elaborated by the Pelton turbine is almost constant throughout the year, this gross economic saving can be also obtained in the upcoming years.

# Chapter 3.

# 3. Energy Recovery in gravity adduction pipelines of a Water Supply System (WSS) for urban areas using Pumps-as-Turbines (PaTs)

## 3.1. Introduction

Energy efficiency interventions have become one of the most important and challenging aspects to tackle the carbon-dioxide ($CO_2$) emissions into the atmosphere [35-37]. Among different applications, energy recovery in Water Supply Systems (WSSs) are taking the field due to their continuous operation throughout the day, which grants a high recovery potential [38, 39]. In this regard, several interventions have been already applied so far and results showed a considerable economic advantage [40, 41].

Generally, the water is collected using a dam located at high altitude and it flows towards one or more head compensation tanks by gravity. The main head compensation tank is connected either to other tanks placed downstream

or directly to the Water Distribution Network (WDN), which supplies water to the end users. In the former case, the water pressure is lowered down to a threshold value, which depends on the local regulations, in order to guarantee the water supply to all the end users and decrease the water leakages in the branches of the WDN as well. The excess of the hydraulic energy is dissipated through Pressure Reducing Valves (PRVs) that significantly contribute to the inefficiency of the entire system [42]. In this regard, Kanakoudis et al. [43] performed a study on the water distribution system located in the town of Kozani (Greece); in particular, they dealt with a mechanism capable of finding the best trade-off between several elements involved in the analysis of such system, namely its consumption, the operating pressure, the water cost and price when an increase of full water costing implementation occurs. Patelis et al. [44] developed a hydraulic simulation model to resemble the behaviour of the WDN located in the town of Kos (Greece) in order to study its behaviour when high-water demands peaks and lows during summer and winter time occur, respectively. In particular, the network has been divided in district metered areas and the simulation of PRVs in the entering node of each metered district allowed them to analyse how the water pressure reduction affects the water leakages throughout the analysed branches.

A possible solution for increasing the energy efficiency of these systems can be the replacement of PRVs with hydraulic turbines to recover part of the hydraulic energy potential [45]. Nevertheless, the installation of hydraulic turbines in WSSs has as an important drawback, since the technology should be one-of-the-kind and thus specifically designed; therefore, this technical

solution would be expensive and not affordable on the economic point of view [46].

In such a context, Pump-as-Turbine (PaT) technology is considered a cheaper and effective solution than traditional hydraulic turbines to be installed in WSSs in order to perform both pressure regulation and hydraulic energy recovery [47-49]. The main advantages addressed to PaTs are: i) their large availability in the market, ii) low investment cost and iii) easiness of installation [3]. The cost of a PaT can be 10-20 times cheaper than a traditional hydraulic turbine [50]. Even though the efficiency of a PaT is generally lower than the one achieved by a conventional hydraulic turbine [51], these machines can reach a relatively high efficiency (up to 85%) according to both typology and appropriateness of the installation site [52]. In order to evaluate the overall economic advantages of using PaTs, a comparison of the PayBack Periods (PBPs) with conventional hydraulic turbines has to be done. PaTs are usually applied in a power range between 5 and 500 kW and lead to a PBP of approximately 6 years [53-55]. However, it is worth noting that PBPs vary according to the different costs involved in both civil and electric works, as well as the availability of constant flow rates and economies of scale [3]. On the other hand, the use of conventional hydraulic turbines in micro-hydropower plants leads to higher PBPs (8-10 years) taking into account the same power range previously mentioned [56]. Despite PaTs are mainly installed in sites with low hydraulic energy availability, these machines can be installed also in applications where a significant recovery potential is available. In this regard, a case study related

to the WSS of Murcia (Spain) showed that a maximum power recovery of 100 kW using a PaT system can be achieved [57]. In Germany, eight PaTs installed in parallel led to a total power capacity of 300 kW [58]. The sizing of a small-scale hydropower plant is a very crucial point, since it affects not only the profitability of the investment, but also the maximum exploitation of the hydraulic power and thus the performance of the total power plant [59].

In order to design and select the PaTs properly, both flow rate and head have to be identified together with the mechanical efficiency of the hydraulic machine [60]. A PaT should be designed to operate at its Best Efficiency Point (BEP) with both adequate flow rate and head. The proper choice of a PaT to be installed in a specific application strongly depends on the definition of its performance in turbine mode; the lack of robust and general methodologies to forecast the performance of these machines has slowed down the deployment of this technology so far. Indeed, pumps manufacturers only supply performance data in pump mode and do not provide the ones in reverse mode. Recently, some models relate BEPs of PaTs to those in pump mode [61-63]. Other studies also supply off-design performance curves of these machines [64-66]. Among them, Stefanizzi et al. [67] proposed a methodology to evaluate the BEP of a PaT relating the specific speed in pump mode to that in turbine mode, together with another one that relates the specific speed in turbine mode to the head coefficient in turbine mode. These relations have been developed using BEPs of 27 different PaTs. Venturini et al. [68] proposed a physics-based model for the prediction of PaTs performance curves, BEP included, starting from BEP data in pump mode.

Barbarelli et al. [69] performed both experimental and theoretical activities on 12 different PaTs in order to validate the theoretical results and then provide a reliable tool capable of predicting the performance of a PaT. Furthermore, they also presented a case study to show the applicability of their model. All the previous models rely on a consistent number of both experimental and numerical data that lead to a good forecast capability. As previously mentioned, PaTs are mainly used to operate with fixed flow rate and head at the BEP. When dealing with off-design operating conditions, the efficiency of a PaT significantly drops [70]. Generally, gravity adduction pipelines have constant flow rate and head, while the pipelines of WDNs present a variable flow rate according to the end users' water demand. In the first case, a methodology capable of estimating the proper yearly average flow rate in gravity adduction pipelines of WSSs is fundamental to correctly assess the BEP of a PaT, since flow meters are not always present.

In literature deterministic, probabilistic and demand time-series approaches are proposed for predicting the peak water demand in WSSs. A literature review performed by Wong et al. [26] analysed most of the approaches previously mentioned, highlighting the advantages of the Bayesian one. Balacco et al. [28] analysed the water demand in several towns located in Puglia (Italy) and found out a relation between the peak factor and the number of inhabitants. In particular, results showed that the design of a WSS can be done without considering the use of both monthly and weekly peak factors. Furthermore, the peak factor values obtained through measured data are considerably lower than those reported in literature, especially for small

towns. However, all the previous methods require detailed information that are rarely available.

The novelty of this work regards the development of a methodology capable of forecasting the yearly average flow rate inside a gravity adduction pipeline of a WSS by knowing only few information related to the operation of the WSS itself. Such a tool would be also useful for the management of the WSS in order to evaluate possible energy recovery interventions, especially when flow meters are not installed, as in the case of gravity adduction pipelines. A methodology related to the PaT selection and performance prediction, already discussed in detail in other works [61, 64], has been used to support the analysis of the energy recovery potential.

This chapter is structured as follows: Section 3.2 describes the methodology related to the estimation of the yearly average flow rate in gravity adduction pipelines. Section 3.3 presents the case study of a WSS in a town located in the Center of Italy and the validation of the proposed methodology using a flow meter installed in a gravity adduction pipeline. Section 3.4 deals with both energy and economic analyses related to the gravity adduction pipeline considered in the previous section and presents the evaluation of the possible energy savings deriving by the installation of PaTs in other gravity adduction pipelines in the analysed WSS. Furthermore, the case with the highest possible energy recovery has been also analysed on the economic point of view. Finally, Section 3.5 reports the conclusions of the work.

## 3.2. Methodology

Most of the WSSs present a water source at a high altitude that feeds one or more head compensation tanks downstream. Subsequently, the water flows towards the WDN to be supplied to all the users. The water source can be a reservoir, a pressure-breaking tank or a head compensation tank refilled by a pumping station. Figure 8 shows a general layout of a WSS.

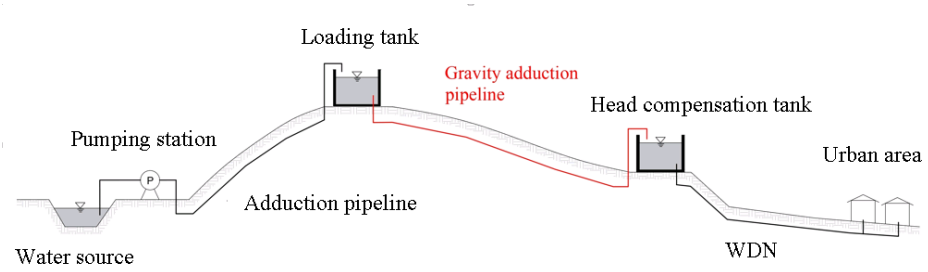


*Figure 8: General layout of a Water Supply System*

Under the WSS management point of view, knowing the instantaneous flow rate in each pipeline is important for monitoring the status of the system and to evaluate both yearly average flow rate and water losses along the pipes. Nevertheless, flow meters are not always installed in all the gravity adduction pipelines, while they are present in the adduction pipelines connected to the pumping stations. The proper evaluation of both yearly average flow rate and net head is also fundamental for selecting the proper hydraulic machine to be used as energy recovery devices.

This Section presents a methodology capable of estimating the yearly average flow rate in the gravity adduction pipelines of a WSS in a town located in the Center of Italy. Furthermore, another methodology to select the most suitable PaT for applying the energy recovery intervention is presented. The forecasts of its BEP [61] and off-design performance [64] have been carried out by applying two methodologies proposed by authors of other works; therefore, the reader is referred to the previous two references for a detailed explanation regarding their development. Finally, the combination of the presented methodologies is intended to provide technicians with a tool to perform both energy and economic analyses of the PaTs installation in specific pipelines of a WSS.

### 3.2.1. Estimation of the yearly average flow rate in gravity adduction pipelines

While several gravity adduction pipelines can feed one or more head compensation tanks, the presented methodology can only be applied to those where a head compensation tank is served by a single pipeline. This condition is the most frequent in the layouts of the WSSs: the main reason is that the connection between the water source and the head compensation tank through a gravity adduction pipeline is, under the same conditions, more reliable than those cases where the head compensation tanks are fed by several branches, since they are more subject to failures with respect to gravity adduction

pipelines [71]. Under this condition, the flow rate in the gravity adduction pipelines can be estimated, also when flow meters are not installed, by:
i) the data mining of the yearly water volume used by each end user $V_{c,i}$ $[m^3]$ through metering devices, directly or indirectly connected to the analysed tank that provides the water, as described by Eq. (13):

$$\overline{Q}_{c,y} = \frac{\sum_{i=1}^{n} V_{c,i}}{8{,}760} \ [m^3/h] \quad (13)$$

ii) the estimation of the water losses along the branches of the WDN connected to the analysed head compensation tank. This process is possible thanks to the knowledge of both water flow rate coming from the pumping stations and water volume sold to the end users. The water losses are calculated through Eq. (14):

$$\overline{Q}_{loss} = \frac{\overline{Q}_{a,d,y} - \overline{Q}_{c,d,y}}{\overline{Q}_{a,d,y}} \ [-] \quad (14)$$

*where* $\overline{Q}_{a,d,y}$ $[m^3/h]$ is the yearly average flow rate supplied to a water district and $\overline{Q}_{c,d,y}$ $[m^3/h]$ is the yearly average flow rate sold to the end users: it is worth noting that both quantities are measured through flow meters.
Nevertheless, the water volume used by the end users has to be compared to the water volume inside the head compensation tank in order to estimate the flow rate coming from the water source properly. It is worth noting that the total capacity of a head compensation tank consists of: i) a compensation volume $\overline{V}_c$ $[m^3]$, which has the aim to regulate the discharge water flow of

the tank according to the end users' water demand, ii) a reserve volume that is used when failures occur and iii) a water volume dedicated to the fire hydrants. The compensation water volume $\overline{\mathrm{V}}_{\mathrm{c}}\,[\mathrm{m}^3]$ is the difference between the total capacity of the tank and the last two volumes, namely the ones related to the reserve and the fire hydrants. $\overline{\mathrm{V}}_{\mathrm{c}}$ can be expressed as a compensation function $\Psi(\mathrm{C_p})$ times the average water volume used by the end consumers $\overline{\mathrm{V}}_{\mathrm{g}}\,[\mathrm{m}^3]$, as reported by Eq. (15):

$$\overline{V}_c = \Psi(\mathrm{C_p}) \cdot \overline{\mathrm{V}}_{\mathrm{g}}\ [\mathrm{m}^3] \qquad (15)$$

$\Psi(\mathrm{C_p})$ depends on the peak coefficient $\mathrm{C_p}\,[-]$, the number of consumers served by the head compensation tank and other seasonal parameters [29]. For sense of clarity, the peak coefficient $\mathrm{C_p}\,[-]$ is estimated through tables and charts available in the design handbooks of WSSs or evaluated by knowing the compensation water volume of the tank. Generally, the value of $\mathrm{C_p}\,[-]$ ranges between 1.00 and 1.82, even though other values can be found in literature as functions of both network size and the number of inhabitants served by the head compensation tank [29]. Finally, Eq. (16) evaluates the yearly average flow rate $\overline{\mathrm{Q}}_{\mathrm{a,t}}\,[\mathrm{m}^3/\mathrm{h}]$ coming from a water source:

$$\overline{Q}_{a,t} = \left[\frac{\overline{Q}_{c,y}}{1-\overline{Q}_{loss}}\right] \cdot C_p = \overline{Q}_{c,y,gross} \cdot C_p\ [m^3/h] \qquad (16)$$

After the estimation of the yearly average flow rate, the calculation of the net head is crucial to assess the proper hydraulic power that can be potentially

recovered. Firstly, the identification of the locations of the head compensation tanks should be carried out: this task is performed through a study of the planimetry of the WSS. After that, the layout of all the gravity adduction pipelines is outlined in order to select the cases where a head compensation tank is filled only by a single gravity adduction pipeline, without any junction. Knowing the location of both water source and head compensation tanks, the gross head is calculated as the difference between the altitudes related to the two previous mentioned elements. However, the pressure losses, mainly the distributed ones [71], have to be evaluated for defining the available net head. Thanks to the study of the planimetry, it is also possible to obtain diameters, lengths, materials and the roughness of each pipeline. The flow rate $\overline{Q}_{a,i}$ $[m^3/h]$ is the sum of all the $\overline{Q}_{a,tj}$ $[m^3/h]$ as described by Eq. (17), where $\overline{Q}_{a,tj}$ $[m^3/h]$ is the flow rate fed to the $j^{th}$ head tank calculated following the same procedure used for the estimation of $\overline{Q}_{a,t}$ $[m^3/h]$ through Eq. (16). In the case of a gravity adduction pipeline without any branch, the flow $\overline{Q}_{a,i}$ $[m^3/h]$ is equal to $\overline{Q}_{a,t}$ $[m^3/h]$:

$$\overline{Q}_{a,i} = \sum_{tj=1}^{n} \overline{Q}_{a,tj} \ [m^3/h] \quad (17)$$

Knowing $\overline{Q}_{a,i}$ $[m^3/h]$ and the physical dimensions of the pipelines, the distributed pressure drop in each pipe is obtained using the Chezy and Gauckler-Stickler formula valid for fully turbulent flow regimes [29]; thus, the net head is calculated as the difference between the gross head and the distributed pressure losses, as described by Eq. (18):

$$H_{net} = H_{gross} - H_{loss} \ [m] \quad (18)$$

where $H_{gross}$ [m] is the gross head available between the altitudes of both starting and ending points related to the gravity adduction pipeline that supplies the tank, while $H_{loss}$ [m] is the pressure drop along the same pipeline. Finally, both $\overline{Q}_{a,t}$ [$m^3/h$] and $H_{net}$ [m] are used for the evaluation of the available average hydraulic power $\overline{P}_h$ [kW], as described by Eq. (19):

$$\bar{P}_h = \frac{\rho_w \cdot g \cdot (\bar{Q}_{a,t}/3600) \cdot H_{net}}{1000} \ [kW] \quad (19)$$

where $\rho_w$ [$kg/m^3$] is the water density at standard conditions (997 kg/$m^3$) and g [$m/s^2$] is the gravity acceleration. Nevertheless, the trend of the flow rate in a WSS is not always constant throughout the year, but it varies according to the daily end users' water demand. Therefore, attention must be paid to the evaluation of the flow rate variation with respect to an average value, since it can strongly affect the choice of the proper hydraulic machine and thus the mechanical power output.

### 3.2.2. Performance prediction models of Pumps-as-Turbines (PaTs)

With regard to the BEP evaluation, in this work the methodology proposed by Renzi et al. [61] was used with the aim of identifying relations between pump and turbine performance of a PaT. This is fundamental to select the proper pump to be used in turbine mode and to

predict the energy recovery potential. The methodology consists on the analysis of a wide range of experimental data related to 59 different PaTs operating in both modes. Most of them refer to radial and mixed-flow machines. In such a context, the yearly average flow rate and net head estimated using the procedure described in Subsection 3.2.1 were used as BEP values of the PaT in turbine mode operation, where the values of both angular rotational speed ω [rad/s] and impeller diameter D [m] were selected using datasheets of pumps. Dimensionless parameters, such as the specific speed and the specific diameter are evaluated with the following correlations, reported in Eq.s (20) and (21):

$$N_S = \frac{(Q/3600)^{0.5}}{(g \cdot H)^{0.75}} \; [-] \tag{20}$$

$$D_S = \frac{(g \cdot H)^{0.25}}{(Q/3600)^{0.5}} \; [-] \tag{21}$$

In order to find a relation between dimensionless parameters in pump and turbine modes, the specific speed and the specific diameter of PaTs operating in both modes were compared. Results showed that two linear relations between the two dimensionless parameters have been found; in particular, the values of the specific speed in pump mode (p) were related to the ones in turbine mode (t), as reported by Eq. (22). The same procedure was done to the specific diameter values, as described by Eq. (23):

$$N_{Sp} = \frac{N_{St}}{0.9051} \; [-] \tag{22}$$

$$D_{Sp} = \frac{D_{St}}{0.9436} \; [-] \tag{23}$$

After the calculation of both $N_{Sp}$ and $D_{Sp}$, the values of $\omega$ $[rad/s]$ and $D$ $[m]$ were calculated through an iterative process in order to evaluate both pump flow rate and head by coupling Eq.s (20) and (21), respectively. Indeed, the flow rate and the head of the PaT operating in pump mode are used to select the hydraulic machine by means of pumps datasheets.

Also the mechanical efficiency $\eta$ $[-]$ of the PaT in turbine mode has to be evaluated in order to have a complete description of the PaTs performance at the BEP in turbine mode: to this aim, Eq. (24) provides a formula that includes both $N_{Sp}$ and the $\eta_p$ as dependent variables:

$$\eta_t = 0.7933 \cdot N_{Sp} + 0.605 \cdot \eta_p - 0.09246 \cdot {N_{Sp}}^2 - 0.8254 \cdot (N_{Sp} \cdot \eta_p) + 0.3936 \cdot {\eta_p}^2 \ [-] \qquad (24)$$

Finally, all design parameters of the PaT operating in both pump and turbine modes at BEP are known.

Unfortunately, the knowledge of the BEP values is not enough to predict the energy recovery of a PaT when flow rate variations are present. As previously said, the trend of the flow rate is not always constant in a WSS, but its change is driven by the end users' water demand throughout the day. The flow rate variation is strictly dependent on the sizes of the WSS and it can be subjected to low or high variabilities. However, the use of a frequency converter to match the available water flow rate with the characteristic curve of the PaT at variable speed is not mandatory because the advantage of following the PaT BEP is not economically justified [72].

Indeed, several works in literature confirm that PaTs maintain a quite flat efficiency trend close to the BEP at both part-load and overload operating conditions (±30% of the BEP flow rate) [64, 68, 69, 70]. Rossi et al. [64] used 32 out of 59 data of [61] related to radial and mixed-flow PaTs operating in both design and off-design conditions in turbine mode to depict the overall characteristic curve of the machine. They developed two different polynomial equations for reconstructing both characteristic and efficiency curves in off-design conditions. The equations depend on the flow coefficient $\phi$ $[-]$ and the head coefficient $\psi$ $[-]$, calculated according to Eq.s (25) and (26), respectively:

$$\phi = \frac{(Q/3600)}{\omega \cdot D^3} \; [-] \tag{25}$$

$$\psi = \frac{g \cdot H}{\omega^2 \cdot D^2} \; [-] \tag{26}$$

It is worth noting that the use of the dimensionless analysis extends the results of the study to other hydraulic machines that operate in fluid dynamic similarity conditions. Furthermore, the normalization process with respect to the magnitude achieved at BEP gets rid of the typology of the used machine, which otherwise has to be considered in the dimensionless analysis. Eq.s (27) and (28) describe the dimensionless characteristic and efficiency curves, both normalized with respect to the magnitudes achieved at BEP:

$$\frac{\psi}{\psi_{BEP}} = 0.2394 \cdot \left(\frac{\phi}{\phi_{BEP}}\right)^2 + 0.769 \cdot \frac{\phi}{\phi_{BEP}} \; [-] \tag{27}$$

$$\frac{\eta}{\eta_{BEP}} = -1.9778 \cdot \left(\frac{\phi}{\phi_{BEP}}\right)^6 + 9.0636 \cdot \left(\frac{\phi}{\phi_{BEP}}\right)^5 - 13.148 \cdot \left(\frac{\phi}{\phi_{BEP}}\right)^4 + 3.8527 \cdot \left(\frac{\phi}{\phi_{BEP}}\right)^3 + 4.5614 \cdot \left(\frac{\phi}{\phi_{BEP}}\right)^2 - 1.3769 \cdot \frac{\phi}{\phi_{BEP}} \; [-] \qquad (28)$$

These curves globally characterize the performance of a possible PaT that can be installed in a gravity adduction pipeline of a WSS. According to operational data of the site of interest, as well as of the PaT, different installation layouts, namely in series or in parallel, can be adopted. This approach has been already evaluated in literature and the installation solution depends on the operative data of the WSS and the characteristics of the adopted energy recovery machines in terms of flow rate, head and, if present, rotational speed control [3]. In this work, different installation solutions are evaluated in order to define the optimal arrangement for the energy recovery purpose related to the analysed WSS. In parallel to the PaT, at least a by-pass valve should always be installed in order to grant the operation of the WSS when the machine is damaged or in maintenance. Furthermore, a PRV has to be always installed downstream the PaT in order to regulate the pressure in case the available head is higher than the one exploited by the machine, for example when a flow rate lower than the rated one is elaborated.

## 3.3. Case study

The methodology presented in Section 2 was applied to a WSS of a town located in the Center of Italy. The layout of the analysed WSS presents several gravity adduction pipelines without any branches that connect a water source to one or more head compensation tanks downstream. The remarkable altitudes of both water source and head compensation tanks make the gravity adduction pipelines suitable for applying energy recovery interventions.

Figure 9 shows the layout of the analysed WSS along with the altitudes where each head compensation tank is placed. These data were obtained by the analysis of both scale-study and contour-lines map of the site of interest. Furthermore, the flow meters installed along the pipelines are shown as well.

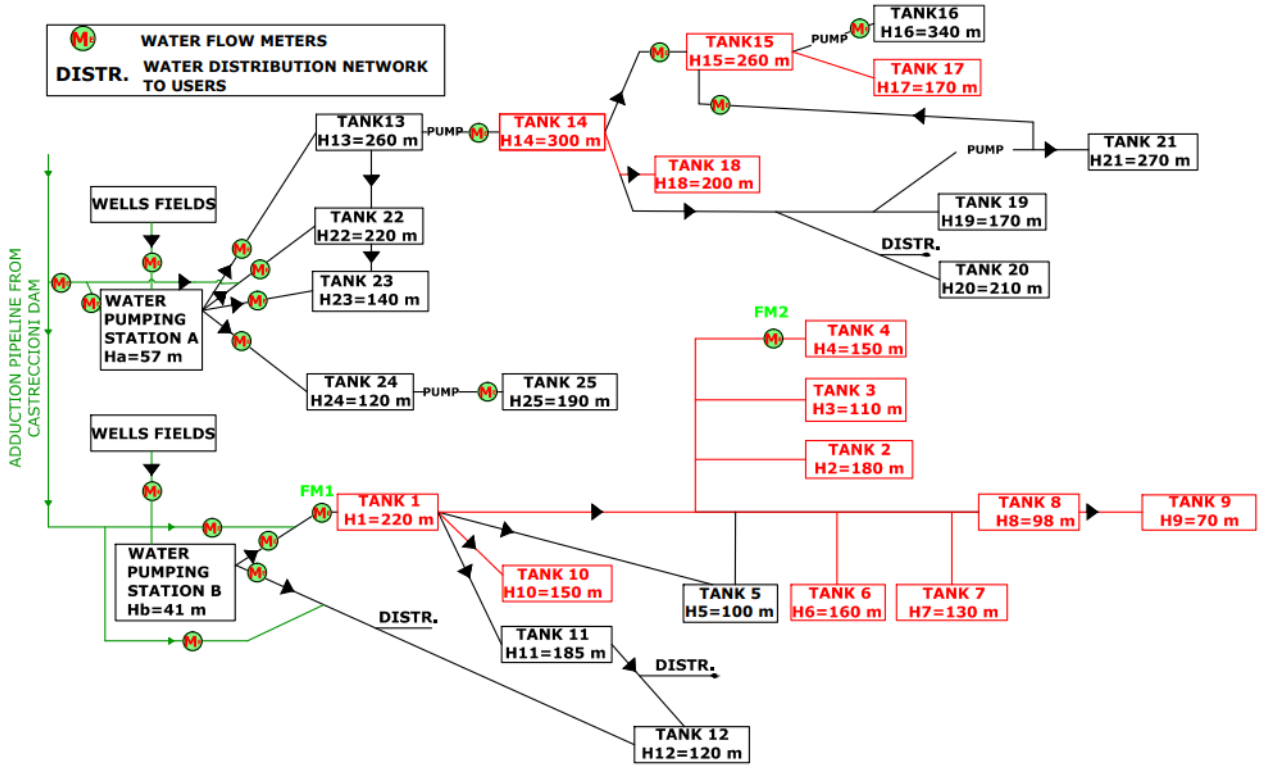


*Figure 9: Layout of the analysed WSS with the gravity adduction pipelines of interest highlighted in red*

Table 8 lists the water sources and the head compensation tanks shown in Figure 9 along with the respective altitudes, gross head and the number of users connected to each head compensation tank.

*Table 8: Characteristics of both water sources and head compensation tanks shown in Figure 9*

| **Water source** | **Altitude [m]** | **Head compensation tank** | **Altitude [m]** | **Gross head [m]** | **# of end users** |
|---|---|---|---|---|---|
| **TANK 1** | **220** | TANK 2 | 180 | 40 | 274 |
| | | TANK 3 | 110 | 110 | 584 |
| | | **TANK 4** | **150** | **70** | **772** |
| | | TANK 6 | 160 | 60 | 337 |
| | | TANK 7 | 130 | 90 | 798 |
| | | TANK 8 | 98 | 122 | 1025 |
| | | TANK 10 | 150 | 70 | 11 |
| TANK 8 | 98 | TANK 9 | 70 | 28 | 410 |
| TANK 14 | 300 | TANK 18 | 200 | 100 | 20 |
| TANK 15 | 260 | TANK 17 | 170 | 90 | 405 |

The gravity adduction pipeline that connects Tank 1 to Tank 4, which is in bold in Table 1, has been selected in order to validate the yearly average flow rate estimated with the methodology presented in Section 2. This choice depends on the presence of a flow meter close to Tank 4 that allows to compare the estimated flow rate $\overline{Q}_{c,y,gross}$ $[m^3/h]$ with the real one, as well as the evaluation of $\overline{Q}_{a,t}$ $[m^3/h]$ with the modal value obtained using the flow rates measured in one year of operation. The first comparison aims at verifying the correct evaluation of the yearly average that flows towards the

distribution network connected to Tank 4. The second comparison assesses the correct evaluation of $C_p$ $[-]$ in order to calculate the flow rate in the gravity adduction pipeline, which is connected to Tank 4, due to the compensation water volume.

### 3.3.1. Estimation of the yearly average flow rate, the net head and the available hydraulic power

The water volume $\overline{Q}_{c,i}$ $[m^3]$ consumed by each end user was extracted from the dataset available for the analysed WSS; thus, the consumed yearly average flow was calculated using Eq. (13), resulting equal to 11.88 $m^3/h$. In order to evaluate the water losses, a water balance of the district supplied by Tank 1 is performed. The water district includes the end users supplied by Tank 4, whose inlet water is measured by the flow meter FM1 (see Figure 9). In this way, the yearly average flow rate $\overline{Q}_{a,d,y}$ $[m^3/h]$ that flows from the pumping station B to Tank 1, as well as from the Castreccioni dam to Tank 1, is equal to 202.52 $m^3/h$, while the one consumed by the end users $\overline{Q}_{c,d,y}$ $[m^3/h]$ is equal to 144.92 $m^3/h$. The water losses are evaluated through Eq. (14), being equal to about 30% of $\overline{Q}_{a,d,y}$ $[m^3/h]$ according to the average value related to the zone of interest. Before estimating the yearly average flow rate $\overline{Q}_{a,t}$ $[m^3/h]$ coming from Tank 1, the peak coefficient $C_p$ $[-]$ has to be evaluated to take into account the compensation water volume $\overline{V}_c$ $[m^3]$ of Tank 4. The reserve water volume $\overline{V}_r$ $[m^3]$ can be considered equal to

one fifth of the maximum daily water volume consumed by the end users $\overline{V}_{g\_max}$ $[m^3]$, thus being equal to 74 $m^3$ [71]. It is worth noting that the water volume related to the firefighting services is already included in $\overline{V}_r$ $[m^3]$. The compensation water volume $\overline{V}_c$ $[m^3]$ of Tank 4 is then obtained by subtracting $\overline{V}_r$ $[m^3]$ from $\overline{V}$ $[m^3]$, providing a value of 209 $m^3$.

The compensation function $\Psi(C_p)$ was evaluated through Eq. (15) and it is equal to 0.73 considering $\overline{V}_c$ $[m^3]$ and $\overline{V}_g$ $[m^3]$ of 209 $m^3$ and 285 $m^3$, respectively. Finally, considering the value of $\Psi(C_p)$ and the number of inhabitants supplied by Tank 4, a peak coefficient $C_p$ $[-]$ of 1.13 was obtained [29]. After this evaluation, the gravity adduction pipeline presents a yearly average flow rate $\overline{Q}_{a,t}$ $[m^3/h]$ of 18.58 $m^3/h$ that was evaluated by means of Eq. (16). It is worth noting that the yearly average flow rate $\overline{Q}_{a,t}$ $[m^3/h]$ considers the monthly compensation capacity of Tank 4 used for managing the variability of the end users' water consumption curve within a month. Table 9 sums up the results obtained according to the procedure presented in Subsection 2.2.

*Table 9: Magnitudes evaluated for the estimation of the yearly average flow rate $\bar{Q}_{a,t}$ $[m^3/h]$*

| **Magnitude [Unit of Measure]** | **Value** |
|---|---|
| $\overline{Q}_{c,y}$ $[m^3/h]$ | 11.88 |

| | |
|---|---|
| $\overline{Q}_{a,d,y}[m^3/h]$ | 200.52 |
| $\overline{Q}_{c,d,y}[m^3/h]$ | 144.92 |
| $\overline{Q}_{loss}$ (%) | 27.70 |
| $\overline{V}$ $[m^3]$ | 283 |
| $\overline{V}_r$ $[m^3]$ | 74 |
| $\overline{V}_c$ $[m^3]$ | 209 |
| $\overline{V}_g$ $[m^3]$ | 285 |
| $\overline{V}_{g\_max}$ $[m^3]$ | 371 |
| $\Psi(C_p)[-]$ | 0.73 |
| $C_p$ $[-]$ | 1.13 |
| $\overline{Q}_{a,t}$ $[m^3/h]$ | 18.58 |

In order to demonstrate the effectiveness of the proposed methodology related to the estimation of the flow rate, the yearly average flow rate value without the presence of the peak coefficient $\overline{Q}_{c,y,gross}$ $[m^3/h]$ was compared to the flow rate $\overline{Q}_{mis}$ $[m^3/h]$ measured by the flow meter FM2 (see Figure 9) close to Tank 4. The two values are 16.44 $m^3/h$ and 16.90 $m^3/h$, respectively. For sense of clarity, Table 10 lists the monthly average flow rates in each month of the year 2019 and Figure 10 shows the curve associated to the values of Table 10 together with $\overline{Q}_{mis}$ $[m^3/h]$.

*Table 10: Monthly average flow rates together with $\bar{Q}_{mis}$ $[m^3/h]$ in the year 2019*

| Month - Year 2019 | Monthly average flow rate [$m^3/h$] |
|---|---|
| January | 14.35 |
| February | 13.84 |
| March | 14.88 |
| April | 15.87 |
| May | 16.54 |
| June | 18.28 |
| July | 20.58 |
| August | 21.30 |
| September | 17.43 |
| October | 16.92 |
| November | 16.59 |
| December | 15.99 |
| **Yearly average** | **16.90** |

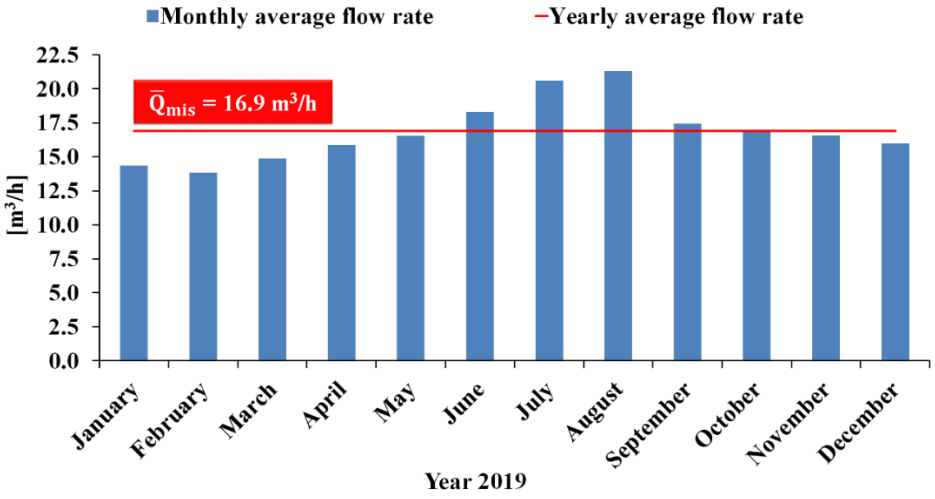

*Figure 10: Measured monthly average flow rate curve coming from Tank 4 in the year 2019*

The accuracy of the methodology was evaluated on the tested case through the relative percentage error related to $\overline{\mathrm{Q}}_{\mathrm{c,y,gross}}$ $[\mathrm{m}^3/\mathrm{h}]$, as reported in Eq. (29):

$$\Delta\overline{Q}_{c,y,gross}\ (\%) = \frac{\overline{Q}_{c,y,gross} - \overline{Q}_{mis}}{\overline{Q}_{mis}}\ (\%) \qquad (29)$$

An error of -2.72% was obtained. Together with the previous analysis, the modal value $\overline{\mathrm{Q}}_{\mathrm{mis,t}}$ $[\mathrm{m}^3/\mathrm{h}]$ related to the flow rates during the year 2019 was evaluated, being equal to $18\ \mathrm{m}^3/\mathrm{h}$. The modal value was calculated considering the number of occurrences of the measured flow rates that flow into Tank 4.

Table 11 and Figure 11 show the flow rate values sorted by the number of occurrences in one year of operation, together with $\overline{\mathrm{Q}}_{\mathrm{mis,t}}$ $[\mathrm{m}^3/\mathrm{h}]$.

*Table 11: Flow rates values sorted by number of occurrences in the year 2019 together with* $\bar{Q}_{mis,t}$ $[m^3/h]$

| **Flow rate** $[\mathbf{m^3/h}]$ | **# of occurrences (%)** |
|---|---|
| 0.9 | 5% |
| 3.6 | 4% |
| 7.2 | 5% |

| | |
|---|---|
| 10.8 | 7% |
| 14.4 | 18% |
| 18.0 | 30% |
| 21.6 | 17% |
| 25.2 | 10% |
| 28.8 | 3% |
| 32.4 | 1% |
| 36.0 | 1% |
| **Modal value: 18.0** | **30%** |

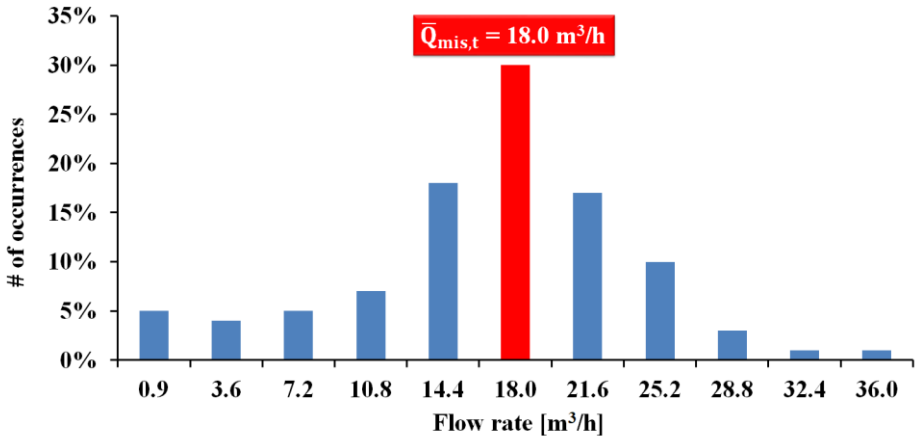


*Figure 11: Number of occurrences of the flow rate values in the year 2019*

Eq. (30) is used to calculate the relative percentage error related to $\bar{Q}_{a,t}$ [m³/h]:

$$\Delta\overline{Q}_{a,t}\ (\%) = \frac{\overline{Q}_{a,t} - \overline{Q}_{mis,t}}{\overline{Q}_{mis,t}}\ (\%) \qquad (30)$$

A value of 3.2% has been obtained; thus, the two comparisons that have been performed so far demonstrate the accuracy and the reliability of the presented methodology, since errors lower than 5% were obtained.

Before evaluating the pressure drop along the gravity adduction pipeline that connects Tank 1 to Tank 4, the flow rate $\overline{\mathrm{Q}}_{\mathrm{a,i}}\ [\mathrm{m}^3/\mathrm{h}]$ flowing inside each branch of the gravity adduction pipeline must be evaluated. The procedure for calculating $\overline{\mathrm{Q}}_{\mathrm{a,ti}}\ [\mathrm{m}^3/\mathrm{h}]$ is the same as the one applied to Tank 4 and described in Section 2 through Eq. (16). Finally, the pressure drop in each branch of the pipeline is evaluated using the Chezy and Gauckler-Stickler formula, which is valid for fully turbulent flow regimes [29]. Figure 12 shows the operational data and the geometric characteristics of the pipeline of interest, which was used to evaluate the pressure drop between Tank 1 and Tank 4.

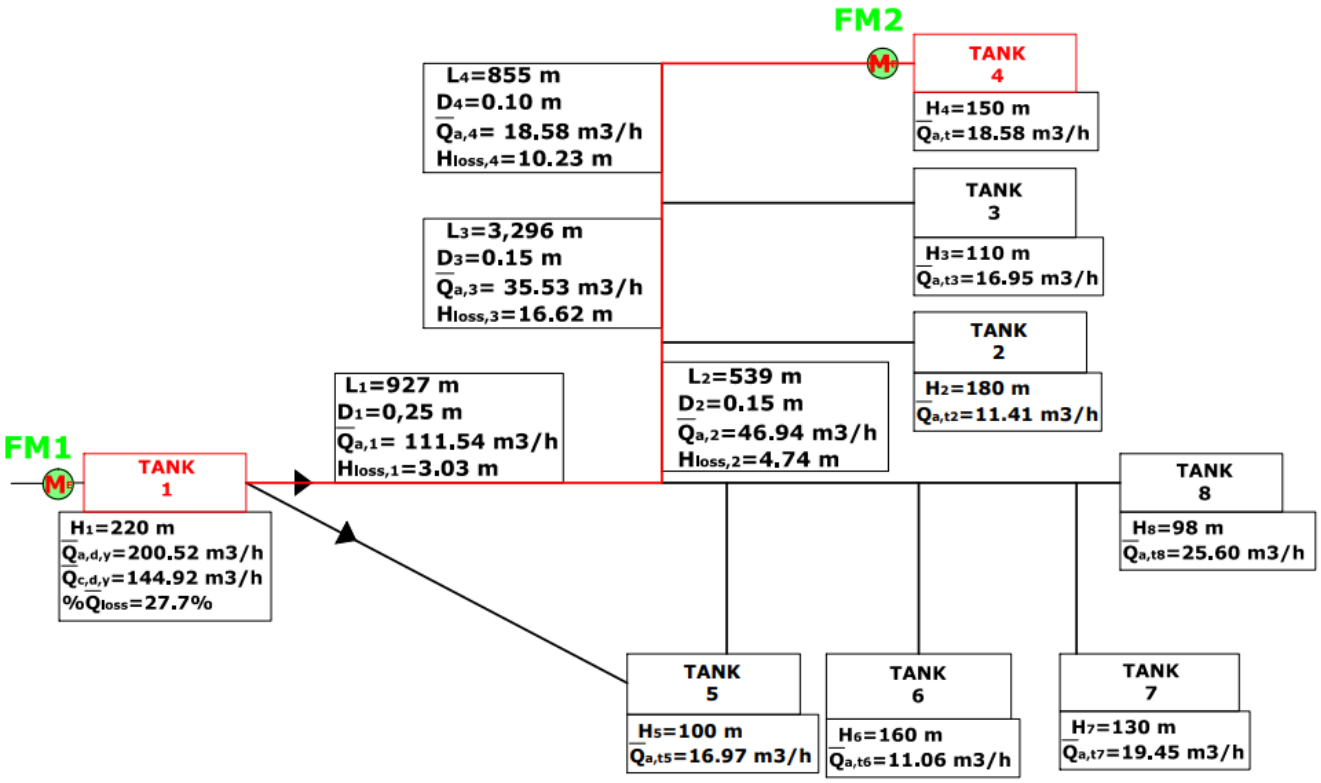


*Figure 12: Analysed pipeline with its operational data and geometric characteristics*

The pressure drop $H_{loss}$ [m] between Tank 1 and Tank 4 is equal to 34.6 m: therefore, the available net head $H_{net}$ [m], considering the respective altitudes of Tank 1 (220 m) and Tank 4 (150 m), is equal to 35.4 m. Knowing the yearly average flow rate $\overline{Q}_{a,t}$ [$m^3$/h] that flows into Tank 4 and the available net head $H_{net}$ [m], a potential yearly average hydraulic power $\overline{P}_h$ [kW] of 1.79 kW is obtained.

### 3.3.2. Selection of the Pumps-as-Turbines (PaTs)

The measured yearly average flow rate $\overline{Q}_{mis,t}$ (18 $m^3/h$) and the available net head $H_{net}$ (35.4 m) have been considered to select the proper PaT to be installed in the pipeline of interest. The previous values correspond to the BEP of the hydraulic machine.

Precisely, two different PaTs were selected. PaT A was chosen as the only hydraulic machine to be installed in the pipeline of interest, while PaT B was selected for a parallel installation layout. It is worth noting that a frequency converter was not considered in this case study; thus, the regulation of the flow rate that can be exploited by the PaT is performed through a regulation valve installed upstream the PaT itself. The regulation valves are installed between the PaT and the head compensation tank in order to lower the water pressure down to the atmospheric one, as shown in Figure 13. Nevertheless, in case of failure or maintenance of the hydraulic machine, the water can flow in a parallel circuit where a by-pass valve is installed. Using the performance prediction models discussed in Section 2, the main characteristics of the selected PaTs are obtained and reported in Table 12 together with the BEP values in both pump and turbine modes. Furthermore, Tables 13 and 14 list both design and off-design operating values of PaTs A and B in turbine mode, respectively.

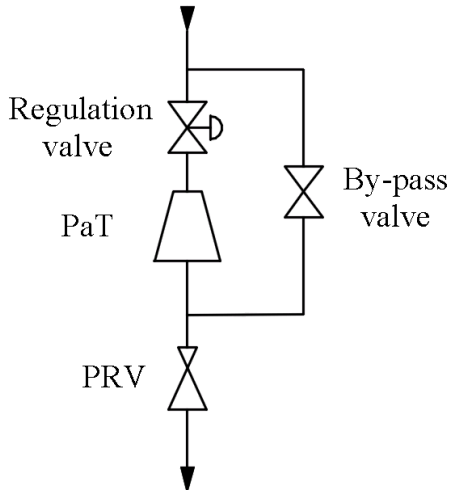


*Figure 13: Scheme related to the installation of a PaT together with the by-pass valve*

*Table 12: Characteristics of the selected PaTs together with the respective BEP values*

| | **PaT A** | | **PaT B** | |
|---|---|---|---|---|
| | Pump mode | Turbine mode | Pump mode | Turbine mode |
| Flow rate [$m^3/h$] | 10.81 | 18.00 | 7.06 | 9.00 |
| Head [m] | 21.6 | 35.4 | 25.8 | 35.4 |

| | | | | |
|---|---|---|---|---|
| Efficiency [-] | 0.66 | 0.64 | 0.45 | 0.44 |
| Power [kW] | 0.96 | 1.10 | 1.10 | 0.38 |
| Rotational speed [rpm] | 2900 | 2900 | 2900 | 2900 |
| Specific speed [-] | 0.30 | 0.27 | 0.21 | 0.19 |
| Impeller diameter [m] | 0.150 | 0.150 | 0.164 | 0.164 |
| Specific diameter [-] | 10.44 | 9.85 | 14.77 | 13.94 |

*Table 13: Performance of the PaT A with the BEP conditions in bold*

| **Flow rate [m³/h]** | **Head [m]** | **Efficiency [-]** | **Power [kW]** |
|---|---|---|---|
| 12.60 | 25.5 | 0.46 | 0.40 |
| 14.40 | 29.9 | 0.54 | 0.63 |
| 16.20 | 34.4 | 0.59 | 0.90 |
| **18.00** | **35.4** | **0.64** | **1.10** |
| 19.80 | 44.1 | 0.61 | 1.46 |
| 21.60 | 49.3 | 0.60 | 1.74 |
| 23.40 | 54.6 | 0.59 | 2.04 |

*Table 14: Performance of the PaT B with the BEP conditions in bold*

| **Flow rate [m³/h]** | **Head [m]** | **Efficiency [-]** | **Power [kW]** |
|---|---|---|---|

| | | | |
|---|---|---|---|
| 6.30 | 25.5 | 0.31 | 0.14 |
| 7.20 | 29.9 | 0.37 | 0.22 |
| 8.10 | 34.4 | 0.40 | 0.31 |
| **9.00** | **35.4** | **0.44** | **0.38** |
| 9.90 | 44.1 | 0.42 | 0.50 |
| 10.80 | 49.3 | 0.41 | 0.59 |
| 11.70 | 54.6 | 0.40 | 0.70 |

After the evaluation of the performance related to the selected PaTs, the estimation of the possible energy recovery deriving by the application of these hydraulic machines was obtained by means of Eq. (31):

$$P_r(\%) = \frac{P_{m\_BEP}}{P_h}\ (\%) \qquad (31)$$

Using one PaT A, the recovered power is equal to 62% of the overall potential one, while it is equal to roughly 44% considering two PaTs B installed with a parallel layout. It is worth noting that, even though the available hydraulic power is low, this case study has been considered due to the presence of a flow meter in the pipeline of interest; thus, reference values are available for validating the results obtained through the presented methodology.

## 3.4. Energy and economic analysis

In this section, energy, environmental and economic analyses related to the energy recovery intervention in the analysed WSS is discussed. The operating values obtained in Section 3 were considered for the further calculations. Firstly, the energy saving due to the use of PaTs is evaluated by Eq. (32):

$$En_{saving} = \eta_{el} \cdot P_{m\_BEP} \cdot t \ [kWh] \quad (32)$$

where $\eta_{el}[-]$ is the electric efficiency of the generator, which was assumed equal to 0.87 according to [73], and t [h] refers to the operational hours of the WSS equal to 7,884 h according to the end users' water demand. Knowing the saved electric energy, which otherwise would have been taken from the national grid, the saved Tonnes of Oil Equivalent (TOE) are calculated by means of Eq. (33):

$$TOE_{saving} = En_{saving} \cdot Fc_{TOE} \ \ [TOE] \quad (33)$$

where $Fc_{TOE}$ [TOE/kWh] is the conversion factor from [kWh] to [TOE], equal to 0.000187 [TOE/kWh] [31]. Knowing the energy saving, the gross economic saving is then obtained through Eq. (34):

$$Ec_{saving\_gross} = En_{saving} \cdot ec \ \ [€/year] \quad (34)$$

where $ec$ [€/kWh] is the lowest price guaranteed by the Italian Authorities that vary according to different produced electrical energy ranges [74]. However, also the yearly maintenance cost has to be calculated in order to obtain the net economic saving $Ec_{saving\_net}$ [€/year] of the overall energy recovery intervention. Besides evaluating the Net Present Value (NPV)

obtained per each year, it is fundamental to calculate also the capital cost (cc) of the intervention. To this aim, the cost of PaTs together with electric generators, civil works, piping, fittings and manpower were considered in the calculation of the cc. It is worth noting that the cost of PaTs, as well as the one related to electric generators, were taken from a price list of an Italian pumps manufacturer, while the remaining ones were provided by the purchasing department of the company that manages the analysed WSS. Table 8 sums up the items previously mentioned along with the respective values related to one PaT A and two PaTs B installed in parallel.

*Table 15: Energy and economic evaluation of the energy recovery interventions*

| **Item** | **1 x PaT A** | **2 x PaTs B** |
|---|---|---|
| Energy saving $(\mathrm{En_{saving}})$ [kWh] | 7,545 | 5,213 |
| Gross Economic saving $(\mathrm{Ec_{saving\_gross}})$ [€/year] | 1,178 | 814 |
| Capital cost (cc) [€] | 11,003 | 7,902 |
| Maintenance [€/year] | 220 | 158 |
| Net Economic saving $(\mathrm{Ec_{saving\_net}})$ [€/year] | 958 | 656 |

The values listed in Table 15 were used to evaluate the NPV, whose formula is expressed by Eq. (35), where a discount rate (dr) of 2% was considered, as

suggested by the purchasing department of the company that manages the analysed WSS:

$$NPV = -cc + \sum_{t=1}^{n} \frac{Ec_{saving\_net}}{(1+dr)^t} \ [€] \quad (35)$$

The PayBack Period (PBP) of both investments, considering two different installation layouts, is equal to almost 14 years. By analysing the obtained NPVs, it is worth noting that the first layout grants a higher NPV equal to 4,658 € after twenty years, while the second one leads to an NPV equal to 2,824 € considering the same time period. Besides the economic and energetic results presented so far, an additional evaluation should be carried to take into account the local regulations of the selected installation site. Italy provides energy efficiency certificates to boost the use of renewables, as well as energy efficiency interventions in industrial plants. The number of these certificates depends on the TOE saved after the application of the energy efficiency intervention with respect to the baseline. In this case, the possible economic revenue that can be obtained through these certificates is evaluated by Eq. (36):

$$Ec_{cert} = EPS \cdot rc \ [€/year] \quad (36)$$

where rc [€/TOE] is the market remuneration obtained per each energy efficiency certificate. Adding $Ec_{cert}$ [€/year] to the net economic saving $Ec_{saving\_net}$ [€/year] listed in Table 15, a new $Ec_{saving\_net}$ [€/year] of 1,325 €/year and 908 €/year can be achieved when considering the installation of one PaT A and two PaTs B in parallel, respectively. These $Ec_{saving\_net}$

[€/year] take into account the incomes from the energy efficiency certificates and lower the previous PBP down to almost 11 years per each solution. Furthermore, NPVs after twenty years from the completion of the energy efficiency interventions are equal to 7,064 € and 4,361 € considering the installation of one PaT A and two PaTs B in parallel, respectively. Figure 14 shows the trend of the cash flows related to the two analysed investments, as well as PBPs obtained with or without the further economic saving coming from the use of the energy efficiency certificates.

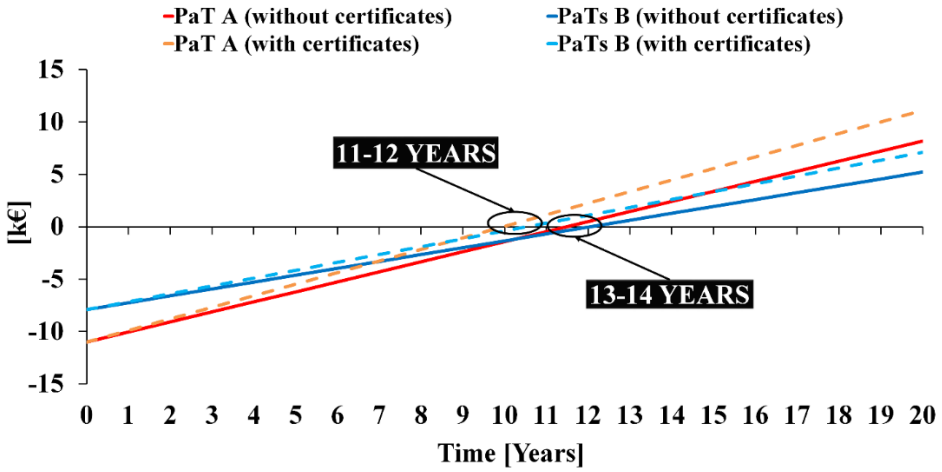


*Figure 14: Trend of the cash flows and the respective PBPs considering a discount rates (dr) of 2%*

Finally, using the presented methodology reported in Section 2, it is interesting to evaluate the possible gross economic savings $Ec_{saving\_gross}$ [€/year] that can be obtained considering some of the tanks listed in Table 8, where flow meters are not installed and thus where no reference values are

available (see Table 16), but where a higher energy recovery potential is available. It is worth noting that the gross economic saving $Ec_{saving\_gros}$ [€/year] is affected by the number and the installation layout of different PaTs, as well as the peak coefficient $C_p$ [−] values that are chosen. Therefore, Table 16 has the aim to present only the best results that can be achieved using the pumps available from the catalogue of the same Italian manufacturer presented in this Section.

*Table 16: Gross economic savings $Ec_{saving\_gros}$ [€/year] achievable in some of the tanks presented in Table 1*

| **Water source** | **Head compensation tank** | **Estimated flow rate [m³/h]** | **Net head [m]** | **Mechanical power [kW]** | **Energy saving $En_{saving}$ [kWh]** | **Gross economic saving $EC_{saving\_gross}$ [€/year]** |
|---|---|---|---|---|---|---|
| **TANK 1** | TANK 2 | 11.41 | 32.23 | 0.57 | 4,493 | 701 |
| | TANK 3 | 16.95 | 85.17 | 2.35 | 18,494 | 2,887 |
| | TANK 6 | 11.06 | 46.61 | 0.46 | 3,610 | 564 |
| | TANK 7 | 19.45 | 73.40 | 1.74 | 13,745 | 2,146 |
| | **TANK 8** | **25.60** | **102.12** | **3.39** | **26,701** | **4,168** |
| TANK 8 | TANK 9 | 9.51 | 27.38 | 0.22 | 1,765 | 276 |
| TANK 15 | TANK 17 | 19.04 | 58.13 | 1.83 | 14,404 | 2,949 |

As anticipated, the analysed case of the gravity adduction pipeline that connects Tank 1 to Tank 4 presents a low potential energy recovery due to the low values of both flow rates and head: this is the main reason of

longer PBPs that make the choice of PaTs not profitable on the economic point of view. The case that presents the highest potential energy recovery in the analysed WSS is the one related to the gravity adduction pipeline that connects Tank 1 to Tank 8 (see text bold in Table 16); for this reason, the results for this test case are evaluated as well. Table 17 sums up the performance of the selected PaT C in both pump and turbine modes, while Table 18 lists the economic outcomes related to three PaTs C installed in series.

*Table 17: Performance of the PaT C at BEP in both pump and turbine modes*

| | **PaT C** | |
|---|---|---|
| | Pump mode | Turbine mode |
| Flow rate [$m^3/h$] | 19.47 | 25.60 |
| Head [m] | 24.7 | 33.9 |
| Efficiency [-] | 0.53 | 0.55 |
| Power [kW] | 2.47 | 1.29 |
| Rotational speed [rpm] | 2900 | 2900 |
| Specific speed [-] | 0.36 | 0.33 |
| Impeller diameter [m] | 0.204 | 0.204 |
| Specific diameter [-] | 10.95 | 10.33 |

*Table 18: Energy and economic evaluation related to the installation of three PaTs C in series*

| **Item** | **3 x PaTs C** |
|---|---|
| Energy saving $(\mathrm{En_{saving}})$ [kWh] | 26,701 |
| Gross Economic saving $(\mathrm{Ec_{saving\_gross}})$ [€/year] | 4,168 |
| Capital cost (cc) [€] | 16,541 |
| Maintenance [€/year] | 551 |
| Net Economic saving $(\mathrm{Ec_{saving\_net}})$ [€/year] | 3,617 |

Considering the energy efficiency certificates released by the Italian Authorities, a new $\mathrm{Ec_{saving\_net}}$ [€/year] of 4,915 €/year can be obtained. In this case, the NPV after twenty years from the completion of the energy efficiency intervention is equal to 52,843 € and the PBP of the investment is approximately 6 years, being aligned to the values reported in the literature [53-55]. Figure 15 shows the trend of the cash flow and the obtained PBP by analysing the case with the highest potential energy recovery of the analysed WSS, with and without the use of energy efficiency certificates.

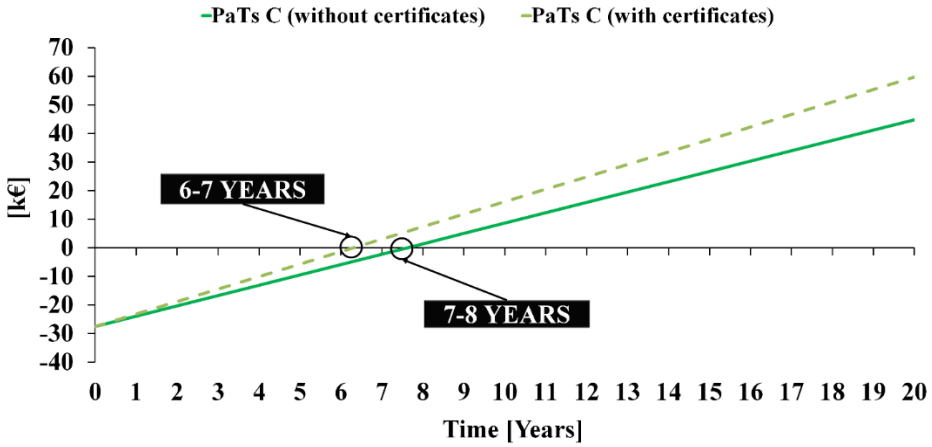


*Figure 15: Trend of the cash flows and the respective PBPs related to three PaTs C installed in series*

Through the installation of the PaTs in all the gravity adduction pipelines of the analysed WSS, an overall energy recovery of 90,757 kWh and a gross economic saving of 14,167 €/year can be reached. The former value can increase up to 18,580 €/year considering the revenues coming from the energy efficiency certificates released by the Italian Authorities. Furthermore, it is worth noting that both potential energy savings and economic incomes can be further boosted by extending these analyses to all the other gravity adduction pipelines of the studied WSS, which have been excluded due to the constraint of the proposed methodology highlighted in Section 2 related to the presence of branches. The methodology can be improved and extended by collecting more measured data from different WSSs in order to create a freely accessible database.

## 3.5. Conclusions

In this second study a methodology capable of estimating the yearly average flow rate in gravity adduction pipelines of a Water Supply System (WSS) is performed. This procedure is useful to monitor the WSS network and to consider possible energy efficiency interventions, since flow meters are not always present due to their high cost.

Generally, the estimation of the peak flow rate is generally performed by using different deterministic, probabilistic and demand time-series approaches based on the peak water demand of the end-users that require a detailed knowledge of the operative and design parameters of the WSS, which are not always available. To the authors' knowledge, the estimation of the yearly average flow rate in gravity adduction pipelines has not been analysed so far. Furthermore, the proper monitoring of the pipelines in WSSs helps their management to identify possible failures and to evaluate the application of energy efficiency interventions.

The proposed methodology consists on a straightforward procedure based on the water consumption of the end users connected to a WSS. Indeed, these data can be used to assess the energy recovery potential: specifically, in this work, the application of Pumps-as-Turbines (PaTs) was considered. The performance evaluation of these machines was carried out through a methodology, already available in literature, that consists on forecasting both

Best Efficiency Point (BEP) and off-design performance of the hydraulic machines in turbine mode.

The yearly average flow rate flowing in a selected gravity adduction pipeline was estimated and compared to the modal value obtained through the measured flow rates in one year of operation, showing a relative error of 3.2%. In addition, the available net head was evaluated to assess the yearly average available hydraulic power $\overline{P}_h$ [kW], equal to of 1.79 kW.

Two different hydraulic machines (PaTs A and B) were selected according to two different layouts, namely one PaT A and two PaTs B in parallel. The energy savings $En_{saving}$ [kWh] obtained through PaTs A and B were equal to 7,545 kWh and 5,213 kWh, respectively, considering 7,884 h of operation of the WSS per year. Subsequently, the net economic savings $Ec_{saving\_net}$ [€/year] of 958 €/year and 656 €/year were achieved considering the two installation layouts. Even higher economic savings are achieved when considering energy efficiency certificates. Finally, the same PayBack Period (PBP) of almost 14 years was obtained considering the installation of PaTs A and B, respectively. However, comparing the Net Present Values (NPVs) after twenty years from the completion of the energy efficiency interventions, it is evident that the case with one PaT A is preferable on the economic point of view, since it leads to 4,658 € instead of 2,824 € obtained with the installation of two PaTs B in parallel. Taking into account the energy efficiency certificates, a PBP of almost 11 years can be achieved with NPVs of 7,064 € and 4,361 € for PaTs A and B, respectively. However, more interesting results can be obtained when analysing other

WSSs with different operating conditions; thus, the most profitable installation layout of PaTs has to be discussed in detail according to the operational values of each site.

Considering the installation of PaTs in some of the gravity adduction pipelines of the analysed WSS, the possible total energy recovery is equal to 90,757 kWh and the total gross economic saving is 14,167 €/year, with further advantages if energy efficiency certificates are also taken into account. In particular, the installation with the highest potential energy recovery can lead to an NPV after twenty years equal to 52,843 € and a PBP of approximately 6 years. These values are consistent to the outcomes reported in literature that assess the economic profitability of PaTs as energy recovery devices in WSSs.

# Chapter 4.

# 4. WSS efficiency improvement through water losses reductions

## 4.1 Water losses in WSSs

Nowadays, the water loss in WSSs is one of the main issues that their management has to face with. Few years ago, techniques related to loss containments were implemented exclusively for critical conditions, repairing visible or particularly large losses.

Since average water losses are greater than one third of the total drinking water, this problem is still growing and has to be remedied [75]. Indeed, the continuous expansion of water consumption, as well as the increase of standards related to the water quality, lead to environmental contaminations, over-exploitation of the aquifers and an increase of the standard qualities required by end users [75].

Therefore, water losses can have a strong impact on the society through various aspects, which can be summarized and classified as follows [75]:

- economic and financial aspects: a high level of water losses leads to a deficit between the costs water collection and supply, as well as revenues due to the considerable cost to supply water to end users. The previous aspects increase water costs, as well as decrease the availability of founding to make new investments. Indeed, according to the "Galli" 36/94 Law, both capital and supply costs are used to determine tariffs of the water service [76],

- ethical-social aspect: huge water losses in WSSs lead to water deficits in Water distribution Networks (WDNs) and, as already mentioned, an increase of the service costs; in general, a high level of water losses causes a decrease of the service / tariff ratio for end users. This aspect goes against the principle of solidarity and it is necessary to deal with the management of the water service, as also sanctioned in Law "Galli" 36/94 [76]:
- environmental aspect: water losses inevitably increase the exploitation of supply sources, as the level of the demand cannot be reduced. Sometimes it happens that, considering the same number of end users, it is necessary to identify new supply sources or, alternatively, the prolonged over-exploitation of those available. This situation is clearly in contrast with the principle of sustainability related to the use of sources, enshrined Law "Galli" 36/94 [76].
A great step forward in the development of best-practice methods related to both analysis and prediction of water losses was made between 1999 and 2000 thanks to the publication of a manual by the Task Force of the International Water Association (IWA) related to "Water Losses" and "Performance Indicators". The practical approach for the control of losses in distribution systems is based on the fundamental importance of pressure control and on the need of distinguishing different components related to those losses. Many countries tried to improve their performance on managing water losses. New performance indicators, which have been proposed by IWA, allowed more rational comparisons between systems operators with different characteristics in terms of loss controls.

The main indications provided by the IWA experiences have been incorporated in Italy also through the D.P.C.M. 04/03/1996 [77] and, in particular, the ministerial decree 99/97 [78].

## 4.2. District metering areas (DMAs) in Water Distribution Networks (WDNs)

### 4.2.1. Main features

The growing interest on the issue related to the rational and sustainable use of water sources, as well as the quality of water, has led to new elements in the definition of the distribution system. One of the solutions is the “districting” of the water network, also defined as “district metering”. In Article 2.2 of Annex 2, Ministerial Decree LL.PP. 99/97 containing "Regulation on the criteria and method on the basis of which to evaluate the losses of aqueducts and sewers" it is specified as follows:

"Concerning the control of leaks in a WSS, it is useful to divide the water network into districts, which may include entire elements related to both production and distribution portions whose dimensions are decided according to configuration and size of the network. Each district is defined by the characteristic of having continuous tools that measure the input water flow rate. Districts are characterized by the possibility of being intercepted and isolated from the general system” [78].

Therefore, districting stands for the creation of distribution areas that are disconnected one to each other, fed through few entry points by a supply

network. These access points allow to measure flow rates remotely and limit the distribution pressure to fixed values by acting on the remote regulation of the set-point.

It should be borne in mind that this strategy is useful not only for identifying parts of the network in which the losses are greater, but also for obtaining information on the functioning of the network itself, thus allowing to acquire important information for WSSs management. Hence, the interest on distribution network districts can lead to an increase of possible solutions to control water systems and be sure that its reliability is confirmed, minimizing the water sources [79].

Water network districts were introduced and theorized in the early 90s (Cheong, 1993) as an alternative approach to traditional measures, which spread especially in the post-war period and aimed at favoring large-mesh distribution systems [80]. It is known that completely meshed distribution schemes have been often adopted so far; however, they offer some advantages such as greater flexibility of operation, containment of pressure drops, greater safety distribution in case of maintenance in a branch of the network, greater ease of expansion of the distribution system and greater standardization of the plant [79]. On the other hand, these systems have also some disadvantages such as poor network governance in terms of remote control, difficulty on monitoring losses, inability to identify the origin of critical events on the network [79]. Therefore, new schemes and new water system management philosophies have been developed. One of the most significant examples is represented by the division of the network in DMAs, consisting of the

division of the distribution system in water districts [79]. This is the so-called "district metering", aimed to obtain a more effective control of the inlet and outlet pressures together with flow rates in order to regulate the piezometric load in the network and reduce water losses. This kind of intervention requires the installation of remote control equipment and, obviously, the revision of the network architecture: however, it is not enough to simply superimpose the remote control on a pre-existing system. Districting optimizes the hydraulic operation of a water system with beneficial effects on both losses and frequency breakages.

### 4.2.2. Water losses seeking procedure with DMAs

As part of the identification and design of districts, it is important to foresee methods for finding losses. Seeking operations are normally divided in two phases: a pre-localization, which makes possible to restrict the field of researches from the totality of the district networks to one or more portions of the network, and a localization, which allows to identify the exact location of the water losses.

As regards the first phase, the Minimum Night Flow (MNF) is identified and then compared to the night consumption of the household and non-household users $NC = (HNU + NHNU)$ obtained on the basis of the average hourly consumption per end user of the various districts in literature. However, the best approach provides that the night users consumption $NC$ is not estimated, but measured by end user smart flow meter to have a dynamic and real value

of night consumption. Through the Eq. (37) the water losses can be estimated [81] and then it is possible to determine the future actions.

$$\bar{Q}_{loss,d} = MNF - (HNU + NHNU) \quad (37)$$

In the case of a value of $\bar{Q}_{loss,d}$ higher than the value related to the unavoidable and physiological losses of the network, or its progressive increase over time, the second phase is carried out, namely the location of the losses; otherwise, another district is examined. The advantage of having a district network is to operate only on areas where losses are foreseeable. The seeking then continues with the step-by-step analysis technique (step test), which consists of progressively close all the gate valves at decreasing distances from the flow meter (operation carried out at night). In this way, the research area is limited by isolating smaller and smaller portions of the network in order to appreciate the consequent variations in flow rate measured at the entrance of the sector. It becomes possible to delimit the pipeline sections that present the most significant losses and then proceed to the localization with traditional techniques. Following the repairs of the identified leaks, it is possible to quantify the water recovery by comparing the $\bar{Q}_{loss,d}$ before and after the repair. Subsequently, the control of losses in the districts will simply consists of measuring, from time to time, the $\bar{Q}_{loss,d}$ and comparing it with the reference updated after repairs: the result of the comparison will provide the priorities for intervention districts, activating the subsequent field research. Naturally, it is suggested to have data loggers that allow to download measured data remotely, with considerable time savings and more effective monitoring control. It is also important to select a software that includes [79]:

- archiving data in a database to easily keep the "history" of the district;
- reporting of particular events (exceeding the high / low threshold);
- the possibility to download data at any time.

Within each district, if necessary, the piezometric head can also be checked, which, as already reported several times, implicitly leads to a reduction of losses, regardless of the actual leak seeking procedure. In fact, even modest reductions of excessively high levels pressure lead to a reduction of leakage volumes and the number of failures in the network [79]. Obviously, it must be ensured that minimum pressure values are enough to supply end users with the required water in all the operating conditions. Compliance with an ideal or strictly sufficient piezometric head to meet all the operational needs can be pursued by means of regulating valves with variable opening.

## 4.3. Water losses in the WSS of Osimo

### 4.3.1. Strategies implemented to seek and reduce water leakages until 2015

In the three-year period 2013-2015, a study was started to seek and reduce water losses in the WSS of the municipality of Osimo. The methodology used is divided into the following phases:

- Phase 1: the water network of Osimo was divided into water districts based on the presence of flow meters and / or volumetric flow meters, some connected to the remote control and remote-readable, others read periodically during the maintenance. The presence of few meters installed in the main

pipes coming from the main tanks prevented the subdivision of the network into restricted districts. Furthermore, the availability of remote data of some flow meters allowed to monitor the water volumes when the operator read measured data. Regarding the water balance between the entering volumes and those consumed by the end users of each district, it was possible to list end users according to the tank to which they are connected and the consumed volumes consumed. These informations are obtained by annual or semi-annual measures of the end user counters, manually collected. Considering the critical issues on the flow meters installed at the entrance of each district and the availability of only annual data of the water volumes consumed by the end users, the water balance is carried out annually. Using the values measured by the flow meters placed in the pipes serving the districts, assessments were made on the minimum night flow (MNF) compared with the estimated average daily consumption. This assessment is approximated due to the large size of the districts and the absence of the measured consumption value on the day in which MNF was assessed.

- Phase 2: To make the assessments limited to more restricted areas, temporary districts were used by the temporary installation of clamp-on ultrasonic flow meters with transducers mounted outside the pipe. This procedure allowed to assess the extent of the water losses made in phase 1, during the period in which the meters were installed, for districts where data of water flow rates were not available.

- Phase 3: Once the water losses in phase 1 and 2 were identified and quantified, the active leak seeking activity was started, carried out by mechanical rod, portable ultrasonic flow meter. The information obtained in the first two phases were limited and purely indicative, leading the punctual research for water losses with low effectiveness. Indeed, the installation of the noise loggers and the punctual research was based more on reports of evident leaks than on the identification and localization of hidden leaks through data analysis.

#### 4.3.2. Results and limitations

This method of seeking water leaks allowed to intervene on evident failures in pipelines, while other leaks remained hidden until their manifestation. The repairs were piloted by the instruments that lead to the identification of only a small part of the losses, reducing water losses only temporarily without the possibility to manage the effects of the interventions in the medium and long term. Indeed, despite the efforts, the average losses in the WSS of Osimo were constant over time (about 30% with respect to the supplied flow rate).

## 4.4. New approach: Smart water grid and remote monitoring of district metering areas of a Demosite in Osimo

#### 4.4.1. Innovative contribution and benefits

To overcome the limitations that arose with the methods used in the previous years, a different approach to the problem of finding water leaks is studied. It

is necessary to divide the water network into DMAs to have a smart grid, adopting technologies aimed at actively monitoring and real-time managing the network. This innovative approach overcomes the limited mentality of seeking and quantifying water losses by manually and annually executing water balances of districts of considerable size. This way of operation is time consuming for identifying leaks, repair small breakages that cause hidden leaks and monitor the effects of the maintenance on the identified break. Indeed, the annual manual balance of an extended district and the flow data measured by ultrasonic meters temporarily installed in some pipelines allowed to have a brief idea of the situation of the leaks, but they cannot represent a tool for monitoring, quantifying and locating the leaks themselves. The acquisition of these data allowed to understand the most critical areas in which installing noise loggers for the detection of reported burst losses, thus losing the concept of background loss control, the identification of losses from unreported breakages and, more generally, the daily monitoring of the water balance, of the MNF, of the night consumption related to the end users of districts of reduced size. The new methodology, on the other hand, can control all the previous elements, thus allowing the sub-districts to be monitored with an hourly time step and to accurately quantify the extent of the losses and reduce the time to locate the losses. The use of smart flow meters located at the entrance of small districts and upstream each end user's private network, the installation of a fixed infrastructure for remote reading and the preparation of a software for managing and analysing the remote

collected data allow to reduce water losses through hourly monitoring of the network, leading to the following benefits and opportunities:

- Possibility to repair the pipeline when losses are still hidden to prevent the onset of significant losses that would lead to a huge energy waste. The use of the monitoring system will lead to the reduction of damage and inconvenience caused to third parties due to water losses and the number of interventions by water service operators.
- Reduction of costs for electricity used for the transportation of water and for the supply of water from external sources.
- Reducing water losses in addition to the environmental benefit, leading to the reduction of water to be raised in pumping stations and to be purified or purchased from external sources.
- Obtaining energy efficiency certificates (White Certificates).

The monitoring of the water network allows to have data of the water volumes entered to DMAs. These measures are necessary during the presentation of the report for obtaining energy efficiency certificates. The TOE reduction resulting from the reduction of electricity consumption can be reported with a final project to be sent to the GSE, which issues the energy efficiency certificates in proportion to the saved TOE.

The research of water losses based on smart metering leads to the following additional benefits, beyond energy efficiency:

- Improvement of the service and operational management of the water network. The replacement of residential meters with water smart flow meters will be accompanied by a mapping of the water supply points and

the derivation pipes for the connection of the end users' internal networks to the road pipes. This mapping with barcode labels will be functional to better manage the water network. In addition, making the data available online, the residential smart water meter allows users to monitor their consumed hourly water volume and, therefore, to check for any internal losses and anomalies.

- Deleting the charges due to periodic water consumption readings and automation of the billing system. The smart flow meters together with the remote reading infrastructure allow to have the hourly water consumption data of each end user, accessible through the cloud system that is able to send periodic and automatic consumption reports.

### 4.4.2. Case study

To test this new approach and the good functioning of the remote reading technologies offered on the market, it was necessary to design the water losses monitoring system of a distribution network divided in DMAs, starting from a demo site. The water district of the historic Center of Osimo has been selected as demo site, served by a single pipeline leaving tank 14.

Figure 16 shows the identification of the tested district:

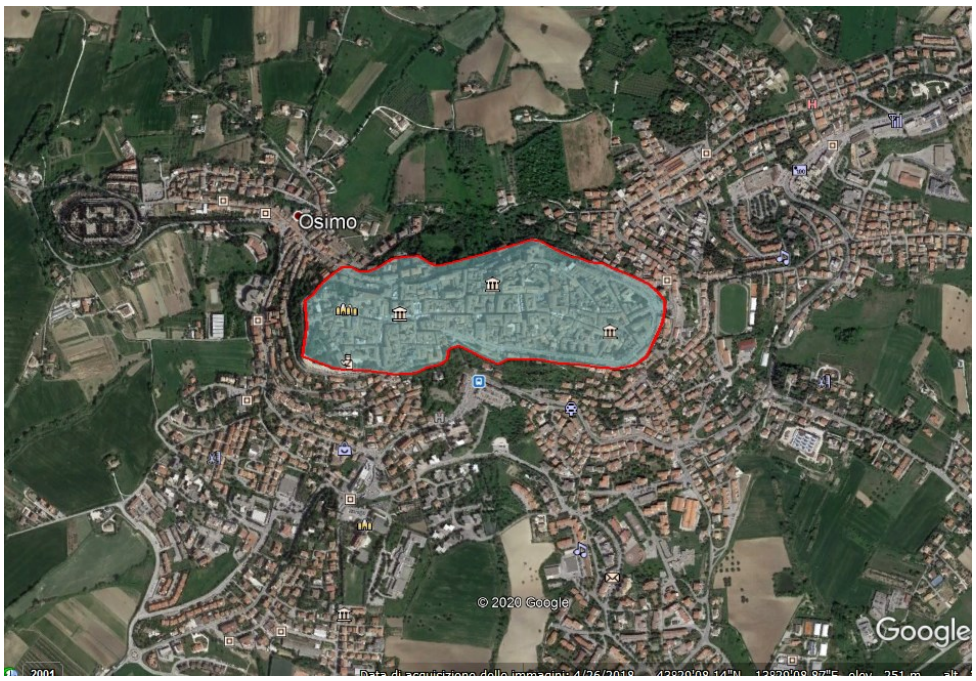


*Figure 16: Localization of the water district located in the historic Center of Osimo*

The choice of this demo site was addressed by the following reasons:

1) The percentage of water losses in this distribution network is greater than the average value of the municipality of Osimo. In the past years, pipe breaks and repairs were frequent. In addition, in the historic Center there are load-bearing masonry caves below the ground where the pipes are placed. These caves are cyclically subject to flooding phenomena due to water infiltrations from leaks. The identification and reduction of water losses undertaken between 2013 and 2015 also demonstrated the greater vulnerability of the water distribution

network in the district of the historic Center of Osimo compared to the rest of the Osimo network;

2) Greater sensitivity due to questions of structural safety of the caves mentioned in the previous point. Huge water losses, if not foreseen in advance, can cause dangerous structural instability of the masonry vaults of the underground caves, endangering the stability of the foundations of the buildings;
3) Significant energy costs due to the pumped water. High heads are needed to overcome the significant geodesic difference between the source of water represented by the well fields located at 57m and the historical Center, where the location of highest end user is 260 m in addition to the 25 m minimum pressure height to be guaranteed to provide the service. Therefore, even small reductions in water losses lead to significant savings in terms of energy required by the water pumping station A and by the pumps that bring the water from tank13 to tank 14.

### 4.4.3. Futures of the water district

The following pipes depart from tank 14:

- DN150 steel adducting pipe, which feeds tank 15 at an altitude of 260 m;
- DN150 steel adducting pipe that serves the tanks 18-19-20-21 branching along its extension in several branches;

- HDPE PN 10, De63 high density polyethylene distribution pipe, which distributes the water to some end users located outside the water district of the historic Center of Osimo;
- DN 150 steel distribution pipe serving the end users of the district in question located in the historic Center.

The last pipeline acts as an approach pipeline for a short section of 54 m, which serves the mixed type distribution network between closed links and the open system of the water district. The distribution network consists of 13 mesh, 151 nodes and 165 sections of pipeline. The nodes placed at a geodesic height vary between a minimum of 230 m and a maximum of 261 m excluding tank 14. The pipelines are quite oversized for the number of served end users, the flow rates and the considerable hydraulic and topological redundancy of the water network. The internal diameters range from 160.3 mm of a DN150 steel pipeline (for example the pipe leaving the tank 14 and those branching from it) to 26 mm of a HDPE PN16 De32 pipeline that is located in the most peripheral part of the network. The most used material is high density polyethylene, especially for pipes with a smaller diameter, while for larger diameters both coated steel with polyethylene and high density polyethylene are used. In rare cases the pipes were made of cast iron. The overall length of the network is 6,438 m. Below there are Tables 19,20,21 that report information about the percentage distribution of the diameters and materials used:

*Table 19: Length of pipelines classified by materials*

| Material | Lenght | % |
|---|---|---|
| HDPE | 5.015 | 78% |
| Cast iron | 373 | 6% |
| Steel | 1.050 | 16% |
| TOTAL | 6.438 | 100% |

*Table 20: Length of pipelines classified by internal diameter*

| Internal Diameter | Lenght | % |
|---|---|---|
| 0<Di<50 | 472 | 7% |
| 50<Di<75 | 2.627 | 41% |
| 75<Di<100 | 825 | 13% |
| 100<Di<125 | 1.206 | 19% |
| 125<Di<150 | 876 | 14% |
| Di>150 | 432 | 7% |
| TOTAL | 6.438 | 100% |

*Table 21: Main material of pipelines classified by internal diameter*

| Internal Diameter | Main Material | % |
|---|---|---|
| 0<Di<50 | HDPE | 92% |
| 50<Di<75 | HDPE | 90% |
| 75<Di<100 | HDPE | 74% |
| 100<Di<125 | HDPE | 89% |
| 125<Di<150 | Steel | 68% |
| Di>150 | Steel | 100% |

### 4.4.4. Flow and pressure data acquisition

The acquisition of pressure data, as well as flow rates, is necessary to calibrate and verify real data of the hydraulic model related to the district network. Furthermore, the acquisition of data on the volumes of water consumed by end users in the district and the evaluation of the water volumes introduced

in the same district are necessary to evaluate the situation of current water losses occurring along the distribution network. During the planning phase of the DMAs in the district of the historic Center of Osimo, no flow meters were installed, considering the data available from the existing meters enough.

**Flow rate adduced to tank "Duomo Alto"**

As already described in the previous paragraph related to the characteristics of the district, several pipes depart from tank 14, of which only one serves the district in exam. With the exception of the pipeline that connects tank 14 to tank 15 on which a flow meter is installed before the outlet of tank 15, there are no flow meters in other pipes. Therefore, to evaluate the flow rates introduced by tank 14 in the water district, it is started from the flow rate supplied from tank 13 to tank 14 by means of a pumping system consisting of 2 centrifugal pump 30 kW, one of them a reserve pump. At the end of this adduction pipeline, an electromagnetic flow meter connected to the remote control system is installed. From the software interface of this system, the hourly progressive data of water volume supplied to tank 14 has been extracted for the year 2018. Subtracting the progressive water volume with that of the previous hour, the hourly flow rate values have been obtained. The total volume given to Tank 14 in 2018 is equal to $V_{mis} = 651557\ m^3$ which corresponds to a yearly average flow rate $\overline{Q}_{y,mis} = 20{,}66\ l/s$. With the hourly flow rate data extracted, the daily consumption curve and the relative

average hourly coefficients $\overline{K}_{hi}$ is also calculated as the ratio between the average hourly flow rates $\overline{Q}_{hi,mis}$and the average daily flow rate $\overline{Q}_{g,mis} = 20{,}78\ l/s$. The average hourly coefficient curve is shown in Figure 17:

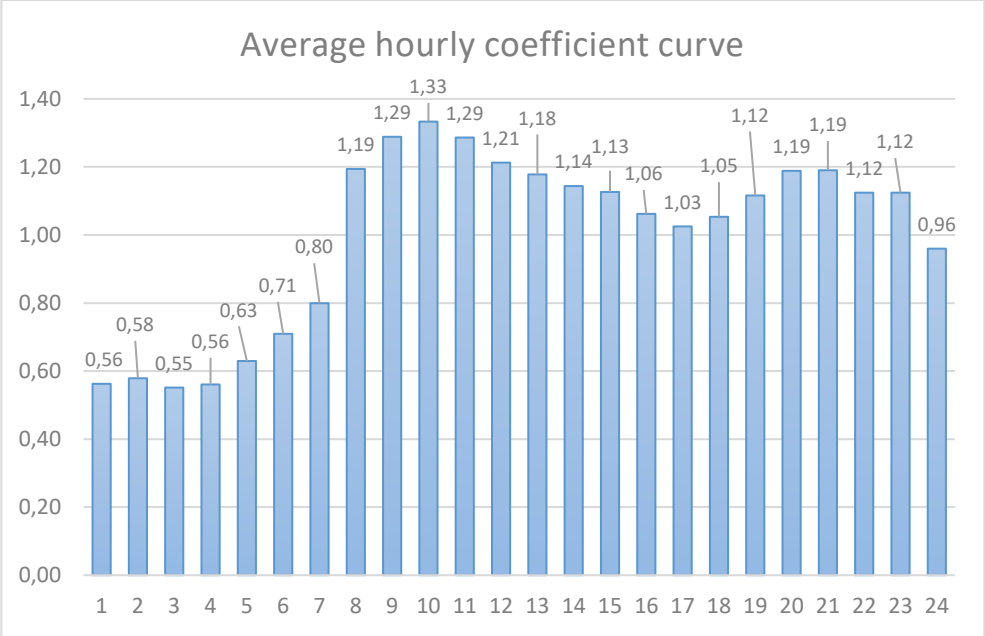


*Figure 17: Average hourly coefficient curve of flow rates supplied to Tank 14*

From the analysis of the extracted data, the following considerations can be made:

- The absolute maximum flow rate that occurs in the hour of maximum consumption of the year is equal to $\overline{Q}_{hmax,mis} = 37{,}45\ l/s$, the minimum one is $\overline{Q}_{hmin,mis} = 8{,}33\ l/s$, instead the average flow rate is $\overline{Q}_{y,mis} = 20{,}66\ l/s$, as already reported;

- In practice, the minimum flow rate in the night never drops below $\overline{Q}_{hmin,mis} = 8{,}33\ l/s$. This suggests the presence of rather conspicuous water losses along the water network served by tank 14, which also includes the water district of the historic Center of Osimo. This phenomenon is even more evidenced by the absence of significant water consumption in the night, being a residential area with little presence of activities during the night;
- The average daily fluctuations of the flow rate around the average value are not evident with an average daily peak coefficient of $\overline{K}_{hmax} = 1{,}33$ and a minimum one $\overline{K}_{hmin} = 0{,}55$. It can be deduced the presence of a constant basic flow rate represented by water losses that dampens the fluctuations around the average value. The monthly flow rate curves for July and the respective daily coefficients are also obtained $\overline{K}_{gi}$ as a ratio of the average daily flow of the i-th day of July $\overline{Q}_{gi,mis}$ and of the average monthly flow $\overline{Q}_{m,mis} = 24{,}85\ l/s$. The daily coefficient curve of July is shown in Figure 18:

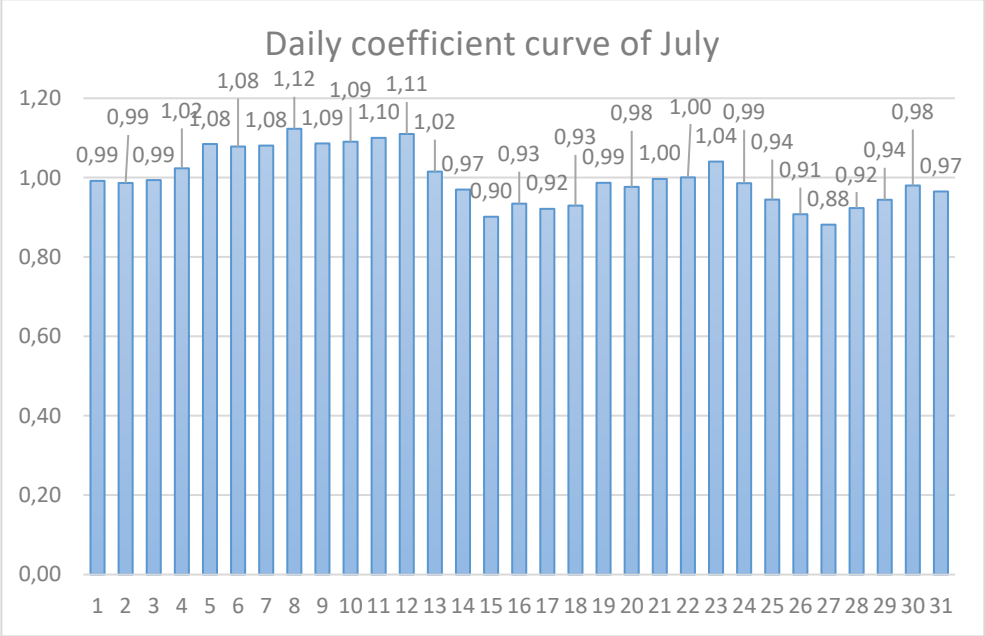


*Figure 18: Daily coefficient curve of July about flow rates supplied to Tank 14*

Finally, the annual flow rate curves and the respective monthly coefficients $\overline{K}_{mi}$ are evaluated as the ratio between the average monthly flow rates $\overline{Q}_{mi,mis}$ and the average annual flow rate $\overline{Q}_{y,mis} = 20{,}66\ l/s$. Figure 19 shows the monthly coefficient $\overline{K}_{mi}$ curve in the year 2018:

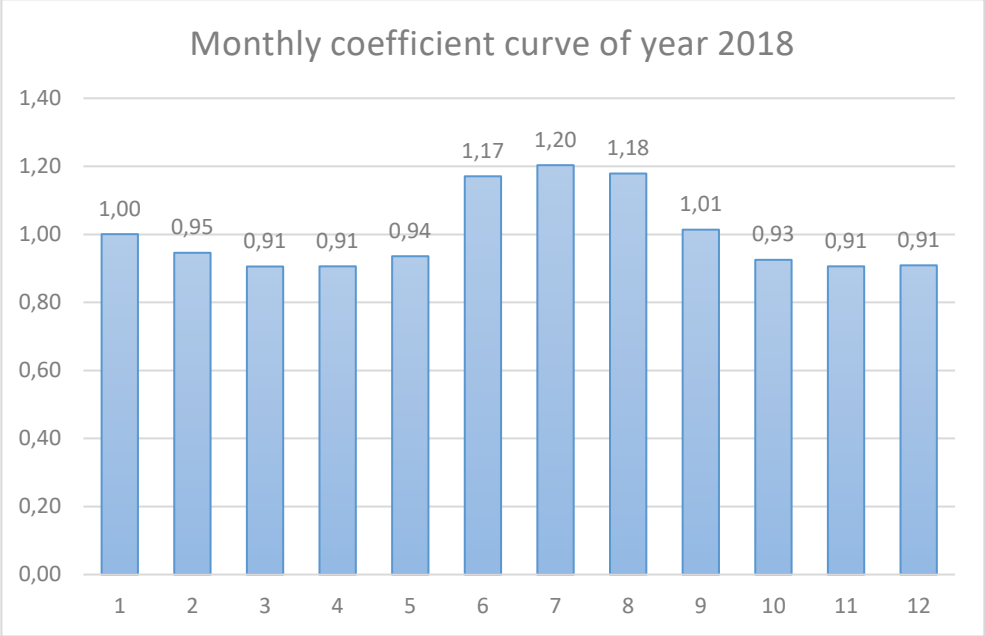


*Figure 19: Monthly coefficient curve of year 2018 about flow rates supplied to Tank 14*

These coefficients are enough to define the maximum and minimum flow conditions introduced in the district network by tank 14 throughout the year. These conditions must be imposed on our hydraulic model to proceed with the design of the smart flow meters of each DMA and the appropriate hydraulic checks of the network divided in DMAs.

**Flow rate consumed by end users**

The calculation of the authorized consumption billed by users is necessary for the evaluation of water losses and for the definition of the hydraulic network.

In fact, to proceed with the hydraulic simulation, it will be necessary to attribute to each node of the network an appropriate annual average flow rate that simulates the withdrawal from the network by the group of end users belonging to the relevant network node. For the year 2018, the values of the volumes of water consumed are extracted using an integrated water service management software called NETA H2O. This procedure is not done only for the end users of the streets present in the water district in exam, but for all the end users served both directly and indirectly by the tank 14. Since the water meter is not installed on the distribution pipeline that fed the water district in exam, it is necessary to have also the consumption related to the end users outside the district served by the tank 14 to estimate proportionally the flow rate introduced into the district starting from the total flow rate distributed by tank 14. Therefore, data extraction will also involve the end users served by the tank 15,16, 17,18,19,20,21 which in turn are fed by the tank 14. Table 22 reports the annual water volumes $V_{s,i}$ $[m^3]$ and the corresponding average yearly flow rate consumed by the end users of each street in the district $\bar{Q}_{s,i,y}$ $[l/s]$:

*Table 22: Users, annual water volume and average yearly flow rate consumed for each street of district*

| STREET | USERS NUMBER | $V_{s,i}$ $[m^3]$ | $\bar{Q}_{s,i,y}$ $[l/s]$: |
|---|---|---|---|
| C.SO MAZZINI | 90 | 5,025 | 0.1593 |
| P.ZZA A. GALLO | 11 | 5,205 | 0.1650 |
| P.ZZA BOCCOLINO | 32 | 2,238 | 0.0710 |
| P.ZZA DANTE | 53 | 4,537 | 0.1439 |

| | | | |
|---|---|---|---|
| P.ZZA DEL CARMINE | 9 | 679 | 0.0215 |
| P.ZZA DEL COMUNE | 34 | 2,620 | 0.0831 |
| P.ZZA DON MINZONI | 2 | 60 | 0.0019 |
| P.ZZA DUOMO | 36 | 2,703 | 0.0857 |
| P.ZZA GRAMSCI | 10 | 817 | 0.0259 |
| P.ZZA LEOPARDI | 31 | 1,676 | 0.0531 |
| P.ZZA MARCONI | 11 | 1,608 | 0.0510 |
| P.ZZA MONTANARI | 10 | 477 | 0.0151 |
| P.ZZA ROSSELLI | 13 | 684 | 0.0217 |
| P.ZZA S. GIUSEPPE DA COPERTINO | 6 | 335 | 0.0106 |
| P.ZZA SANT'AGOSTINO | 6 | 561 | 0.0178 |
| V.LO A. NICCOLI | 9 | 736 | 0.0233 |
| V.LO BONFIGLI | 7 | 745 | 0.0236 |
| V.LO BUON VILLANO | 17 | 1,467 | 0.0465 |
| V.LO CENTONARI | 10 | 904 | 0.0287 |
| V.LO CROCCANO | 1 | - | 0.0000 |
| V.LO LIPPACCIO E GUZZOLINO | 14 | 900 | 0.0285 |
| V.LO MALAGRAMPA | 16 | 1,118 | 0.0355 |
| V.LO MARTORELLI | 39 | 2,856 | 0.0906 |
| V.LO SENTINELLA DEL MUSONE | 14 | 785 | 0.0249 |
| VIA ANDREA DA RECANATI | 22 | 1,126 | 0.0357 |
| VIA ANTICA ROCCA | 11 | 1,275 | 0.0404 |
| VIA ANTICO POMERIO | 24 | 1,957 | 0.0621 |
| VIA ARCO VECCHIO | 5 | 210 | 0.0067 |
| VIA B. PONTELLI | 2 | 176 | 0.0056 |
| VIA BONDIMANE | 20 | 1,399 | 0.0444 |
| VIA CAGIAROLO | 6 | 580 | 0.0184 |
| VIA CAMPANA | 25 | 2,340 | 0.0742 |
| VIA CAPPUCCINI | 84 | 6,309 | 0.2001 |
| VIA CASTEL DE PULCI | 2 | 100 | 0.0032 |
| VIA CIALDINI | 9 | 692 | 0.0219 |
| VIA CINQUE TORRI | 48 | 2,777 | 0.0881 |
| VIA COMPAGNONI | 38 | 2,719 | 0.0862 |
| VIA CONERO | 15 | 1,169 | 0.0371 |
| VIA COSTA DEL BORGO | 12 | 697 | 0.0221 |
| VIA F. FIORENZI | 2 | 68 | 0.0022 |

| | | | |
|---|---|---|---|
| VIA FONTE MAGNA | 77 | 7,148 | 0.2267 |
| VIA FUINA | 22 | 1,631 | 0.0517 |
| VIA G. LEOPARDI | 54 | 11,125 | 0.3528 |
| VIA GIULIA | 24 | 2,738 | 0.0868 |
| VIA GOMERO | 8 | 1,486 | 0.0471 |
| VIA GUASINO | 17 | 1,493 | 0.0473 |
| VIA L. BALEANI | 34 | 2,076 | 0.0658 |
| VIA LEON DI SCHIAVO | 8 | 382 | 0.0121 |
| VIA LIONETTA | 40 | 2,503 | 0.0794 |
| VIA MACELLI | 33 | 3,876 | 0.1229 |
| VIA MATTEOTTI | 116 | 19,543 | 0.6197 |
| VIA N. ROMANI | 14 | 1,416 | 0.0449 |
| VIA OPPIA | 24 | 2,166 | 0.0687 |
| VIA ORSO | 1 | 92 | 0.0029 |
| VIA ORTI TRAIANI | 10 | 814 | 0.0258 |
| VIA PAOLO VI | 45 | 4,474 | 0.1419 |
| VIA POMPEIANA | 138 | 10,369 | 0.3288 |
| VIA PORTA MUSONE | 11 | 544 | 0.0173 |
| VIA SACRAMENTO | 49 | 2,667 | 0.0846 |
| VIA SAFFI | 10 | 980 | 0.0311 |
| VIA SALUSTRIANA | 16 | 1,135 | 0.0360 |
| VIA SAN BARTOLOMEO | 40 | 3,470 | 0.1100 |
| VIA SAN FILIPPO | 54 | 7,397 | 0.2346 |
| VIA SAN FRANCESCO | 44 | 3,421 | 0.1085 |
| VIA SAN MARCO | 19 | 2,245 | 0.0712 |
| VIA SAN SILVESTRO | 11 | 777 | 0.0246 |
| VIA SANTA LUCIA | 40 | 3,719 | 0.1179 |
| VIA SCALETTE | 52 | 4,092 | 0.1298 |
| VIA SOGLIA | 23 | 3,227 | 0.1023 |
| VIA STRIGOLA | 25 | 1,988 | 0.0630 |
| VIA TALLEONI | 5 | 460 | 0.0146 |
| VIA VENTIDIA | 11 | 601 | 0.0191 |
| VIA VINCENZO ACQUA | 11 | 624 | 0.0198 |
| VIA VITALIONI | 7 | 591 | 0.0187 |
| VIA Z. CESARI | 9 | 369 | 0.0117 |
| TOTAL | 1908 | 173,969 | 5.5165 |

Therefore, the total authorized volume invoiced in the district is $V_{c,d} = 173.969\ [m^3]$, which corresponds to an average annual flow rate of $\bar{Q}_{c,d,y} = 5{,}52\ [l/s]$.

The same evaluation extended to all users served by the tank 14 led to a volume consumed by users of $V_{c,t14} = 438.680[m^3]$, which corresponds to an average annual flow rate of $\bar{Q}_{c,t14,y} = 13{,}91\ [l/s]$.

**Evaluation of flow rate distributed inside the water district**

Knowing the flow rate adduced $\overline{Q}_{y,mis} = 20{,}66\ l/s$ from tank 13 to tank 14 by means of a pumping station and the flow rate consumed by users of tank 14 and other connected $\bar{Q}_{c,t14,y} = 13{,}91\ [l/s]$ and the flow rate consumed by users of the Osimo historic center district served by a pipeline of the tank 14 $\bar{Q}_{c,d,y} = 5{,}52\ [l/s]$, the annual average flow rate introduced into the district in proportion to the flows consumed is obtained:

$$\bar{Q}_{d,y} = 20{,}66 * \frac{5{,}52}{13{,}91} = 8{,}20\ l/s$$

Obviously this assessment is based on the following simplifying assumptions:

- absence of water losses in tank 14;
- proportional relation between flow rates distributed in the district and end users' consumption assuming the presence of uniform water losses along the entire adduction and distribution network downstream of the tank14.

**Daily curve of pressure measurement in two nodes**

As regards the evaluation of the pressures involved in the current district, two pressure probes were installed to monitor the daily trend of the pressure head in two significant points of the network:

1) The first pressure probe in correspondence to an utility placed in via Antica Rocca located in node 4 of the network at geodetic altitude +260 m a.s.l.;
2) The second pressure probe in correspondence to a user in via Scalette located in node n30 of the network at geodetic altitude +240 m a.s.l.

The pressure head on 10 October 2018 at node 4 varied from a minimum of 30.5 m to a maximum of 32.35 m for an average value of 31.56 m, while in node n30 a minimum pressure of 49 m, maximum of 51.21 m and average of 49.85 m.

These measurements will be used to verify in the hydraulic modelling phase the correspondence between the simulated average pressure height data and the real one in these nodes and the correlation that exists between the simulated daily trend and the real one of the piezometric head of these nodes.

### 4.4.5. District water balance

Based on the assessments made about the flow introduced in the district and the flow consumed by the end users of the district, the water balance of the water network of the historic Center of Osimo using the "Top Down" technique (IWA, 2000) is performed. Considering that the average annual flow introduced in the network (SYSTEM INPUT VOLUME) $\bar{Q}_{d,y} =$

8,20 $l/s$ and the average annual flow rate consumed and billed to the end user (BILLED AUTHORIZED CONSUMPTION) is equal to $\bar{Q}_{c,d,y} = 5{,}52\ [l/s]$, the non-invoiced flow attributed to network losses in the district is $\bar{Q}_{loss,d} = 2{,}68\ [l/s]$. From the water balance it can therefore be deduced that the overall water losses, both physical and apparent, are equal to 32.68% of the total flow introduced in the district, a value in line with the average water losses of the entire municipality of Osimo. It should be noted that within the apparent component of the losses are also included for simplicity the authorized consumption not invoiced, thus separating the NRW (non-revenue water) into only two components: the apparent losses (including authorized consumption not invoiced) and the physical losses.

Certainly, this evaluation is affected by the approximation of the measurement error of the residential meters and of the flow meter raised from tank 13 to tank 14. Furthermore, the assumption of the hypothesis of homogeneous distribution of water losses over the entire network related to tank 14. This last hypothesis had to be assumed due to the absence of the flow meter on the pipeline that feeds the water district in exam.

To reduce significant water losses, it has to immediately assess the effect of local interventions on the distribution network and preserve the effects of reducing losses achieved over time and to overturn the precise methods of research and reduction of water losses implemented in previous years, as described in the chapter 4.3, and to approach the problem by building a real-time monitoring system of the water network. To do this, the identification of DMAs to be monitored by means of remote-readable flow meters has to be

done. The starting point is the construction of a hydraulic model of the district in exam to simulate its behaviour before and after the subdivision into DMAs, as explained in the following paragraphs.

### 4.4.6. Water district modelling with Epanet2

The hydraulic simulations of the water district related to the historic Center of Osimo were carried out using the EPANET version 2.0 software.
EPANET is a program implemented by the United States Environmental Protection Agency (EPA). The version used, developed by the Water Supply and Water Resources Division of the National Risk Management Research Laboratory in Cincinnati-Ohio, works in a Windows environment and is freely downloadable from the EPA website.
The software allows simulations of pressurized hydraulic networks relating to hydraulic phenomena and water quality. The capabilities of EPANET include:

- networks of unlimited size;
- use of the formulas of Hazen-Williams, Darcy-Weisbach or Chezy-Manning for the calculation of the distributed head losses;
- calculation of local head losses;
- constant or variable rotation speed of the pumps;
- calculation of energy consumption and pumping costs;
- modelling of various types of valves;

- head compensation tanks of any shape;
- water requests at the nodes of various types including those that vary over time;
- the system configuration both on the level of a tank and through the use of a timer.

The EPANET hydraulic simulation model calculates the pressure heads at the nodes and the flow rates passing through the pipelines throughout the day. The program allows to evaluate the dynamic trend of the water network by setting hourly curves of daily consumptions, curves that describe the total head in the "reservoir" during the day, internal operating curves of the pumping system. The tank levels, on the other hand, are calculated hour by hour by integrating the continuity equations applied to the tanks. The solution for the loads and flow rates at a particular point in time is identified by simultaneously solving the flow conservation equation in each node and the energy balance of each pipeline taking into account the dissipation of energy by friction. This process, known as hydraulic balance, requires an iterative technique to solve the nonlinear equations involved; For this purpose, EPANET uses the gradient algorithm, defined by Todini and Pilati (1987) and subsequently by Salgado (1988).

**Water network simplification method**

The water network of the district to be modelled can undergo to a simplification process without causing alterations in terms of hydraulic

behaviour. In this way, its hydraulic modelling is made less expensive without altering the validity of the results. Two models are called equivalent if they produce the same head pressure distribution and the same flow rate values due to the same water demand and the same contour conditions [82].

The simplification process is called “skeletonization” and consists of a combination of simplification procedures on the network applied in series. Given a water distribution system, it is thus possible to pass from an initial hydraulic model, characterized by certain dimensions, to an equivalent model of smaller dimensions.

The properties of pipes and nodes that are excluded in the equivalent model are not cleared but, rather, are incorporated into the simplified model.

The different skeletonization procedures can be divided into two different levels [79]:

1. removals and unifications: consists of the set of skeletonization procedures that allow to simplify the network without changing the hydraulic characteristics of the pipelines such as length, diameter or roughness. These procedures include:

- simple removal of pipelines with respect to a reference factor (for example, diameter or length below the assigned threshold values);
- removal of the ramifications or elimination of the pipelines of ends;
- removal of single-access micro-networks;

2. transition to equivalent pipelines: it consists of a set of procedures that allow to simplify the network by switching to equivalent smaller size

schemes; these procedures inevitably change the hydraulic characteristics of the pipelines such as length, diameter or roughness, passing from values that have their own intrinsic physical significance to others obtained by mathematical equivalence. These procedures include:

- replacement of pipelines in series and in parallel with one pipeline equivalent: two pipelines in series (in succession to each other) or in parallel (i.e. having the same end nodes) are replaced by a third pipeline with physical characteristics (length, diameter, roughness, etc.) to represent the two pipes hydraulically removed taking into account the flows circulating in each section and those delivered in the end nodes;
- star-triangle transformation (Hamberg and Shamir 1988): a very common transformation in the analysis of electrical systems, is that from the "triangle", that is a three-sided mesh, to the "star", that is, three pipes that meet in a central node [82].
- elimination of pipes characterized by poor conveying capacity (opening of the closed meshes).

The hydraulic scheme used in the simulation of the network of the historic Center of Osimo comes from a skeletonization procedure carried out in order to unify the sections having the same diameter and roughness, replacing the branches and micro-networks with single access with appropriate concentrated supplies. During the simplification process, the flow rates consumed by the end users served by the open end networks are attributed to

the end nodes of the new modelled network. After that, the hydraulic network was constituted by13 closed links, 151 knots and 165 pipeline sections to 13 closed meshes, 115 knots and 129 pipeline sections.

**Planimetry and altimetry of the district network in Epanet**

The simplified network obtained by means of the above procedure is represented in graphic form through a CAD drawing in .dwg format. The nodes and pipelines that compose the network already have as attributes and properties the information necessary to describe its elevation and planimetry. The nodes have longitude, latitude and geodetic elevation as properties, while the pipelines have their length, the material in which they are made and the nominal diameter as properties. Once the drawing in .dwg was acquired, the EpaCAD software was used to convert the water network made up of nodes and pipes into a format compatible with the Epanet 2.0 software. In this way, the network with its planimetry and altimetry arrangement was imported into Epanet 2.0, while this procedure does not allow to import directly the diameters and the roughness coefficient depending on the material of the pipes into the hydraulic model. These last information are manually introduced at a later time for each pipeline, just as the compensation tank with the relative characteristics.

**Water source characterization of district network**

To create a hydraulic model that strictly reflects the structure of the WSS of the water district in exam, it would be necessary to model the tank 13 through

the "reservoir" element connected by means of a centrifugal pump to the tank 14, which should be modelled with the element "tank". Considering that the tank 13 presents a variable water tie and its water is supplied by another pumping station, it should be necessary to set a tank with a variable "total head" throughout the day and to define the characteristics of the pump introducing its head-flow operating curve. Instead a simpler modelling is preferred to this more complex approach, neglecting all that is present upstream of the tank 14. The tank14 is modelled as a “reservoir” with an average daily “total head” with respect to the sea level, the value of which varies during the day due to the fluctuations of its water tie. To simulate this daily variation, a "pattern head" is introduced into the software to be associated with the reservoir. First, the water tie data of tank 14 were extracted from the remote control system. Below Table 23 shows the average hourly water tie values that are realized:

*Table 23: Average hourly water tie of Tank 14*

| hour | 1 | 2 | 3 | 4 | 5 | 6 | 7 | 8 | 9 | 10 | 11 | 12 |
|---|---|---|---|---|---|---|---|---|---|---|---|---|
| Water level [m] | 5 | 5.1 | 5 | 4.95 | 4.9 | 4.8 | 4.68 | 4.5 | 4.55 | 4.7 | 4.95 | 4.65 |

| hour | 13 | 14 | 15 | 16 | 17 | 18 | 19 | 20 | 21 | 22 | 23 | 24 | average |
|---|---|---|---|---|---|---|---|---|---|---|---|---|---|
| Water level [m] | 4.5 | 4.78 | 4.86 | 4.56 | 4.97 | 4.7 | 4.65 | 4.5 | 4.67 | 4.7 | 4.73 | 4.85 | 4.76 |

The geodetic height of the bottom tank is 286.5 m deduced from the graphic drawings of the construction sections of the hanging tank. By adding hour by

hour the geodetic elevation of the bottom with the water tie, the daily curve of the total head, shown in Table 24, is obtained:

*Table 24: Daily curve of total head of Tank 14*

| hour | 1 | 2 | 3 | 4 | 5 | 6 | 7 | 8 |
|---|---|---|---|---|---|---|---|---|
| Total head [m] | 291.50 | 291.60 | 291.50 | 291.45 | 291.40 | 291.30 | 291.18 | 291.00 |
| coeff.of head pattern | 1,0008 | 1,0012 | 1,0008 | 1,0007 | 1,0005 | 1,0001 | 0,9997 | 0,9991 |
| hour | 9 | 10 | 11 | 12 | 13 | 14 | 15 | 16 |
| Total head [m] | 291.05 | 291.20 | 291.45 | 291.15 | 291.00 | 291.28 | 291.36 | 291.06 |
| coeff.of head pattern | 0,9993 | 0,9998 | 1,0007 | 0,9996 | 0,9991 | 1,0001 | 1,0003 | 0,9993 |
| hour | 17 | 18 | 19 | 20 | 21 | 22 | 23 | 24 |
| Total head [m] | 291.47 | 291.20 | 291.15 | 291.00 | 291.17 | 291.20 | 291.23 | 291.35 |
| coeff.of head pattern | 1,0007 | 0,9998 | 0,9996 | 0,9991 | 0,9997 | 0,9998 | 0,9999 | 1,0003 |

The average value of total head 291.26 m is attributed as total head in Epanet and as coefficients of the head pattern reported in Table 24.

The low variability of the water level in the tank 14 justifies the choice of simplified modelling in place of modelling the reality. In fact, the flow rate values in the pipes and the pressure values in the nodes are almost negligibly influenced by the variability of the free surface of the water contained in the tank 14. As regards the energy analysis of the savings achievable with the

reduction of water losses, it is not necessary to model the pumps in Epanet, but it is enough a more practical method that is explained in detail in the paragraph 4.4.10.

**Pipelines characterization**

In Epanet it is necessary to insert the internal diameter, the roughness coefficient and the initial status of the pipes. The internal diameter can be obtained by using the technical tables of the pipes for each material starting from the information in the .dwg file of the nominal diameter for steel and cast-iron pipes and the external diameter for plastic pipes (PVC, HDPE). Instead, the Hazen-Williams formula implemented in the software is used to simulate the distributed pressure drops in the pipelines. For the choice of roughness coefficients C to be used for each material, the age of the pipeline should also be taken into account based on the year of installation. The differentiation by age is burdensome and superfluous considering the limited incidence of pressure drops on the pressure that occurs at the network nodes. Therefore, uniform values will be considered as roughness coefficients C for all pipelines of a given material according to Table 25:

*Table 25: Roughness coefficient for each pipeline material*

| Material | C Roughness coefficient |
|---|---|
| Steel | 100 |
| Cast Iron | 120 |
| PVC, PEAD | 140 |

**Characterization of nodes**

The geographic coordinates of the nodes and their geodetic height (elevation) have already been defined during the import of the geometry related to the water network in Epanet. However, it is necessary to evaluate the flow rate passing through the node according to the network losses that occur and the water consumption of the end users that withdraw water near the node in question.

To consider the different nature of the components that contribute to the average annual flow passing through each node as a whole, it is necessary to evaluate the total average annual flow as the sum of three components:

- Average annual allowed water flow billed by end users $\bar{Q}_{c,y,m}$ related to the m-th node that feeds a group of end users located in the streets near the node. The flow rate for the m-th node is calculated with the following Eq. (38):

  $$\bar{Q}_{c,y,m} = \sum_{i=1}^{n} \bar{Q}_{s,i,y} \quad [l/s] \qquad (38)$$

  where $\bar{Q}_{s,i,y}$ is the yearly allowed billed flow rate consumed by end users located on i-th street. In Epanet the flows obtained will be addressed to the nodes as "Base Demand";
- Average annual apparent losses $\bar{Q}_{app,y,m}$. For classification within the apparent losses, unauthorized consumption and measurement errors are considered. In our analysis, the unmeasured authorized

consumption due to the washing of the pipes and tanks. The opening of the drains is also included in the apparent losses. Given the nature of these losses, they are considered to be evenly distributed over all the distribution nodes of the network. Average annual real losses $\bar{Q}_{real,m}$ are those that occur due to failures in the pipelines and are considered to be evenly distributed throughout the network. Therefore, the flow rate related to the real losses are distributed on all nodes, both emitters and losers.

Considering the temporal variability of these three components, in each m-th node the flow rate at each instant t can be evaluated with Eq. (39):

$$Q_{t,m} = Q_{c,t,m} + Q_{app,t,m} + Q_{real,t,m} \quad (39)$$

- The authorized billed flow rate consumed at time t is calculated through Eq. (40):

  $$Q_{c,t,m} = \bar{K}_{hi} \cdot \bar{K}_{gi} \cdot \bar{K}_{mi} \cdot \bar{Q}_{c,y,m} \quad (40)$$

  where the peak coefficients allow to simulate the consumption of utilities at any time of the year. The peak consumption coefficients are the same for all nodes given the uniformity of the residential fabric of the district. The daily consumption curve will be taken into account in the Epanet model by defining a Demand Pattern, to be attributed to the network nodes, through the average hourly peak coefficients $\bar{K}_{hi}$ reported in Figure 17. Instead, the product of the peak coefficients $\bar{K}_{gi} \cdot \bar{K}_{mi}$ must be entered within the "Demand Multiplier" of the

Epanet "Analysis Options" to consider end users' water consumption in a specific day of the year.

- Apparent losses are instead calculated with Eq. (41) [79]:

$$Q_{app,t,m} = A_c \cdot Q_{c,t,m} \quad (41)$$

In this way, the temporal trend of apparent losses will be the same as the billed flow rates consumed by end users. Furthermore, it is practical to write the apparent losses as a function of the consumption billed because in Epanet they can be easily considered by increasing for each m-th node the flow rate supplied as "Base Demand" ( $\bar{Q}_{c,y,m}$) by a factor equal to $A_c$ o be considered in the "Demand Multiplier" of the "Anlaysis Options".
To calculate $A_c$, the quantification of the real losses has to be done. To do this, the following Eq. (42) is used:

$$MNF = HNU + NHNU + ONU + \bar{Q}_{real,d} \quad (42)$$

where $MNF$ is the minimum night flow, $HNU$ is the household night use, $NHNU$ è il non-household night use, $ONU$ is the operational use in the night and $\bar{Q}_{real,d}$ is the flow rate associated to real water losses [81]. For sake of clarity, all the end users are considered as household and the operational consumption in the night is included in household one. Literature values indicate for the estimate of the HNU to consider

active the 6% of the total number of inhabitant $N_{inh}$ with a water consumption for inhabitant of 9 l/h [81]. To take into account also the NHNU and the ONU, the HNU can be evaluated considering active the 10% of the inhabitants living in the district using the following Eq. (43):

$$HNU = 0{,}1 \cdot N_{inh} \cdot \frac{9}{3600}\ [l/s] \tag{43}$$

$N_{inh}$ is equal to 4746, so $HNU$ is 1,19 l/s. Using Eq.(42)it is obtained $\bar{Q}_{real,d}$ = 2,12 l/s. From the water balance with the Top-Down method, it is calculated the average annual total water losses in the district $\bar{Q}_{loss,d} = 2{,}68\ l/s$ including apparent and real losses,. Therefore the annual average apparent losses is equal to $\bar{Q}_{app,y,d} = 0{,}56\ l/s$, which corresponds to 20,9% of total water losses. Total water losses represents the 32,7% of the average annual water supplied to the district. From this double correlation, it is deduced that $\bar{Q}_{app,y,m} = 0{,}1 \cdot \bar{Q}_{c,y,m}$ from which is highlighted the coefficient $A_c = 0{,}1$.
Ultimately, based on the day of the year, the "Demand Multiplier" will be equal to $(A_c + 1) \cdot \overline{K}_{gi} \cdot \overline{K}_{mi}$.

- The real physical losses in the m-th node vary over time according to the pressure value that occurs in the node. The relationship that links the real water losses flow rate with the pressure is expressed by Eq. (44):

$$Q_{real,t,m} = C \cdot p_{t,m}^{\alpha} \quad (44)$$

Where C is the "emitter coefficient" to be obtained in the calibration phase of the hydraulic model and α is the "emitter exponent " and, according to literature values, it is set equal to 0.8, higher than the Torricellian value of 0.5. The same coefficient C is considered for all nodes [79, 81].

The total flow rate introduced into the network at time t is evaluated by Eq. (45):

$$Q_{d,t} = \sum_{m=1}^{n}(1{,}1 \cdot \overline{K}_{hi} \cdot \overline{K}_{gi} \cdot \overline{K}_{mi} \cdot \overline{Q}_{c,y,m}) + \sum_{m=1}^{l} C \cdot p_{t,m}^{\alpha} \quad (45)$$

Where $n$ represents the number of emitter nodes and $l$ the number of loss nodes.

To summarize the value of the components that compose the overall average annual flow introduced into the district of the historic Center of Osimo, it is shown below the Table 26 with the average values of authorized billed flow, apparent losses and real losses.

*Table 26: Quantification of each components of the total yearly average flow rate flowing in the analysed district*

<table>
<tr><td rowspan="3">Total Yearly average Flow rate<br>$\bar{Q}_{d,y}$<br>$8.20\ l/s$</td><td>Billed authorized flow rate</td><td colspan="2">$\bar{Q}_{c,d,y} = 5.52\ [l/s]$<br>67.3% of $\bar{Q}_{d,y}$</td></tr>
<tr><td rowspan="2">Water Losses (included authorized consumption unbilled)</td><td rowspan="2">$\bar{Q}_{loss,d}$<br>$2.68\ l/s$<br>32.7 % of $\bar{Q}_{d,y}$</td><td>Apparent Losses<br>$\bar{Q}_{app,y,d}$<br>$0.56\ l/s$<br>20,9 % of $\bar{Q}_{loss,d}$<br>6,8 % of $\bar{Q}_{d,y}$</td></tr>
<tr><td>Real Losses<br>$\bar{Q}_{real,d}$<br>$2.12\ l/s$<br>79,1% of $\bar{Q}_{loss,d}$<br>25.9% of $\bar{Q}_{d,y}$</td></tr>
</table>

**Water network calibration to determine C coefficient**

At this point, the hydraulic model is ready and it is only necessary to find the correct value of the "emitter coefficient" C to be attributed to the nodes to correctly simulate the water losses. Its value, as already mentioned, is not obtained from the literature as for α the "emitter exponent", but is the result

of the calibration of the model. The calibration of the hydraulic model is carried out by choosing values of C such as the average annual flow out of the tank converges to the value represented by the real average annual flow supplied to the district $\bar{Q}_{d,y} = 8{,}20\ l/s$. By setting the value of C = 0.0012, the analysis of the model has the output value $\bar{Q}_{d,y} = 8{,}20\ l/s$ in the hour of the years in which $\overline{K}_{hi} = \overline{K}_{gi} = \overline{K}_{mi} = 1$, when the average annual flow rate is achieved.

**Analysis of the results of the actual district network**

Once all the characteristics of the hydraulic model have been defined, the analysis is run. The software automatically solves the hydraulic problem through all the equations of the energy balance in each branch and the conservation of mass in each node. In this paragraph the pressures and flow rates that occur at the nodes and pipelines in the hour of the maximum water consumption of the year are reported. These values are obtained on Epanet setting 1.49 as a "demand multiplier" and displaying the values at 10:00, maximum point of the daily curve.
Figure 20 is a "contour plot" graph that depicts the areas of the district divided by pressure head ranges:

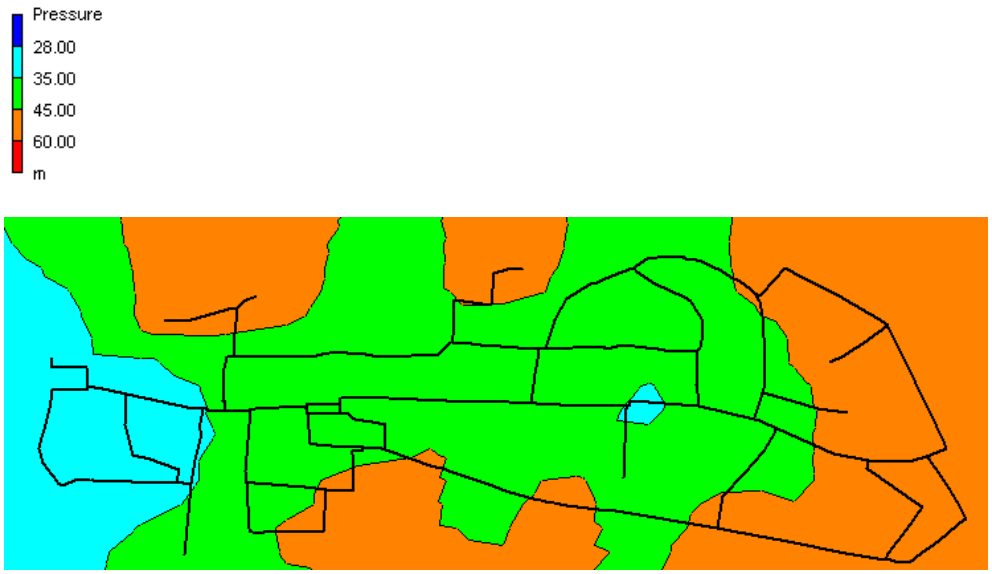


*Figure 20: Pressure head ranges of the water distribution network in exam*

The minimum pressure head that occurs in the water district is 29.44 m, while the maximum one is 59.81 m. On the one hand, the pressure head is always higher than 5 m compared to the roof slab of the top floor of the tallest building, guaranteeing the service. However, on the other hand, the graph shows areas of the distribution network that exceed 45 m of pressure, which is above the minimum pressure head necessary to guarantee the service. These high pressures increase the real water losses and breakage of pipelines.

Then, the simulation has been run setting the Demand Multiplier equal to 1.02 to calculated the pressure curves that occur in nodes 4 and n30 on 10 October. The choice of these two nodes is due to the need to compare the real values obtained during the pressure measurement campaign with the simulated

values to verify the correspondence of the hydraulic model to the values that actually come true. The simulated mean pressure head is equal to 30.44 m for node 4, which has an error of 3.6% with respect to the 31.56 m measured value, while for node n30 Epanet calculates 50.04 m as the average value of pressure head compared to a measured value a measured value of 49.85 m, with an error of -0.4%. Figures 21-22 show the comparison between the measured pressure head curve and the simulated one on Epanet in nodes 4 and 30:

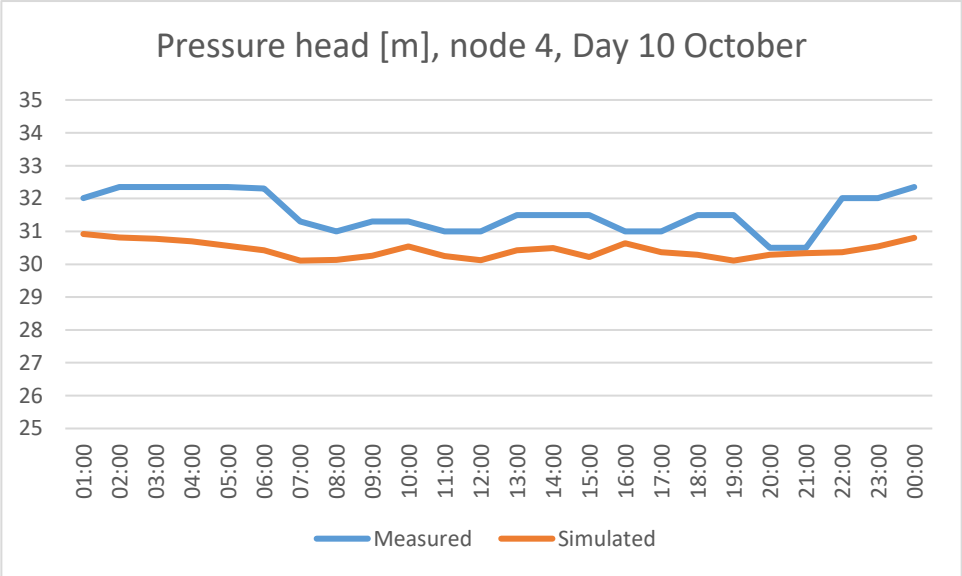


*Figure 21: Comparison between measured and simulated pressure head of node 4 during the day 10/10/2018*

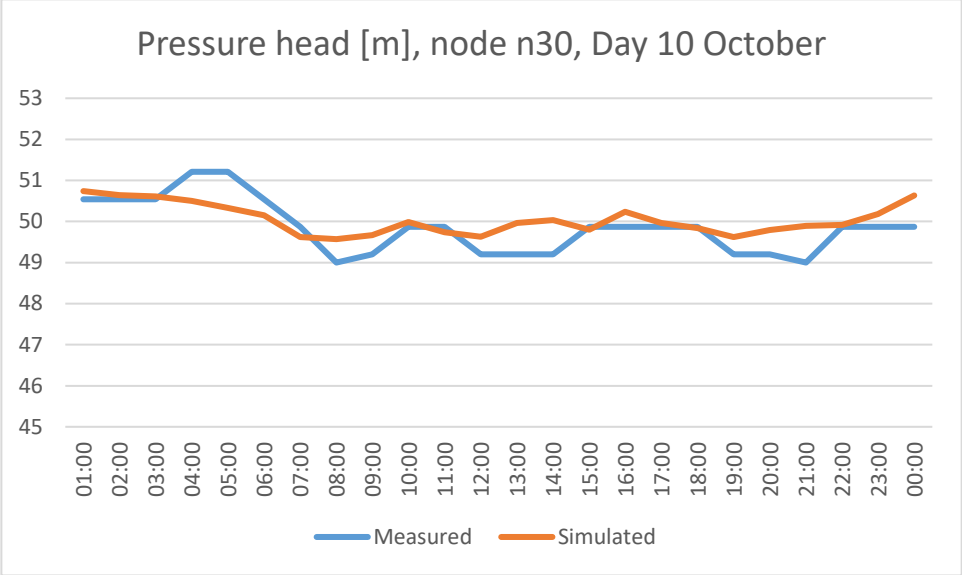


*Figure 22: Comparison between measured and simulated pressure head of node 30 during the day 10/10/2018*

Figure 23 shows the flow rate curve [l/s] that occur along the main distribution pipeline from tank 14 to distribution network during the day of maximum water consumption.

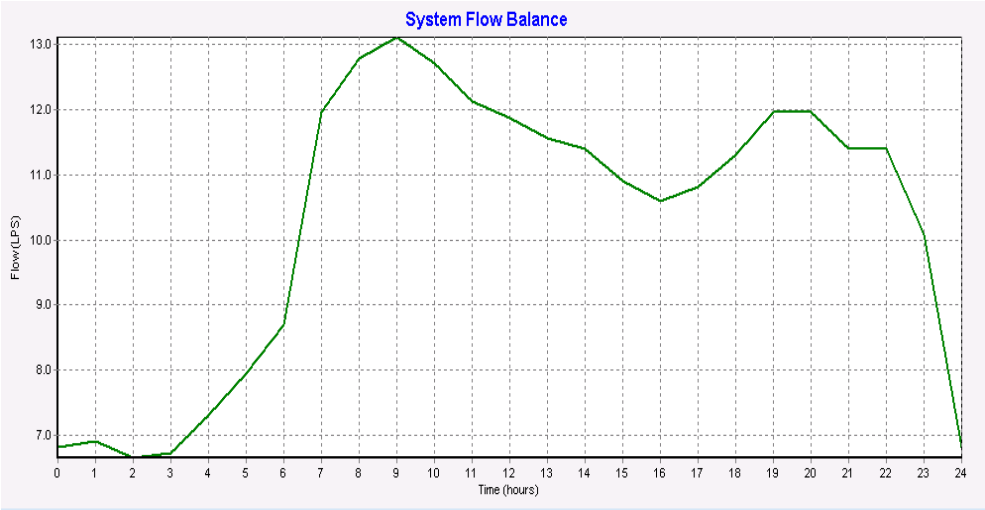


*Figure 23: Flow rate curve exported by Epanet of the main distribution pipeline during the day of maximum water consumption*

Figure 24 shows the Epanet plotter of the hydraulic model, indicating the range of flow rates in each pipeline:

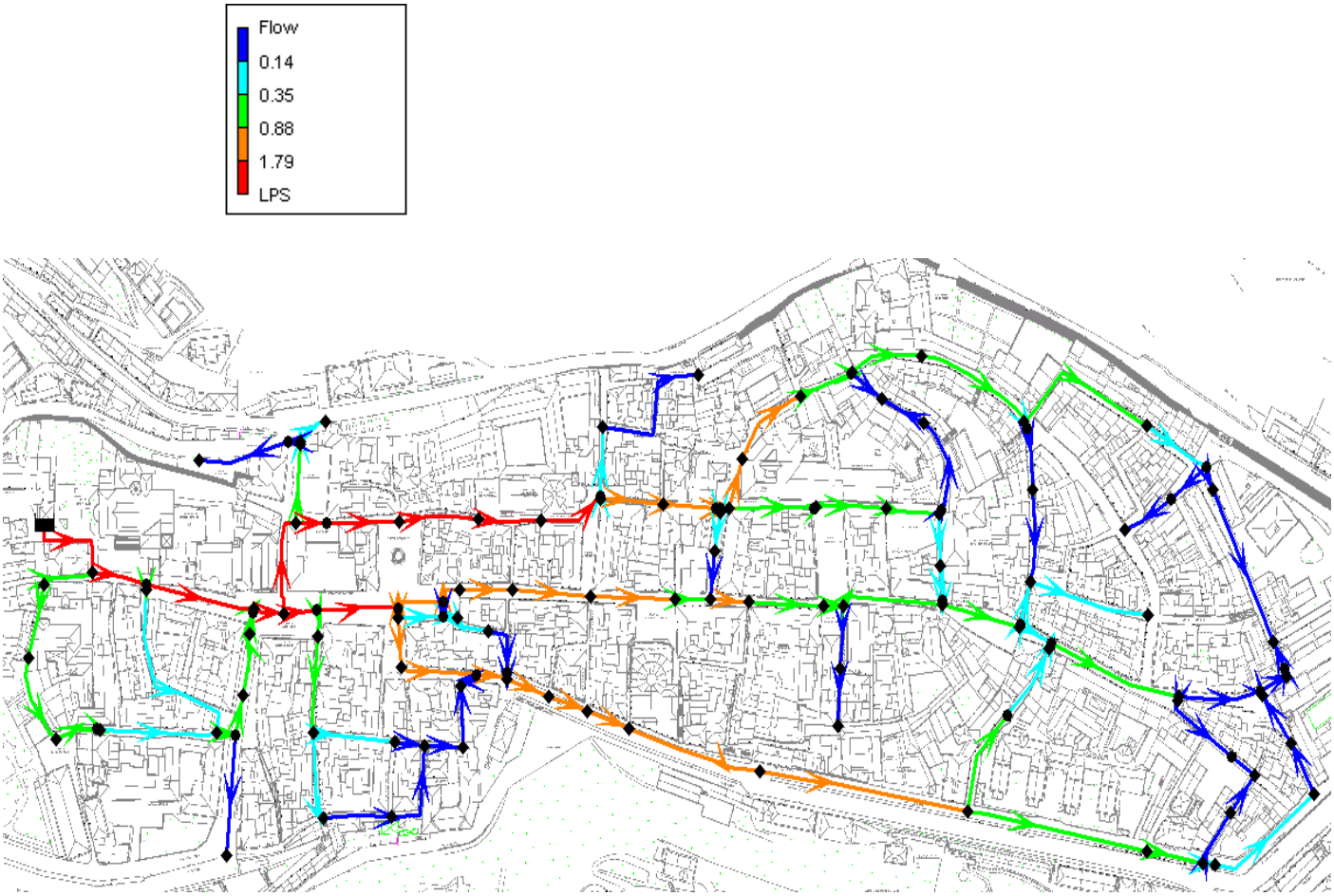


*Figure 24: Hydraulic network model in Epanet with indication of flow rate ranges flowing the pipelines.*

### 4.4.7. Procedure of Network subdivision in DMAs

**Identification of DMAs**

Genetic algorithms and other optimization criteria were not used to choose the DMAs in which divide the water district in exam, but it is preferred an empirical approach based on the minimization of the civil and hydraulic works to be carried out. After a careful analysis of the gate valves present and their maintenance, the network is divided into the following 5 sub-districts as shown in the Figure 25:

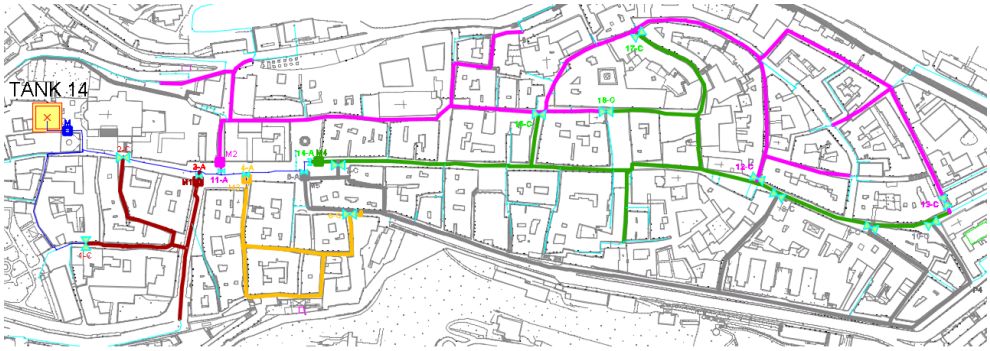


*Figure 25: District water network of historic Center of Osimo divided into 5 DMAs*

This subdivision allows to limit the intervention area related to the installation of all flow meters for monitoring the flow rates entering the districts. Another ways of dividing the district in DMAs would have led to greater installation costs and the need to install flow meters both inside and outside the DMAs. The only drawback of this re-layout of the WSS in the historic Center of Osimo is the high redundancy reduction of the hydraulic network. In fact,

before the subdivision in DMAs, the network had a remarkable reliability due to a topology composed of several closed meshes. After the process of subdivision into sub-districts, the closed meshes were cut at the closure of the gate valves, obtaining 5 branched open networks and only one of them connected to one closed mesh. Therefore, the subdivision carried out with the aim of minimizing the costs for civil and hydraulic works must be appropriately verified in terms of reliability and satisfaction of the water supply service provided to the end users of the network divided in DMAs.

**Evaluation of the reliability and hydraulic resilience of the network divided into DMAs**

The permanent subdivision in DMAs water distribution network modifies the original configuration of the acquired system by inserting numerous gate valves, which alter its hydraulic behaviour by increasing the hydraulic resistance and decreasing the redundancy of the water system. The goal is to define network structures compatible with the service levels of the end users and the good functioning of the WSS. It is advisable to use synthetic performance indices that allow to analyse the effects of performance alterations introduced with sub-districts [83].

The design of the water distribution networks has always been set up with the aim of obtaining reliable systems, in the sense of being able to ensure compliance with the standards pre-established service in the presence of extremely variable water requests in space and time [83].

The most commonly procedure followed for the design of water networks consists of creating meshed topologies, on the assumption that these structures guarantee high reliability thanks to the redundancy of the paths available in the network for the movement of water [84].

To verify the behavior of the network divided in DMAs, the same hydraulic model made for the starting network is elaborated, simulating the division in DMAs by inserting portions of pipeline with negligible length to be placed in the "closed" state on EPANET. In this way, these closed ducts simulate the behaviour of the penstocks that are closed for the division in the 5 DMAs.

Figure 26 shows the color map, indicating the range of pressures that occur in the network divided into DMAs in the peak hour of utility consumption:

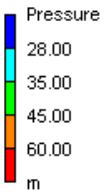

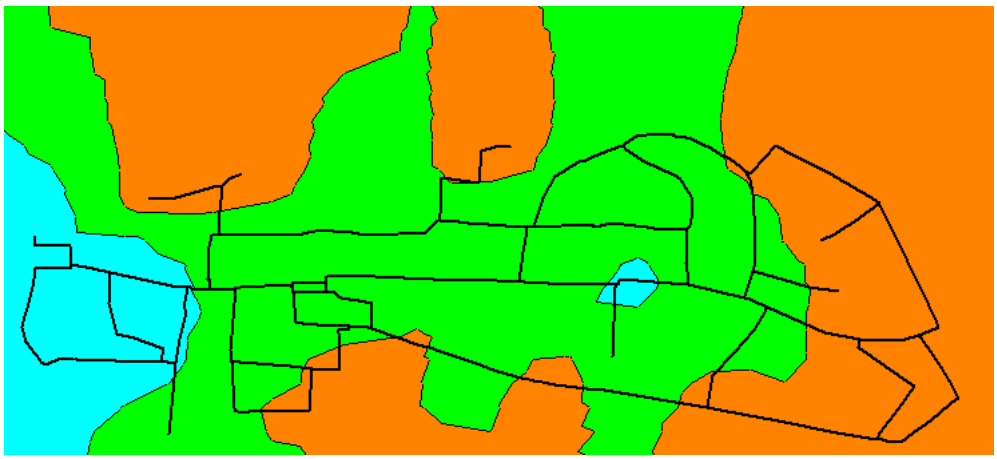

*Figure 26: Pressure head ranges of the water distribution network in exam divided into 5 DMAs*

From this first approximate visualization, the distribution of pressures in the nodes remained almost unchanged compared to that obtained for the water network without districts. The main reason lies in the size of the pipes, which is high compared to the supplied flow rates. Therefore, the pressure drops are low and the transformation of the closed mesh network into an open network does not have a great impact on the pressure drops thanks to the oversizing of the network.

To accurately assess whether the network divided in DMAs is reliable and resilient, the following assessments are made:

1. Check that the minimum pressure is always higher than the minimum one that must be guaranteed for the service;

2. Comparison between the minimum average and maximum pressure that occur in the network divided in DMAs and those without divisions [83];
3. Calculation of the performance index based on the resilience of the network, before and after the division in DMAs. It is clear that districts of an existing water network, carried out by inserting valves that cut one or more pipelines, change the topology of the network by increasing the internal energy dissipation. Therefore, the resilience index is an effective tool for comparing different district configurations, also presenting a close correlation with the average pressure of the network [83].

The minimum pressure head in the sub-districted network is equal to $h_{min}$= 29.44 m, higher than the minimum pressure head of 25 m to ensure 5 m of pressure head above the roofs of the highest building. After verifying that the pressure value is always higher than that necessary to guarantee the service to end users, minimum, maximum and average pressure in the original network are compared to those divided in DMAs in Table 27:

*Table 27: Minimum, average and maximum pressure head comparison between actual network and divided in DMAs one*

| | $h_{min}$[m] | $h_{av}$ [m] | $h_{max}$[m] |
|---|---|---|---|
| Starting Water network | 29.44 | 42.49 | 59.81 |
| Water network in DMAs | 29.44 | 42.38 | 59.76 |
| Difference % | 0 | 0.3% | 0.1% |

The minimum pressure did not change because it occurred in the node located near the compensation tank and it is not hydraulically involved in the re-layout of the network. The average and maximum pressure in the two situations also vary slightly. It can be deduced that the changes made to the network with the subdivision into DMAs did not greatly affect the pressures involved, making it reliable.

Finally, the absolute and relative resilience indexes are calculated, according to the following equations Eq. (46,47) [85, 86]:

$$I_r = 1 - \frac{P_D}{P_{Dmax}} = 1 - \frac{\gamma \cdot \sum_{j=1}^{Np} q_j \cdot H_{loss,j}}{\gamma \cdot \sum_{i=1}^{Nt} q_i \cdot H_i - \gamma \cdot \sum_{s=1}^{Nn} Q_s \cdot \bar{H}_s} \quad (46)$$

$$I_{r,d} = \left(1 - \frac{I_r^*}{I_r}\right) \cdot 100 = \left(\frac{P_D^* - P_D}{P_{Dmax} - P_D}\right) \cdot 100 \quad (47)$$

where $P_D$ is the power dissipated along the network, $P_D^*$ is the power dissipated along the network divided in DMAs, $P_{Dmax}$ is the maximum power that can be dissipated and it is evaluated as the difference between $P_A$, available power, and $P_N$, minimum total power required by the nodes for provide the service [85], $I_r^*$ is the resilience index of the network divided in DMAs. Instead, $H_{loss,j}$ is the head loss in the j-th pipeline, $q_j$is the water flow in the j-th pipeline, $q_i$ is the water flow supplied by the i-th tank, $H_i$is the total head of i-th tank, $Q_s$ is the flow rate delivered by the s-th node, $\bar{H}_s$ is the minimum hydraulic head required at the s-th node to guarantee the service. The resilience index of the original network is $I_r = 0{,}947$, while the index of the network divided in DMAs is equal to $I_r^* = 0{,}941$, both calculated with Eq.

(46). The relative resilience index, evaluated with Eq. (47), is therefore equal to $I_{r,d} = 0{,}64\%$. These values of $I_r$and $I_r^*$ close to 1 confirm that both the starting network and the one divided in DMA are hydraulically reliable [87] and the low relative value $I_{r,d}$ indicates that in the re-layout of the network the resilience of the network has not been affected [86]. After making these necessary checks, it is possible to proceed with the subdivision into previously designed 5 DMAs without compromising the service and good functioning of the distribution network.

### 4.4.8. District and end users smart meters design

**Smart flow meters in districts**

At this point it is necessary to design the hydraulic works and the smart flow meter to be installed on the pipelines of each DMAs. The following elements are important at this stage:

- The correct sizing of the flow meters, whose diameter does not always coincide with that of the pipeline on which it has to be installed. The correct choice of the diameter of the district meter must be based on the study of the range of flows that pass through it during the year. In fact, each flow meter is characterized by an error curve as a function of the flow rate that passes through it and by a range of operative flow rates. Therefore, the flow meters must have the diameters such that, for the annual range of flow rates passing through

the pipelines during the year, an error of between -2% and 2% is obtained. In this way, the precision of the meter measurements, especially at low flow rates, allows to accurate evaluate the water losses;

- Remote reading of the flow meters by means of a radio module for continuous transmission and integrated battery with a sufficiently long duration;
- The design of a correct civil-hydraulic work that allows to access to the flow meter for its inspection, maintenance and possible replacement and enable the continuity of the water service to end users in case of failures;

To evaluate the range of flows that pass through the districts that will be monitored by the smart flow meters, it is proceeded with two hydraulic simulations in Epanet, the first to evaluate the minimum annual flows and the second to verify the maximum annual flows. For the first aim, the "demand multiplier" is set on Epanet equal to $1{,}1 \cdot \overline{K}_{g,min} \cdot \overline{K}_{m,min} = 1{,}1 * 0{,}88 * 0{,}91 = 0{,}88$ evaluating the flow rates at 3.00, hour of minimum consumption with $\overline{K}_{h,min} = 0{,}55$.

For the second evaluation, it is used a "demand multiplier" equal to $1{,}1 \cdot \overline{K}_{g,max} \cdot \overline{K}_{m,max} = 1{,}1 * 1{,}12 * 1{,}20 = 1{,}49$ evaluating the flow rates at 10.00, hour of maximum consumption with $\overline{K}_{h,max} = 1{,}33$.

Figure 27 shows a planimetry that reports the range of flow rates that pass through the pipelines, where the district smart flow meters will be installed:

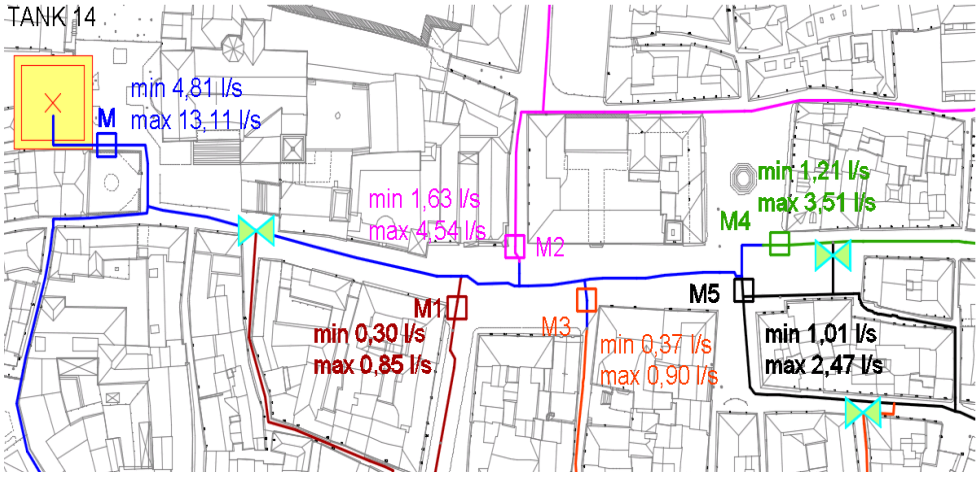


*Figure 27: Planimetry with positioning of the district smart flow meters and indication of the flow rate range*

It has been chosen the smart flow meter WESAN WP G, equipped with a clip-on radio module for the transmission of data using 868 Mhz radio frequency, to achieve the purpose of remote reading of the measurements of flow rates supplied in each district. In this way, building a fixed receiving infrastructure, it is possible to have remote reading of the hourly water flow rate curve entered in each district. Table 28 lists the operating flow rates of the Wesan meter, presenting the nominal diameter of each one:

*Table 28: Operating flow rates of Wesan smart flow meters*

| WESAN WP G | | | | |
|---|---|---|---|---|
| Nominal diameter | Q1 (l/s) (minimum flow rate) | Q2 (l/s) (transitional flow rate) | Q3 (l/s) (permanent flow rate) | Q4 (l/s) (Overload flow rate) |
| DN 50 | 0.18 | 0.28 | 11.11 | 13.89 |
| DN65 | 0.18 | 0.28 | 17.50 | 21.88 |
| DN80 | 0.28 | 0.44 | 27.78 | 34.72 |
| DN100 | 0.44 | 0.71 | 44.44 | 55.56 |
| DN125 | 0.44 | 0.71 | 44.44 | 55.56 |
| DN150 | 1.39 | 2.22 | 69.44 | 86.81 |

According to Figure 28 that shows the error diagram as a function of the flow rate, the error remains around 0% in the range of flow between the transitional flow rate $Q_2$ and the overload flow rate $Q_4$.

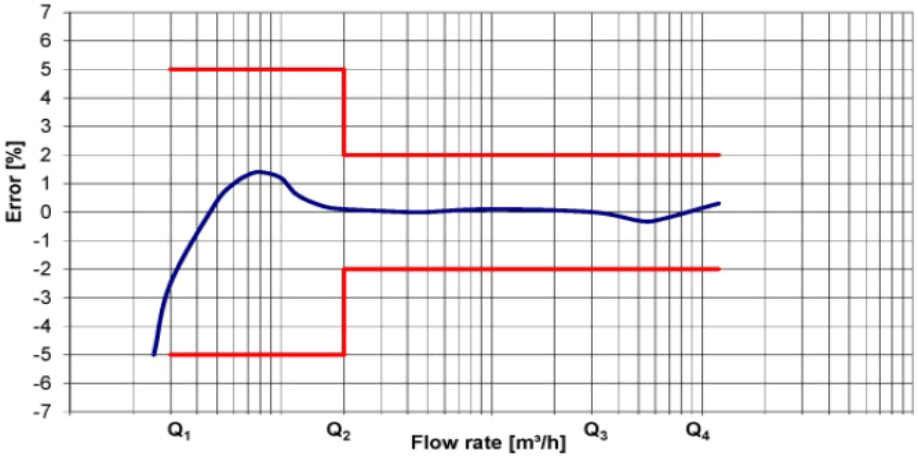


*Figure 28: Error curve of Wesan flow meter*

For this reason, a DN65 nominal diameter is chosen for the district meters, while it is installed a DN80 on the pipeline coming from the tank 14, as shown in Table 29. The choice of these diameters corresponds to the need for accuracy of measurement and preserves a high safety margin when greater flow rates with respect to rated conditions must pass through the pipeline.

*Table 29: Design of nominal diameter of district smart flow meters*

| District smart meter | Pipeline Diameter | Qmin [l/s] demand multiplier = 0,88 at hour 3:00 | Qmax [l/s] demand multiplier = 1,49 at hour 10:00 | Nominal Diameter Smart meter |
|---|---|---|---|---|

| | | | | |
|---|---|---|---|---|
| M (in distribution pipeline of the tank) | DN150 | 4.81 | 13.11 | DN80 |
| M1 | DN100 | 0.30 | 0.85 | DN65 |
| M2 | DN150 | 1.63 | 4.54 | DN65 |
| M3 | DN100 | 0.37 | 0.90 | DN65 |
| M4 | DN150 | 1.21 | 3.51 | DN65 |
| M5 | DN150 | 1.01 | 2.47 | DN65 |

The district flow meter is installed on a hydraulic by-pass in parallel to the existing main pipeline. The by-pass pipeline is the same as the nominal diameter of the meter so that neither diverging nor converging elements have to be used. Two sections having 5 times the nominal diameter of the meter are placed downstream and upstream of the flow meter so that the flow is as laminar and undisturbed as much as possible. Two gate valves are placed at the beginning and at the end of the by-pass. Another gate valve is installed on the main pipe. In normal operating conditions, the water passes through the by-pass, while the gate valve of the main pipeline is kept closed. On the other hand, in case of failures or its maintenance, the gate valves of the by-pass are closed, while the one situated on the main pipeline is reopened allowing the continuity of the water supply to end users. Figure 29 shows a graphic

diagram of the by-pass with water meter, while Figure 30 displays a photo taken during the realization of by-pass.

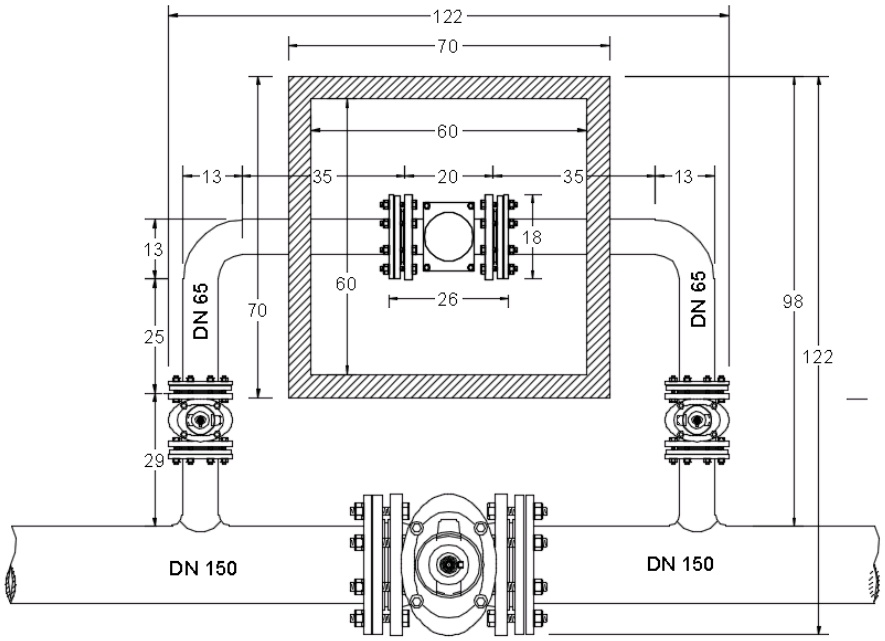


*Figure 29: District smart flow meter installation diagram*

*Figure 30: Photo of hydraulic by-pass with smart flow meter*

**End users smart flow meters**

It is necessary to proceed with a massive replacement campaign of end user meters with smart flow meters in order to have the hourly data of the water consumption of each user that can be remotely read. These data allow to elaborate water balances in each district, to investigate and eliminate the water losses downstream of the user meters, to quantify the consumption of end users in the night in each district in order to accurately calculate the total water losses in each district, starting from the measured MNF from the district flow meters using the following equation Eq. (48) applied to a time t:

$$\bar{Q}_{loss,d,t} = MNF(t) - HNU(t) - NHNU(t) \quad (48)$$

At the end of the massive replacement campaign, it will be possible to have the hourly curves of the authorized consumption measured, to identify any unauthorized consumption, to reduce measurement errors related to the measured consumptions thanks to the greater precision of the new flow meters. In the experimentation phase of this technology, it is decided to use both ultrasonic static meters equipped with an integrated 868 Mhz radio module and volumetric meters equipped with an 868 Mhz clip-on radio module applied above the meter.,

The volumetric flow meter transmits a non-programmable telegram via radio every 15 minutes and measures the volumes of water, while the static meter transmits a programmable telegram every 64 seconds and it is able to measure in addition to the volumes transited, also the water flow rate, the temperature and the water volumes that passes through the flow meter in the opposite direction. Both flow meters interact with the remote reading infrastructure in a unidirectional manner by means of 868 MHz radio waves, i.e. they transmit signals, but they do not receive the signals and, during the data transmission phase, they communicate with two protocols, one wireless M-bus OMS (open metering system) and the other wireless M-bus R4 (proprietary protocol).

Table 30 lists the number of active flow meters to be replaced in each district:

*Table 30: Number of active end users in each DMA*

| DMA | M | M1 | M2 | M3 | M4 | M5 |
|---|---|---|---|---|---|---|
| END USER ACTIVE METERS | 100 | 110 | 650 | 140 | 400 | 250 |

Figures 31a-b shows images related to the substitution of meters in two niches, one with smart volumetric meters and one with smart ultrasonic meters.


*Figure 31 a: Battery of smart volumetric meters*


*Figure 31 b: Battery of smart ultrasonic meters*

### 4.4.9. Infrastructure and cloud system for remote reading and water network management

In parallel with the design and installation of the flow meters, the design and installation of the remote reading infrastructure and the data management of the districts, as well as the water loss analysis, must be done.
The study of the different technologies led to the creation of the solution for remote reading and monitoring of the districts, which is essentially based on

an infrastructure used for remote reading the data plus a platform for their visualization, management, extraction and analysis.

The infrastructure for remote reading consists of 2 radio receiving stations located in the Center of Osimo that allow to cover the entire territory where the flow meters are installed. A high reading frequency generates a significant amount of data that allows managers to view real-time, log consumption and analyse/verify them. Consumptions can be displayed when required, reading intervals that are freely programmable and modifiable at any time. The meters send the data only in one direction to the RDC receivers, which communicate via GPRS to the FTP server using a SIM card (one for each receiver) with active data service. In this way, the flow meter data is collected by the FTP server.

The remote reading system with 868 MHz frequency has been adopted, resulting in the best in terms of signal stability, hybrid solutions, standard protocols, possibility of billing and use for monitoring and analysis, ensuring the reception of signals from flow meters placed in places shielded. The 169 MHz frequency was excluded because it was inadequate for transmission through thick obstacles and within dense urban fabrics.

In the investigation and design phase, the various 868 MHz radio technologies for remote reading of meters were evaluated, leading to the choice of the reception infrastructure with double protocol:

- wireless M-bus 868 MHz OMS (open metering system);
- 868 MHz R4 wireless M-bus which, compared to the OMS standard 868 W-MBus protocol, offers far superior performance.

R4 technology has the following benefits [88]:

- Distance increase of 3 times (coverage range for W-MBus 868 Mhz OMS of 500m, for R4 of 1500m) and 9 times the area covered;
- Increase of performances;
- high reception stability;
- drastic reduction of receivers, no concentrator.

The double radio communication protocol used by both flow meters and infrastructure offers the following advantages:

- in standard conditions, the greater coverage area of the proprietary protocol is exploited by acquiring telegram R4;
- this system integrates with the mobile radio walk-by / drive-by remote reading technology which acquires the standard wireless W-bus 868 MHz OMS protocol;
- the infrastructure remains is prepared to acquire any other type of smart flow meter equipped with 868 MHz OMS radio transmission, with the limitation of the reduced acquisition distance.

The technology based on the LORAWAN protocol was discarded because it is subject to temporary authorizations by the MISE of 180 days' renewable for experimentation for private use (Article 123 of the Electronic Communications Code, Legislative Decree 259/2003). However, nothing excludes that in the future the LORA system may be deepened by virtue of greater liberalization in the use of this protocol.

Figure 32 illustrates a satellite display of planimetry with the identification of the sites, where the two radio receiving stations are located with the

representation of the guaranteed radio coverage in the water district of the project:

**Receiver location ABAE:**
On top of water tank
Assumed height: 27m
Latitude: 43.486336
Longitude: 13.479662
Antenna directions: 100° and 190°

**Receiver location Astea 1:**
On top of Church
Assumed height: 17m
Latitude: 43.485550
Longitude: 13.489299
Antenna directions: 180° and 280°

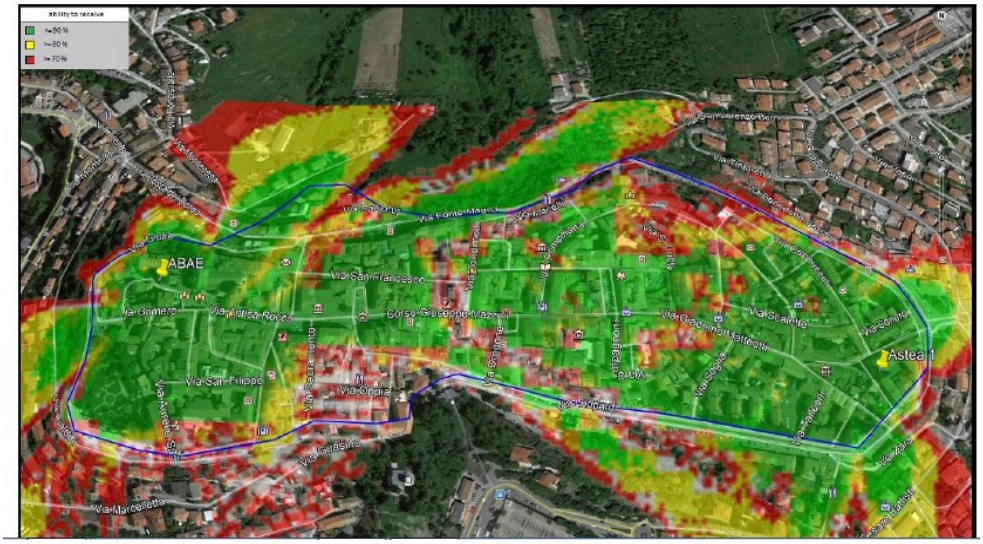


*Figure 32: Satellite representation of the radio area covered by the two radio receiving stations*

For the visualization, management and analysis of data there are two possible choices:

1) Have an internal company Server in which to collect the data sent by the meters installed remotely and use a management software on a PC connected to the internal Server. This system has the advantage of not having to pay

annual fees for data management through a cloud portal provided by third parties, but the burden of having to have a Server, of having to program the management software by yourself and the fact of not being a versatile and open system in case the data serves a superior control architecture;

2) Purchase the license for accessing a cloud portal set up by third parties that communicates with the external server that acquires the data of the meters that allow access from any laptop with internet. This solution allows considerable flexibility for its communication with other monitoring platforms, does not require the installation of an internal server and has already implemented all those useful functions for the management and analysis of the available data.

For this research project, it is chosen the solution with the cloud portal which is a web-based application of a flow meter data management software running as a service on an external high security data center.

This cloud portal provides all key features for efficient processing of metering data and easy administration of meter reading via Fixed Network or Walk-By / Drive-By. The used system integrates a map view for easy organisation of devices and readout tours; in-built task scheduler to facilitate meter import/export and analysis jobs and use REST API (Application Programming Interface) for easily connecting third party software and a quick implementation process. Other important functions are the possibility to create individual analyses for leakage reporting, virtual meters, water network monitoring and optimisation and other media specific analysis. It also allows

you to homogeneously integrate the data acquired with the fixed infrastructure and those received with the mobile walk-by system.

### 4.4.10. Reduction of water losses and economic benefits by real time monitoring of DMAs of water district

**Analysis of water balances of each DMA through the monitoring software**

The research of water losses in each of the 5 sub-districts is carried out with the support of the portal for remote reading and data analysis. In mid-2020, the activities allowed to proceed with the monitoring of water losses using the MNF recorded by the smart flow meters of each sub-district, while the value of the night consumption of the sum of users in each district was not yet available. This is because at the end of the first semester of 2020 the calibration and orientation of the remote reading system antennas had not been completed and the cloud portal module related to the analysis of the water balances of each district had not yet been implemented. Although the end users' smart flow meters had already been replaced by September, their aggregate data was not yet available remotely.

Therefore, the identification and intervention procedure for the reduction of losses and the results obtained may in the future be further refined and improved. In the meantime, the water leak research is done using the hourly curves of the remote read flow rates of the district meters.

To explain how this was done, it is explained the procedure followed to reduce water losses:

1) Analysis of the trend of the hourly curve and the daily curve of the flow rates introduced into each water district;

2) Evaluation of the trend of the minimum night flow and the average daily flow;

3) Identification of a growing trend of both values, an indication of the onset or increasing of water losses in the distribution network located in the water district area. In the case of an increase in the minimum night flow rate, it is necessary to evaluate the overall trend over time to determine whether it is due to an abnormal night consumption of some end users or to the increase in physical and / or apparent losses. When both the remote reading software and the fixed infrastructure are completed, this will be immediately verifiable remotely by comparing hour by hour the MNF with the water night consumption of the district.

4) Reporting the work team assigned to seek water leaks of the onset of a new leak or the worsening of an existing but hidden leak;

5) Local worker research intervention using noise loggers, hydraulic tests and auscultation of the pipelines;

6) Repair of the breaking;

7) Monitoring and quantification of the effects of the repair on water losses;

8) Checking the effectiveness of the intervention over time.

As an example, the identification of the water leakage in the M4 district on 12 October 2020 is reported through the illustration of Figure 33:

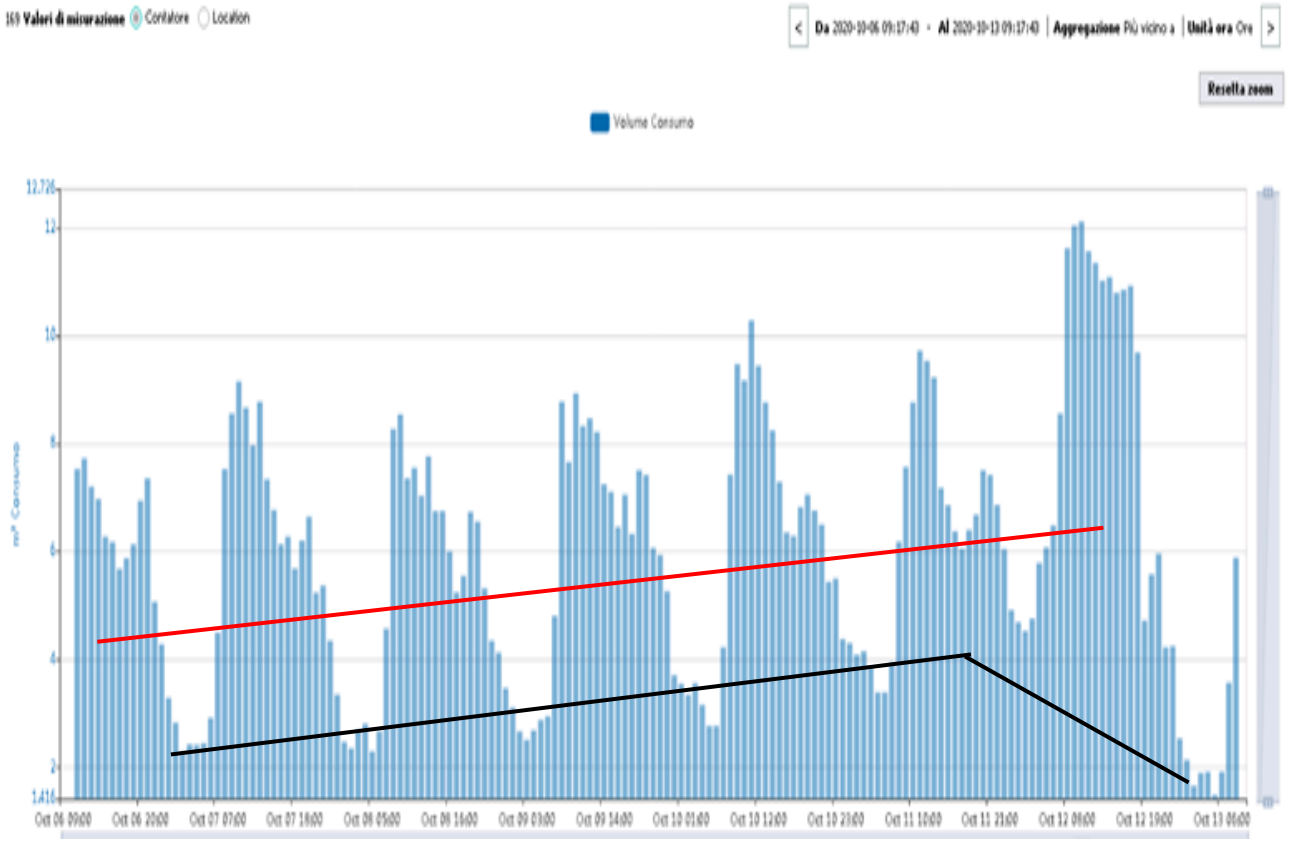
169 Valori di misurazione
Contatore
Location
Da 2020-10-06 09:17:43
Al 2020-10-13 09:17:43
Aggregazione Più vicino a
Unità ora Ore
Resetta zoom
Volume Consumo
m³ Consumo
12.726
12
10
8
6
4
2
1.416
Oct 06 09:00
Oct 06 20:00
Oct 07 07:00
Oct 07 18:00
Oct 08 05:00
Oct 08 16:00
Oct 09 03:00
Oct 09 14:00
Oct 10 01:00
Oct 10 12:00
Oct 10 23:00
Oct 11 10:00
Oct 11 21:00
Oct 12 09:00
Oct 12 19:00
Oct 13 06:00

*Figure 33: Trend of MNF and average daily flow rate of district M4 in the 2° week of October 2020*

The hourly curve shown in Figure 33 shows between 7 October and 12 October a constant increase in the MNF from 2.09 $m^3/h$, reaching the value of 4.53 $m^3/h$.

The average daily flow rate and the maximum daily flow rate are also gradually increased over the same time period by an amount similar to the increase in MNF. These data have been interpreted as a rupture arising in the pipelines of the M4 district, which has expanded over the days. After the report, the workers went to the field, effectively detecting a hidden leak in c.so Mazzini (course of the historic center of the M4 sub-district) and repairing it. Immediately after this repair, which took place between 18:00 and 19:00 on 12 October, the flow rates circulating in the district decreased and on the night of 13 October there was a MNF equal to 1.52 $m^3/h$. These data also allow to quantify the effect of the repair on water losses which is equal to 4.53-1.52 = 3.01 $m^3/h$. tTe non-timely intervention reported by these data would have caused the worsening of this breakage and loss, the repair of which would have taken place only when its extent allowed the identification upon notification.

**Estimation of the energy and economic savings by reducing of water losses**

The repairs of the district distribution network pipelines were mainly concentrated in the period of August and then continue in the following

months with further interventions to remedy the onset of new breakage and repairing the remaining ones. Obviously, some sub-districts have been subjected to greater interventions and attention than others, especially in the context where water losses can cause damage to buildings and caves underlying the water network. Therefore, the improvements are more marked in some districts (e.g. M4 and M1) than in others. The baseline value of MNF refers to the month of July and it is used to evaluate the reduction of water losses in the following months.

To evaluate the energy savings in terms of lower electricity consumed by the pumps, it must be considered that every cubic meter of water to be supplied to the district in exam must be pumped from the water pumping station A to the tank 13 and from the tank 13 to tank 14 by another pumping group. The two pumps consume 0.98 $\mathrm{kWh/m^3}$and 0,19 $\mathrm{kWh/m^3}$ respectively. Furthermore, two thirds of the cubic meters supplied to the district come from the water wells whose pumps consume 0,15 $\mathrm{kWh/m^3}$, while the remaining third comes by gravity from the Castreccioni dam at a cost of $C_w$ = 0,28 $€/\mathrm{m^3}$.

To evaluate the avoided water losses $\mathrm{V_{loss,avoided}}$, the reduction in electricity consumption of the pumps $Ee_{saving}$ the following relations Eq. (49,50) are used:

$$\mathrm{V_{loss,avoid}} = \left|\mathrm{MNF_{bas}} - \mathrm{MNF_j}\right| \cdot \mathrm{t} \quad (49)$$

$$Ee_{saving} = \mathrm{V_{loss,avoid}} \cdot \sum_{i=1}^{n} \mathrm{E_{e,i}} \quad (50)$$

The equations Eq. (49 ,50) are determined by considering the current unavailability of the aggregate data of end users' water consumption. When the system will be fully operative, the evaluation of $V_{loss,avoid}$ will be performed by comparing the water balances between the volumes introduced and those consumed in each district during a period of time t. The evaluation in terms of reduction of water losses and energy saving is reported weekly, starting from September, in Table 31:

*Table 31: Water losses reduction and energy savings for each sub-district (M1-M2-M3-M4-M5) during the period September-December 2020*

| DISTRICT M1 | | | |
|---|---|---|---|
| WEEK | MNF[m3/h] | WATER LOSSES REDUCTION [m3] | Energy Savings[kWh] |
| BASELINE | 0.720 | | |
| 1°SEPTEMBER | 0.667 | 8.960 | 11.818 |
| 2°SEPTEMBER | 0.719 | 0.240 | 0.317 |
| 3°SEPTEMBER | 0.811 | - | - |
| 4°SEPTEMBER | 0.691 | 4.800 | 6.331 |
| 1°OCTOBER | 0.574 | 24.480 | 32.289 |
| 2°OCTOBER | 0.283 | 73.440 | 96.867 |
| 3°OCTOBER | 0.177 | 91.200 | 120.293 |
| 4°OCTOBER | 0.159 | 94.320 | 124.408 |
| 1°NOVEMBER | 0.103 | 103.680 | 136.754 |
| 2°NOVEMBER | 0.086 | 106.560 | 140.553 |
| 3°NOVEMBER | 0.063 | 110.400 | 145.618 |

| | | | |
|---|---|---|---|
| 4°NOVEMBER | 0.053 | 112.080 | 147.834 |
| 1°DECEMBER | 0.051 | 112.320 | 148.150 |
| TOTAL | | 842.480 | 1,111.231 |

| DISTRICT M2 | | | |
|---|---|---|---|
| WEEK | MNF[m3/h] | WATER LOSSES REDUCTION [m3] | Energy Savings[kWh] |
| BASELINE | 3.95 | | |
| 1°SEPTEMBER | 3.842 | 18.200 | 24.006 |
| 2°SEPTEMBER | 3.969 | - | - |
| 3°SEPTEMBER | 3.814 | 22.800 | 30.073 |
| 4°SEPTEMBER | 3.756 | 32.640 | 43.052 |
| 1°OCTOBER | 3.531 | 70.320 | 92.752 |
| 2°OCTOBER | 3.391 | 93.840 | 123.775 |
| 3°OCTOBER | 3.621 | 55.200 | 72.809 |
| 4°OCTOBER | 3.526 | 71.280 | 94.018 |
| 1°NOVEMBER | 3.527 | 71.040 | 93.702 |
| 2°NOVEMBER | 3.420 | 89.040 | 117.444 |
| 3°NOVEMBER | 3.360 | 99.120 | 130.739 |
| 4°NOVEMBER | 3.359 | 99.360 | 131.056 |
| 1°DECEMBER | 3.234 | 120.240 | 158.597 |
| TOTAL | | 843.080 | 1,112.023 |

| DISTRICT M3 | | | |
|---|---|---|---|
| WEEK | MNF[m3/h] | WATER LOSSES REDUCTION [m3] | Energy Savings[kWh] |
| BASELINE | 0.40 | | |

| | | | |
|---|---|---|---|
| 1°SEPTEMBER | 0.288 | 18.760 | 24.744 |
| 2°SEPTEMBER | 0.307 | 15.600 | 20.576 |
| 3°SEPTEMBER | 0.353 | 7.920 | 10.446 |
| 4°SEPTEMBER | 0.386 | 2.400 | 3.166 |
| 1°OCTOBER | 0.344 | 9.360 | 12.346 |
| 2°OCTOBER | 0.323 | 12.960 | 17.094 |
| 3°OCTOBER | 0.337 | 10.560 | 13.929 |
| 4°OCTOBER | 0.347 | 8.880 | 11.713 |
| 1°NOVEMBER | 0.294 | 17.760 | 23.425 |
| 2°NOVEMBER | 0.327 | 12.240 | 16.145 |
| 3°NOVEMBER | 0.346 | 9.120 | 12.029 |
| 4°NOVEMBER | 0.329 | 12.000 | 15.828 |
| 1°DECEMBER | 0.334 | 11.040 | 14.562 |
| TOTAL | | 148.600 | 196.003 |

| M4 | | | |
|---|---|---|---|
| WEEK | MNF[m3/h] | WATER LOSSES REDUCTION [m3] | Energy Savings[kWh] |
| BASELINE | 2.97 | | |
| 1°SEPTEMBER | 1.517 | 244.160 | 322.047 |
| 2°SEPTEMBER | 1.699 | 213.600 | 281.738 |
| 3°SEPTEMBER | 1.641 | 223.200 | 294.401 |
| 4°SEPTEMBER | 1.797 | 197.040 | 259.896 |
| 1°OCTOBER | 2.570 | 67.200 | 88.637 |
| 2°OCTOBER | 1.386 | 266.160 | 351.065 |
| 3°OCTOBER | 1.369 | 269.040 | 354.864 |
| 4°OCTOBER | 1.651 | 221.520 | 292.185 |
| 1°NOVEMBER | 1.540 | 240.240 | 316.877 |

| | | | |
|---|---|---|---|
| 2°NOVEMBER | 1.111 | 312.240 | 411.845 |
| 3°NOVEMBER | 1.284 | 283.200 | 373.541 |
| 4°NOVEMBER | 1.279 | 284.160 | 374.807 |
| 1°DECEMBER | 1.191 | 298.800 | 394.117 |
| TOTAL | | 3,120.560 | 4,116.019 |

| M5 | | | |
|---|---|---|---|
| WEEK | MNF[m3/h] | WATER LOSSES REDUCTION [m3] | Energy Savings[kWh] |
| BASELINE | 1.90 | | |
| 1°SEPTEMBER | 1.690 | 35.280 | 46.534 |
| 2°SEPTEMBER | 1.799 | 17.040 | 22.476 |
| 3°SEPTEMBER | 1.953 | - | - |
| 4°SEPTEMBER | 1.574 | 54.720 | 72.176 |
| 1°OCTOBER | 2.096 | - | - |
| 2°OCTOBER | 1.984 | - | - |
| 3°OCTOBER | 1.767 | 22.320 | 29.440 |
| 4°OCTOBER | 1.817 | 13.920 | 18.360 |
| 1°NOVEMBER | 1.799 | 17.040 | 22.476 |
| 2°NOVEMBER | 1.577 | 54.240 | 71.543 |
| 3°NOVEMBER | 1.207 | 116.400 | 153.532 |
| 4°NOVEMBER | 0.981 | 154.320 | 203.548 |
| 1°DECEMBER | 1.193 | 118.800 | 156.697 |
| TOTAL | | 604.080 | 796.782 |

To evaluate the economic savings obtained, it must be considered that each kWh consumed by the pumps costs an average of $F_{ec}$ = 0,16 €/kWh. For its evaluation, it is used Eq. (51) and results reported in Table 32.

$$\mathbf{EC_{saving}} = Ee_{saving} \cdot \mathrm{F_{ec}} + a \cdot \mathrm{V_{loss,avoid}} \cdot C_w \quad (51)$$

*Table 32: Total energy and economic savings obtained with water losses reduction during the period September-December 2020*

| WEEK | TOTAL Energy Savings[kWh] | TOTAL Economic Savings[kWh] |
|---|---|---|
| 1°SEPTEMBER | 429.150 | € 108.72 |
| 2°SEPTEMBER | 325.107 | € 82.36 |
| 3°SEPTEMBER | 334.920 | € 84.85 |
| 4°SEPTEMBER | 384.620 | € 97.44 |
| 1°OCTOBER | 226.024 | € 57.26 |
| 2°OCTOBER | 588.802 | € 149.16 |
| 3°OCTOBER | 591.334 | € 149.80 |
| 4°OCTOBER | 540.684 | € 136.97 |
| 1°NOVEMBER | 593.233 | € 150.29 |
| 2°NOVEMBER | 757.528 | € 191.91 |
| 3°NOVEMBER | 815.459 | € 206.58 |
| 4°NOVEMBER | 873.072 | € 221.18 |
| 1°DECEMBER | 872.123 | € 220.94 |
| TOTAL | 7,332.057 | € 1,857.45 |

In the period between September and November 2020, it is obtained a $Ee_{saving}$=7,332 kWh and $\boldsymbol{EC_{saving}}$=1,857.45 € as reported in Table 32. Considering to keep the result obtained in terms of MNF in each district and water losses reduction in these three months until the end of August 2021, it is achieved a $Ee_{saving}$= 38,728 kWh and $\boldsymbol{EC_{saving}}$= 9,811.214 €.

This is the economic saving linked exclusively to the reduction of pump consumption. In reality, the evaluation is much more complex because it considers the remuneration in the tariff by the authority, the reduction of costs for reading the volumes consumed by end users for issuing of bills and other benefits due to the support of remote reading in the provision of the service and management of the network. Considering that the search for water losses was carried out using only the district water meters in this first period, to get an idea of the PBP and the NPV, it is evaluated as costs only the cost of the fixed remote reading infrastructure and the annual cost of the cloud portal for monitoring the acquired data. Instead, to evaluate the revenues on a 20-year time horizon, it is considered to maintain over time the MNF result achieved at the end of the first week of December 2020. The fixed remote reading infrastructure costs 20,000 €, while the annual cost of the cloud portal for data management is equal to 8,300 € for the first year and 7,500 € for the following years. Instead, the revenues due to the reduction of water losses amounted to 9,811.214 € for the first year and 11,520.33 € for the following years. The PBP of the investment is 7 years with a 20-year NPV equal to 34,405.10 €.

## 4.5 Conclusions

In this third part of the thesis, a procedure for seeking and reducing water losses by subdividing the water distribution networks in DMAs and the hourly monitoring of the flow rates entered in each DMA and the consumption of the end users of the districts has been developed. To achieve the goal of hourly

monitoring, an innovative fixed 868 MHz radio reception infrastructure was installed without the use of radio concentrators with communication protocol that allows to triple the coverage distance and a cloud portal connected to the software was set up.

In the last 4-5 months of the year 2020, the water losses were monitored, determined and quantified by analysing the MNF trend and the hourly trend of the flows introduced in the 5 districts. In this way, it was possible to promptly report the presence or the onset and the trend of water leaks in the different areas of the historic Center of Osimo and it was possible to intervene to repair the broken pipes.

This developed methodology has allowed not only to implement a sub-districtization that does not change the hydraulic resilience and the quality of the water network service, but also to make the system more efficient by reducing the volumes of water supplied to the compensation tank by the pumping, reducing the consumption of electricity and the costs incurred to provide end users with the necessary water. Specifically for this demonstration site in the period between September and November 2020, it was reached an energy saving $Ee_{saving}$= 7,332 kWh and an economic saving $\boldsymbol{EC_{saving}}$= 1,857.45 €, without neglecting the environmental benefit of not having dispersed 5,558.8 $m^3$ of potable water along the network. Considering only the use of district smart meters for water losses detection, the PBP of the investment is 7 years with a 20-year NPV equal to 34,405.10 €.

# 5. Final conclusions

The aim of this thesis is to develop strategies to improve WSS efficiency in terms of reduction of energy consumed by water pumping systems. To pursue this goal, three general methodologies were developed and then applied to the case study of Osimo WSS, achieving significant energy savings.

Chapter 2 deals with energy efficiency interventions where the water is used for the power production through hydropower plant where the water is used for the self-consumption purposes. In particular, preloading tanks installed between the water source and the load/head compensation tanks connected through gravity adduction pipelines have been analysed to apply the previous energy recovery solution. In this first work, a methodology to estimate the average flow rate in a gravity adduction pipeline upstream the preloading tank of a WSS located in Osimo, Center of Italy, has been developed. This methodology is based on the electric energy consumption of the pumping station, since the sum of flow rates supplied by each pump is equal to the one flowing in the gravity adduction pipeline reduced by the flow rate coming from wells. Then, a Pelton turbine has been selected for recovering the water energy content, supplying electricity to the pumping station.

In the year 2018, an energy saving equal to 475.26 MWh (88.87 TOE and 204.36 $tCO_2$) is obtained in year 2018, which results to a gross economic saving of 94.29 k€/year. In year 2019 it is obtained an energy saving equal to

507.77 MWh which corresponds to the electric energy reduction in withdrawal from the grid by the water pumping station A.

Chapter 3 describes the second work, based on a development of a methodology capable of estimating the yearly average flow rate in gravity adduction pipelines of a WSS. This procedure is useful to monitor the WSS network and to consider possible energy efficiency interventions, since flow meters are not always present due to their high cost.

The proposed methodology consists of a straightforward procedure based on the water consumption of the end users connected to a WSS. Indeed, these data can be used to assess the energy recovery potential: specifically, in this second work, the application of Pumps-as-Turbines (PaTs) is considered. The performance evaluation of these machines was carried out through a methodology, already available in literature, that consists of forecasting both Best Efficiency Point (BEP) and off-design performance of the hydraulic machines in turbine mode.

Considering the installation of PaTs in some of the gravity adduction pipelines of the analysed WSS, the possible total energy recovery is equal to 90,757 kWh and the total gross economic saving is 14,167 €/year, with further advantages if energy efficiency certificates are also taken into account. In particular, the installation with the highest potential energy recovery can lead to an NPV after twenty years equal to 52,843 € and a PBP of approximately 6 years.

In the third part of this thesis (Chapter 4), a procedure for seeking and reducing water losses by subdividing the water distribution networks in

DMAs and by the hourly monitoring of the flow rates entered in each DMA and the consumption of the end users in the districts has been developed. This method was applied to a water district network situated in the historical Center of Osimo. To achieve the goal of hourly monitoring, an innovative fixed 868 MHz radio reception infrastructure was realized.

In the last 4-5 months of the year 2020, the water losses were monitored, determined and quantified through the analysis of the MNF trend and the hourly trend of the water flows introduced in the 5 DMAs in which the water network of the historic Center of Osimo was subdivided.

This methodology allowed to make the WSS more efficient by reducing the volumes of water supplied by the pumps to the compensation tanks 13 and 14, reducing the consumption of electricity. In the period between September and November 2020, an energy saving $Ee_{saving}$= 7,332 kWh and an economic saving $EC_{saving}$= 1,857.45 € have been reached together with an environmental benefit of 5,558.8 $m^3$ of potable water saved. This water reduction methodology lead to an investment with a PBP of 7 years with a 20-year NPV equal to 34,405.10 €.

# References

[1] W. Hickman, A. Muzhikyan, A.M. Farid, The synergistic role of renewable energy integration into the unit commitment of the energy water nexus, Renewable Energy, Year 2017, Vol. 108, Pages 220-229.

[2] E. Ahmadi, B. McLellan, T. Tezuka, The economic synergies of modelling the renewable energy-water nexus towards sustainability, Renewable Energy, Year 2020, Vol. 162, Pages 1347-1366.

[3] J.C. Alberizzi, M. Renzi, M. Righetti, G.R. Pisaturo, M. Rossi, Speed and Pressure Controls of Pumps-as-Turbines Installed in Branch of Water-Distribution Network Subjected to Highly Variable Flow Rates, Energies, Year 2019, Vol. 12(24), Article 4738.

[4] M. Stefanizzi, T. Capurso, G. Balacco, M. Binetti, S.M. Camporeale, M. Torresi, Selection, control and techno-economic feasibility of Pumps as Turbines in Water Distribution Networks, Renewable Energy, Year 2020, Vol. 162, Pages 1292-1306.

[5] N.F. Tumen Ozdil, A. Tantekin, Exergy and exergoeconomic assessments of an electricity production system in a running wastewater treatment plant, Renewable Energy, Year 2016, Vol. 97, Pages 390-398.

[6] M. Renzi, P. Rudolf, D. Štefan, A. Nigro, M. Rossi, Installation of an axial Pump-as-Turbine (PaT) in a wastewater sewer of an oil refinery: A case study, Applied Energy, Year 2019, Vol. 250, Pages 665-676.

[7] T. Lydon, P. Coughlan, A. McNabola, Pressure management and energy recovery in water distribution networks: Development of design and selection methodologies using three pump-as-turbine case studies, Renewable Energy, Year 2017, Vol. 114, Pages 1038-1050.

[8] A. Strazzabosco, S.A. Conrad, P.A. Lant, S.J. Kenway, Expert opinion on influential factors driving renewable energy adoption in the water industry, Renewable Energy, Year 2020, Vol. 162, Pages 754-765.

[9] C.M. Papapostolou, E.M. Kondili, D.P. Zafirakis, G.T. Tzanes, Sustainable water supply systems for the islands: The integration with the energy problem, Renewable Energy, Year 2020, Vol. 146, Pages 2577-2588.

[10] X. Liu, Y. Tian, X. Lei, H. Wang, Z. Liu, J. Wang, An improved self-adaptive grey wolf optimizer for the daily optimal operation of cascade

pumping stations, Applied Soft Computing, Year 2019, Vol. 75, Pages 473-493.

[11] W. Chen, T. Tao, A. Zhou, L. Zhang, L. Liao, X. Wu, K. Yan, C. Li, T.C. Zhang, Z. Li, Genetic optimization toward operation of water intake-supply pump stations system, Journal of Cleaner Production, Year 2021, Vol. 279, Article 123573.

[12] X. Zou, H. Huang, L. Li, Z. Liu, An Improved Energy-Saving Design Method for Drive System with Multi Motor-Pumps by Using Genetic Algorithm, Procedia CIRP, Year 2019, Pages 79-83.

[13] C. Zhang, L. Wang, H. Li, Optimization method based on process control of a new-type hydraulic-motor hybrid beam pumping unit, Measurement, Year 2020, Vol. 158, Article 107716.

[14] A. Mamade, D. Loureiro, D. Covas, H. Alegre, Energy Auditing As a Tool for Improving Service Efficiency of Water Supply Systems, Procedia Engineering, Vol. 89, Year 2014, Pages 557-564.

[15] C. Huang, Y. Li, X. Li, H. Wang, J. Yan, X. Wang, J. Wu, F. Li, Understanding the water-energy nexus in urban water supply systems with cities features, Energy Procedia, Vol. 152, Year 2018, Pages 265-270.

[16] M.R. Nogueira Vilanova, J.A. Perrella Balestieri, Energy and hydraulic efficiency in conventional water supply systems, Renewable and Sustainable Energy Reviews, Year 2014, Vol. 30, Pages 701-714.

[17] G. Meirelles Lima, B. Melo Brentan, E. Luvizotto, Optimal design of water supply networks using an energy recovery approach, Renewable Energy, Year 2018, Vol. 117, Pages 404-413.

[18] S. Kucukali, Hydropower potential of municipal water supply dams in Turkey: a case of study in Ulutan Dam, Energy Policy, Year 2010, Vol. 38, Pages 6534-6539.

[19] A. McNabola, P. Coughlan, A.P. Williams, Energy recovery in the water industry: an assessment of the potential of micro-hydropower, Water Environmental Journal, Year 2013, Vol. 27, Pages 1-11.

[20] J. Saldarriaga, C.A. Salcedo, Determination of Optimal Location and Settings of Pressure Reducing Valves in Water Distribution Networks for Minimizing Water Losses, Procedia Engineering, Year 2015, Vol. 119, Pages 973-983.

[21] F. García-Ávila, A. Avilés-Añazco, J. Ordoñez-Jara, C. Guanuchi-Quezada, L. Flores del Pino, L. Ramos-Fernández, Pressure management for

leakage reduction using pressure reducing valves. Case study in an Andean city, Alexandria Engineering Journal, Year 2019, Vol. 58, Pages 1313-1326.

[22] C. Van den Berg, The Drivers of Non-Revenue Water: How Effective Are Non-Revenue Water Reduction Programs?, Policy Research Working Paper, 6997, Year 2014. Available at: http://documents1.worldbank.org/curated/en/949281468161359020/pdf/WPS6997.pdf.

[23] F. Vieira, H.M. Ramos, Hybrid solution and pump-storage optimization in water supply system efficiency: a case of study, Energy Policy, Year 2008, Vol. 36, Pages 4142-4148.

[24] Z. Xu, L. Yao, X. Chen, Urban water supply system optimization and planning: Bi-objective optimization and system dynamics methods, Computers & Industrial Engineering, Year 2020, Vol. 142, Article 106373.

[25] S. Kucukali, Municipal water supply dams as a source of small hydropower in Turkey, Renewable Energy, Vol. 35, Year 2010, Pages 2001-2007.

[26] L-T. Wong, K-W Mui, A Review of Demand Models for Water Systems in Buildings including a Bayesian Approach, Water, Volume 10(8), Year 2018, Article 1078.

[27] L.K. Letting, Y. Hamam, A.M. Abu-Mahfouz, Estimation of Water Demand in Water Distribution Systems Using Particle Swarm Optimization, Water, Volume 9(8), Year 2017, Article 593.

[28] G. Balacco, A. Carbonara, A. Gioia, V. Iacobellis, A.F. Piccinini, Evaluation of Peak Water Demand Factors in Puglia (Southern Italy), Water, Volume 9(2), Year 2017, Article 96.

[29] V. Milano, Acquedotti Guida alla progettazione (in Italian), HOEPLI, Year 2012, Pages 650.

[30] H. Jeon, J. Hoon Park, Y. Shin, M. Choi, Friction loss and energy recovery of a Pelton turbine for different spear positions, Renewable Energy, Year 2018, Vol. 123, Pages 273-280.

[31] Autorità Regolazione Energia Reti e Ambiente (ARERA), Deliberazione dell'Autorità 618/2013/R/EFR (in Italian). Available at: https://www.arera.it/allegati/docs/13/618-13.pdf.

[32] Agenzia nazionale per le nuove tecnologie, l'energia e lo sviluppo economico sostenibile (ENEA), Rapporto Energia e Ambiente 2002 (in Italian). Available at: http://old.enea.it/com/web/pubblicazioni/REA_02/analisi_02.pdf.

[33] European Statistical Office (EUROSTAT). Available at: https://ec.europa.eu/eurostat/web/energy/data/database.

[34] Gestore dei Servizi Energetici (GSE), Certificati bianchi (in Italian). Available at: https://www.gse.it/servizi-per-te/efficienza-energetica/certificati-bianchi.

[35] L. Miller, R. Carriveau, Energy demand curve variables – An overview of individual and systemic effects, Sustainable Energy Technologies and Assessments, Vol. 35, Year 2019, Pages 172-179.

[36] M. Mohsin, A.K. Rasheed, H. Sun, J. Zhang, R. Iram, N. Iqbal, Q. Abbas, Developing low carbon economies: An aggregated composite index based on carbon emissions, Sustainable Energy Technologies and Assessments, Vol. 35, Year 2019, Pages 365-374.

[37] Z. Zhong, B. Peng, L. Xu, A. Andrews, E. Elahi, Analysis of regional energy economic efficiency and its influencing factors: A case study of

Yangtze river urban agglomeration, Sustainable Energy Technologies and Assessments, Vol. 41, Year 2020, Article 100784.

[38] V. Kanakoudis, S. Tsitsifli, A. Papadopoulou, Integrating the Carbon and Water Footprints' Costs in the Water Framework Directive 2000/60/EC Full Water Cost Recovery Concept: Basic Principles Towards Their Reliable Calculation and Socially Just Allocation, Water, Vol. 4(1), Year 2010, Pages 45-62.

[39] V. Kanakoudis, A. Papadopoulou, Allocating the cost of the carbon footprint produced along a supply chain, among the stakeholders involved, Journal of Water and Climate Change, Vol. 5(4), Year 2014, Pages 556-568.

[40] C.T. Cheung, K.W. Mui, L.T. Wong, Energy efficiency of elevated water supply tanks for high-rise buildings, Applied Energy, Vol. 103, Year 2013, Pages 685-691.

[41] M. Lee, A.A. Keller, P.C. Chiang, W. Den, H. Wang, C.H. Hou, J. Wu, X. Wang, J. Yan, Water-energy nexus for urban water systems: A comparative review on energy intensity and environmental impacts in relation to global water risks, Applied Energy, Vol. 205, Year 2017, Pages 589-601.

[42] R. Kernan, X. Liu, S. McLoone, B. Fox, Demand side management of an urban water supply using wholesale electricity price, Applied Energy, Vol. 189, Year 2017, Pages 395-402.

[43] V. Kanakoudis, K. Gonelas, The optimal balance point between NRW reduction measures, full water costing and water pricing in water distribution systems. Alternative scenarios forecasting the Kozani's WDS optimal balance point, Procedia Engineering, Vol. 119, Year 2015, Pages 1278-1287.

[44] M. Patelis, V. Kanakoudis, A. Kravvari, Pressure Regulation vs. Water Aging in Water Distribution Networks, Water, Vol. 12(5), Year 2020, Article 1323.

[45] J. Du, Z. Shen, H. Yang, Study on the effects of runner geometries on the performance of inline cross-flow turbine used in water pipelines, Sustainable Energy Technologies and Assessments, Vol. 40, Year 2020, Article 100762.

[46] P.A. Su, B. Karney, Micro hydroelectric energy recovery in municipal water systems: A case study for Vancouver, Urban Water Journal, Vol. 12, Year 2015, Pages 678-690.

[47] M.R. Nogueira Vilanova, J.A. Perrella Balestieri, Energy and hydraulic efficiency in conventional water supply systems, Renewable & Sustainable Energy Reviews, Vol. 10, Year 2014, Pages 701-14.

[48] M. Patelis, V. Kanakoudis, K. Gonelas, Pressure Management and Energy Recovery Capabilities Using PATs, Procedia Engineering, Vol. 162, Year 2016, Pages 503-510.

[49] A. Morabito, P. Hendrick, Pump as turbine applied to micro energy storage and smart water grids: A case study, Applied Energy, Vol. 241, Year 2019, Pages 567-579.

[50] C. Power, A. McNabola, P. Coughlan, Development of an evaluation method for hydropower energy recovery in wastewater treatment plants: Case studies in Ireland and the UK, Sustainable Energy Technologies and Assessments, Vol. 7, Year 2014, Pages 166-177.

[51] S.V. Jain, A. Swarnkar, K.H. Motwani, R.N. Patel, Effects of impeller diameter and rotational speed on performance of pump running in turbine mode, Energy Conversion and Management, Vol. 89, Year 2015, Pages 808-824.

[52] H.M. Ramos, M. Mello, P.K. De, Clean power in water supply systems as a sustainable solution: from planning to practical implementation, Water Science & Technology-Water Supply - WSTWS, Vol. 79, Year 2010, Pages 39-49.

[53] S. Derakshan, A. Nourbakhsh, Experimental study of characteristic curves of centrifugal pumps working as turbines in different specific speeds, Experimental Thermal and Fluid Science, Vol. 32, Year 2007, Pages 800-807.

[54] A. Carravetta, G. Del Giudice, O. Fecarotta, H.M. Ramos, PAT Design Strategy for Energy Recovery in Water Distribution Networks by Electrical Regulation, Energies, Vol. 6, Year 2013, Pages 411-424.

[55] M. De Marchis, C.M. Fontanazza, G. Freni, A. Messineo, B. Milici, E. Napoli, V. Notaro, V. Puleo, A. Scopa, Energy Recovery in Water Distribution Networks: Implementation of Pumps as Turbine in a Dynamic Numerical Model, Procedia Engineering, Vol. 70, Year 2014, Pages 439-448.

[56] L. Corcoran, A. McNabola, P. Coughlan, Energy Recovery Potential of the Dublin Region Water Supply Network, In Proceedings of the World Congress on Water, Climate and Energy, Dublin, Ireland, 13th-18th May 2012.

[57] J. Peréz García, A. Cortés Marco A, S. Nevado Santos, Use of centrifugal pumps operating as turbines for energy recovery in water distribution networks. Two case study, Advanced Material Research, Vol. 107, Year 2010, Pages 87-92.

[58] S.V. Jain, R.N. Patel, Investigations on pump running in turbine mode: A review of the state-of-the-art, Renewable & Sustainable Energy Reviews, Vol. 30, Year 2014, Pages 841-868.

[59] A. Kurigi, A.N. Pinheiro, A. Sordo-Ward, L. Garrote, Flow regime aspects in determining environmental flows and maximising energy production at run-of-river hydropower plants, Applied Energy, Vol. 256, Year 2019, Article 113980.

[60] J. Du, H. Yang, Z. Shen, J. Chen. Micro hydro power generation from water supply system in high rise buildings using pump as turbines, Energy, Vol. 137, Year 2017, Pages 431-440.

[61] M. Renzi, A. Nigro, M. Rossi, A methodology to forecast the main non-dimensional performance parameters of pumps-as-turbines (PaTs) operating at Best Efficiency Point (BEP), Renewable Energy, Vol. 160, Year 2020, Pages 16-25.

[62] X. Tan, A. Engeda, Performance of centrifugal pumps running in reverse as turbine: Part Ⅱ - systematic specific speed and specific diameter based performance prediction, Renewable Energy, Vol. 99, Year 2016, Pages 188-197.

[63] M. Liu, L. Tan, S. Cao, Theoretical model of energy performance prediction and BEP determination for centrifugal pump as turbine, Energy, Vol. 172, Year 2019, Pages 712-732.

[64] M. Rossi, A. Nigro, M. Renzi, Experimental and numerical assessment of a methodology for performance prediction of Pumps-as-Turbines (PaTs) operating in off-design conditions, Applied Energy, Vol. 248, Year 2019, Pages 555-566.

[65] D. Novara, A. McNabola, A model for the extrapolation of the characteristic curves of Pumps as Turbines from a datum Best Efficiency Point, Energy Conversion and Management, Vol. 174, Year 2018, Pages 1-7.

[66] J. Delgado, L. Andolfatto, D. I. C. Covas, F. Avellan, Hill chart modelling using the Hermite polynomial chaos expansion for the performance prediction of pumps running as turbines, Energy Conversion and Management, Vol. 187, Year 2019, Pages 578-592.

[67] M. Stefanizzi, M. Torresi, B. Fortunato, S. M. Camporeale, Experimental investigation and performance prediction modeling of a single stage centrifugal pump operating as turbine, Energy Procedia, Vol. 126, Year 2017, Pages 589-596.

[68] M. Venturini, L. Manservigi, S. Alvisi, S. Simani, Development of a physics-based model to predict the performance of pumps as turbines, Applied Energy, Vol. 231, Year 2018, Pages 343-354.

[69] S. Barbarelli, M. Amelio, G. Florio, Experimental activity at test rig validating correlations to select pumps running as turbines in microhydro plants, Energy Conversion and Management, Vol. 149, Year 2017, Pages 781-797.

[70] D. Štefan, M. Rossi, M. Hudec, P. Rudolf, A. Nigro, M. Renzi, Study of the internal flow field in a pump-as-turbine (PaT): Numerical investigation, overall performance prediction model and velocity vector analysis, Renewable Energy, Vol. 156, Year 2020, Pages 158-172.

[71] L. Da Deppo, C. Datei, V. Fiorotto, Acquedotti, Cortina (Padova), Year 2003, Pages 561.

[72] M. Stefanizzi, T. Capurso, G. Balacco, M. Binetti, M. Torresi, S.M. Camporeale, Pump as turbine for throttling energy recovery in water distribution networks, AIP Conference Proceedings, Vol. 2191, Year 2019, Article 020142.

[73] KSB, electric motors efficiency class. Available at: https://www.ksb.com/centrifugal-pump-lexicon/efficiency-class/328160/ (last accessed on the 14/12/2020).

[74] Autorità per l'energia elettrica e il gas (AEEG), Deliberazione dell'Autorità EEN 3/08 (in Italian). Available at: https://www.arera.it/it/docs/08/003-08een.htm (last accessed on the 14/12/2020).

[75] Vetrano L., Modica C., Il controllo in tempo reale delle pressioni nelle reti di acquedotto ai fini della riduzione delle perdite idriche, Dottorato di ricerca internazionale in ingegneria idraulica XXIV ciclo, Università di Catania, Year 2011, Pages 1-135.

[76] L. 5.01.1994, n. 36 e s.m.i., Disposizioni in materia di risorse idriche, G.U. 19.01.1994, n.14.

[77] D.P.C.M. 04.03.1996, Disposizioni in materia di risorse idriche, G.U. 14.03.1996, n. 62.

[78] D.M. LL.PP. 08.01.1997, n. 99, Regolamento sui criteri e sul metodo in base ai quali valutare le perdite degli acquedotti e delle fognature, G.U. 18.04.1997, n. 90.

[79] Portolano D., Giugni M., Il controllo delle perdite nei sistemi acquedottistici: criteri innovativi di gestione, Dottorato di ricerca in analisi dei sistemi ambientali XXI ciclo, Università degli studi di Napoli "Federico II", Year 2008, Pages 1-165.

[80] Cheong L.C., International report on unaccounted for water and economics of leak detection, IWA World Conference Budapest, October 1993.

[81] Oberdan Cei, Team Project ASAP, Actions for Systemic Acquifer Protection – Implementation and demonstration of a protocol to scale down groundwater vulnerability to pollution due to overexploitation – Deliverable 4.3, LIFE 06/ENV/IT/255, Year 2009, Pages 1-20.

[82] Hamberg D., Shamir U., Schematic Models For Distribution Systems Design, Journal of Water Resources Planning and Management, ASCE 114(2), Year 1988, Pages 129-141.

[83] A. Di Nardo, M. Di Natale, R. Greco & G.F. Santonastaso, Indici sintetici per la distrettualizzazione di una rete idrica di distribuzione, XXXIII Convegno Nazionale di Idraulica e Costruzioni Idrauliche, Brescia, Year 2012.

[84] Mays, L.W. Water distribution systems handbook, New York, McGraw-Hill, Year 2000.

[85] Todini, E. Looped, Water distribution networks design using a resilience index based heuristic approach, Urban Water, Year 2000, 2(2), Pages 115-122.

[86] Di Nardo, A. & Di Natale, M. A heuristic design support methodology based on graph theory for district metering of water supply networks, Engineering Optimization, Year 2011, 43(2), Pages 193-211.

[87] Greco, R., Di Nardo, A. & Santonastaso, G. F. Resilience and entropy as indices of robusteness of water distribution networks, Journal of Hydroinformatics, doi:10.2166/hydro.2012.037, Year 2012.

[88] Gma Controls, IZAR-tecnologia applicata per soluzioni AMR / AMI, Year 2018.

[89] F. Poggi, A. Firmino, M. Amado, Assessing energy performances: A step toward energy efficiency at the municipal level, Sustainable Cities and Society, Vol. 33, Year 2017, Pages 57-69.

[90] F. Meggers, H. Liebundgut, S. Kennedy, M. Qin, M. Schlaich, W. Sobek, M. Shukuya, Reduce CO2 from buildings with technology to zero emissions, Sustainable Cities and Society, Vol.2, Year 2021, Pages 29-36.

[91] M. Rossi, G. Comodi, N. Piacente, M. Renzi, Energy recovery in oil refineries by means of a Hydraulic Power Recovery Turbine (HPRT) handling viscous liquids, Applied Energy, Vol. 270, Year 2020, Article 115097.

[92] A.S. Babamiri, M.S. Pishvaee, S. Mirzamohammadi, The analysis of financially sustainable management strategies of urban water distribution network under increasing block tariff structure: A system dynamics approach, Sustainable Cities and Society, Vol. 60, Year 2020, Article 102193.

[93] H. Fontenot, K.S. Ayyagari, B. Dong, N. Gatsis, A. Taha, Buildings-to-Distribution-Network Integration for Coordinated Voltage Regulation and

Building Energy Management via Distributed Resource Flexibility, Sustainable City and Society, Year 2021, Article 102832, In Press.

[94] T.L. Oladosu, O.A. Koya, Numerical analysis of lift-based in-pipe turbine for predicting hydropower harnessing potential in selected water distribution networks for waterlines optimization, Engineering Science and Technology, an International Journal, Vol. 21, Year 2018, Pages 672-678.

[95] M. Sinagra, C. Aricò, T. Tucciarelli, G. Morreale, Experimental and numerical analysis of a backpressure Banki inline turbine for pressure regulation and energy production, Renewable Energy, Vol. 149, Year 2020, Pages 980-986.

[96] W. Yang, Y. Hou, H. Jia, B. Liu, R. Xiao, Lift-type and drag-type hydro turbine with vertical axis for power generation from water pipelines, Energy, Vol.188, Year 2019, Article 116070.

[97] M. Rossi, A. Nigro, G.R. Pisaturo, M. Renzi, Technical and economic analysis of Pumps-as-Turbines (PaTs) used in an Italian Water Distribution Network (WDN) for electrical energy production, Energy Procedia, Vol.158, Year 2019, Pages 117-122.

[98] A. Kandi, M. Moghimi, M. Tahani, S. Derakhshan, Optimization of pump selection for running as turbine and performance analysis within the regulation schemes, Energy, Vol. 217, Year 2021, Article 119402.

[99] S. El-Zahab, T. Zayed, Leak detection in water distribution networks: an introductory overview, Smart Water, Vol. 4, Year 2019, Article 5.

[100] G. Cavazzini, G. Pavesi, G. Ardizzon, Optimal assets management of a water distribution network for leakage minimization based on an innovative index, Sustainable Cities and Society, Vol. 54, Year 2020, Article 101890.

[101] G.J. Bonthuys, M. van Dijk, G. Cavazzini, Leveraging water infrastructure asset management for energy recovery and leakage reduction, Sustainable Cities and Society, Vol. 46, Year 2019, Article 101434.

[102] L. Latchoomun, R.T.F. Ah King, K.K. Busawon, J.M. Ginoux, Harmonic oscillator tank: A new method for leakage and energy reduction in a water distribution network with pressure driven demand, Energy, Vol. 201, Year 2020, Article 117657.

[103] A. Naim, A. Aaroud, K. Akodadi, C. El Hacimi, A fully AI-based system to automate water meter data collection in Morocco country, Array, Vol. 10, Year 2021, Article 100056.

[104] C. Bragalli, M. Neri, E. Toth, Effectiveness of smart meter-based urban water loss assessment in a real network with synchronous and incomplete readings, Environmental Modelling & Software, Vol. 112, Year 2019, Pages 128-142.

[105] J.E. Pesantez, E.Z. Berglund, N. Kaza, Smart meters data for modeling and forecasting water demand at the user-level, Environmental Modelling & Software, Vol. 125, Year 2020, Article 104633.